

THESIS
2.



3 1293 01771 8358



This is to certify that the
thesis entitled
OPTICAL EMISSION SPECTROSCOPY INVESTIGATION
OF MICROWAVE PLASMAS

presented by

Jayakumaran Sivagnaname

has been accepted towards fulfillment
of the requirements for
MASTER OF SCIENCE degree in Electrical Engg.


Major professor

Date 12/15/98

PLACE IN RETURN BOX to remove this checkout from your record.
TO AVOID FINES return on or before date due.
MAY BE RECALLED with earlier due date if requested.

DATE DUE	DATE DUE	DATE DUE
NOV 23 2001		
MAY 31 2003		

**OPTICAL EMISSION SPECTROSCOPY INVESTIGATION OF
MICROWAVE PLASMAS**

By

Jayakumaran Sivagnaname

A THESIS

Submitted to
Michigan State University
in partial fulfillment of the requirements
for the degree of

MASTER OF SCIENCE

Department of Electrical and Computer Engineering

1998

ABSTRACT

OPTICAL EMISSION SPECTROSCOPY INVESTIGATION OF MICROWAVE PLASMAS

By

Jayakumaran Sivagnaname

Microwave cavity plasma reactors are being used for a range of materials processing applications including the deposition of diamond thin films and the etching/surface treatment of semiconductor materials during device fabrication. For all these microwave plasma processes a concise understanding of the plasma species concentration and energies are often still lacking. The plasma parameters like gas temperature and species concentration, H, C₂ and CH, for some of the commonly used plasmas for diamond thin film deposition, namely H₂ - CH₄ and Ar - H₂ - CH₄ were analyzed using optical emission spectroscopy.

The addition of small amounts of N₂ has been shown to affect the deposition rate and characteristics of the diamond film. Hence the effect of nitrogen on these plasmas was also studied. With the 0.1 - 1% addition of nitrogen no change in the gas temperature was observed. However an increase in the amount of atomic hydrogen was observed with nitrogen concentration.

The density of high energy electrons in a compact ion source was also analyzed. This was achieved by observing the doubly ionized argon emission lines. The results indicate the presence of high energy electrons (greater than 27eV) in the plasma of a compact ion source.

Dedicated to

Almighty

ACKNOWLEDGEMENTS

I would like to express my profound gratitude to Dr. Timothy Grotjohn. It was his constant encouragement, support and untiring help that led to the completion of this project. He has given his knowledge, his time and his support to guide me through the work presented here. I would also like to thank Dr. Jes Asmussen and Dr. Tim Hogan for their constructive remarks on the project and for being a part of the examining committee. Thanks are due to Dr. Anatoly Vikharev, Alexander(Sasha) Kolysko and Dmitry Radishev of the Russian Academy of Sciences for their contribution to the project, especially the gas temperature measurements. I wish to express my gratitude to my parents and family members for their love and support. I would also like to thank Bo Keu Kim, Meng-Hua Tsai, Mark Perrin, Amir Khan and Wen-Shin Huang for their advice and friendship.

TABLE OF CONTENTS

List of Tables	iii
List of Figures	ix
1 Introduction	1
1.0 Motivation	1
1.2 Objectives	2
1.3 Thesis Outline.....	3
2 Equipment and Experimental Method	4
2.1 Introduction to equipment used.....	4
2.2 Multipolar ECR plasma reactor system.....	4
2.2.1 Description of the Plasma Source - the MPDR 610	4
2.2.2 The microwave apparatus	7
2.2.3 Gas/vacuum systems.....	8
2.3 High power resonant cavity microwave reactor.....	10
2.4 Spectrometer- system #1	12
2.5 Data acquisition and signal processing for spectrometer system #1	13
2.6 Diode array detector - spectrometer system #2.....	14
2.7 Collection Optics.....	16
2.7.1 Arrangement #1	17
2.7.2 Arrangement #2	17
2.7.3 Arrangement #3	18

3	Identification and analysis of Argon Doubly-ionized atoms	19
3.1	Introduction	19
3.2	Theory of the diagnostic technique	19
3.4	Experimental method	22
3.3	Observation and measurement of the doubly ionized lines.....	23
3.5	Results and discussion.....	26
3.6	Conclusion.....	33
4	Gas Kinetic Temperature of H₂ - CH₄ Microwave Plasma	34
4.1	Introduction	34
4.2	Gas kinetic temperature measurement theory	34
4.2.1	Hund's Coupling Cases.....	38
4.3	Experimental setup	40
4.4	Hydrogen rotational temperature.....	41
4.4.1	Estimation of the rotational temperature.....	41
4.5	Rotational temperature results.....	43
4.6	Conclusion.....	50
5	Study of H₂ - CH₄ - N₂ Microwave Plasma	51
5.1	Introduction	51
5.2	Experimental Setup	51
5.3	Results and discussions	52
5.4	Conclusion.....	60

6	Study of Ar - H₂ - CH₄ - N₂ Microwave Plasma	61
6.1	Introduction	61
6.2	Experimental setup	61
6.3	Results and discussion.....	62
6.5	Conclusion.....	78
7	Summary of results	79
7.1	Conclusion.....	79
7.1.1	Argon Doubly-ionized atoms measurements.....	79
7.1.2	Gas Kinetic Temperature of H ₂ - CH ₄ Microwave Plasma	80
7.1.3	Study of H ₂ - CH ₄ - N ₂ Microwave Plasma	80
7.1.4	Study of Ar-H ₂ - CH ₄ - N ₂ Microwave Plasma	81
7.2	Recommendations for future work.....	81
	Appendix A	84
	Appendix B	86
	Appendix C	91
	References	97

LIST OF TABLES

4 Gas Kinetic Temperature of H₂ - CH₄ Microwave Plasma	34
Table 4.1: Energy level for the R-branch rotational lines	43
Appendix A	84
Table A: Identification and analysis of argon doubly ionized atoms	84
Appendix B	86
Table B: Measurements of Ar - H ₂ - CH ₄ - N ₂ Microwave Plasma	86

LIST OF FIGURES

Figure 2.1 MPDR 610 Plasma Source	6
Figure 2.2 Top view of the chamber	7
Figure 2.3 Vacuum system of the plasma source	9
Figure 2.4 High Power Microwave Plasma Reactor	10
Figure 2.5 High Power Microwave Plasma Reactor	11
Figure 2.6 Sketch of the spectrometer	13
Figure 2.7 Sketch of the diode array detector	15
Figure 2.8 Optical set up for light collection - arrangement #1	17
Figure 2.9 Optical set up for light collection - arrangement #2	18
Figure 2.10 Optical set up for light collection - arrangement #3	18
Figure 3.1 Atomic states of the Ar atom	20
Figure 3.2 Experimental Set-up for the identification of Ar ⁺⁺ lines	23
Figure 3.3 Emission spectra of krypton plasma. Pressure: 3 mT, Flow rate: 1sccm, Input Power: 90 W.	24
Figure 3.4 Emission spectra of argon plasma. Pressure: 0.75 mT, Flow rate: 1sccm, Input Power: 100 W.	25
Figure 3.5 Variation of Ar ⁺⁺ density with pressure for argon plasma. Flow rate: 1sccm. Input power: 40 W.	29
Figure 3.6 Variation of Ar ⁺⁺ density with pressure for argon plasma. Flow rate: 1sccm. Input power: 100 W.	30
Figure 3.7 Variation of Ar ⁺⁺ density with input power for argon plasma. Flow rate: 1 sccm. Pressure: 0.9 mT	31
Figure 3.8 Variation of Ar ⁺⁺ density with flow rate of Ar for argon plasma. Pressure: 0.9 mT. Input power: 40 W.	32

Figure 4.1 Diagram of the Observed Electronic States of the H ₂ Molecule.....	36
Figure 4.2 Energy Level Diagram for a Band with P and R Branches.....	37
Figure 4.3 Experimental Set-up for the measurement of rotational temperature of H ₂	40
Figure 4.4 Emission Spectra of the R-Branch rotational lines of H ₂	42
Figure 4.5 Boltzmann plot for the lines R0 and R5-R10	42
Figure 4.6 Variation of rotational temperature of H ₂ with pressure for H ₂ plasma. Flow rate: H ₂ -200 sccm. Input power: 400 W	45
Figure 4.7 Variation of rotational temperature of H ₂ with pressure for H ₂ -CH ₄ plasma. Flow rate: H ₂ -200 sccm, CH ₄ -4 sccm. Input power: 400 W	46
Figure 4.8 Variation of rotational temperature of H ₂ with input power for H ₂ -CH ₄ plasma. Flow rate: H ₂ -200 sccm, CH ₄ -4 sccm. Pressure: 30 Torr	47
Figure 4.9 Variation of rotational temperature of H ₂ with flow rate for H ₂ plasma. Pressure: 30 Torr. Input power: 400 W	48
Figure 4.10 Variation of rotational temperature of H ₂ with flow rate of N ₂ for H ₂ -CH ₄ -N ₂ plasma. Flow rate: H ₂ -200 sccm, CH ₄ -4sccm. Pressure: 30 Torr. Input power: 400 W ..	49
Figure 5.1 Variation of H _α line intensity with N ₂ concentration. Flow rates: CH ₄ -4 sccm, H ₂ -200 sccm. Pressure: 30 Torr. Input Power: 0.8 kW	54
Figure 5.2 Variation of H _β line intensity with N ₂ concentration. Flow rates: CH ₄ -4 sccm, H ₂ -200 sccm. Pressure: 30 Torr. Input Power: 0.8 kW	55
Figure 5.3 Variation of H _β /H _α ratio with N ₂ concentration. Flow rates: CH ₄ -4 sccm, H ₂ -200 sccm. Pressure: 30 Torr. Input Power: 0.8 kW	56
Figure 5.4 Emission spectrum of H ₂ -CH ₄ -N ₂ plasma. Flow rates: CH ₄ -7.2 sccm, H ₂ -144 sccm, N ₂ -0.5 sccm. Pressure: 30 Torr. Input Power: 0.8 kW	57
Figure 5.5 Variation of CH line intensity with N ₂ concentration. Flow rates: CH ₄ -7.2 sccm, H ₂ -144 sccm. Pressure: 30 Torr. Input Power: 0.8 kW	58
Figure 5.6 Variation of CN line intensity with N ₂ concentration. Flow rates: CH ₄ -7.2 sccm, H ₂ -144 sccm. Pressure: 30 Torr. Input Power: 0.8 kW	59
Figure 6.1 Emission spectrum. Flow rates: Ar- 600 sccm, CH ₄ - 3 sccm, H ₂ - 12sccm, N ₂ - 3 sccm. Pressure: 120 Torr. Input Power: 1.09 kW	64

Figure 6.2 Emission spectrum. Flow rates: Ar- 100 sccm, CH ₄ - 8 sccm, H ₂ - 300sccm, N ₂ - 0 sccm. Pressure: 120 Torr. Input Power: 1.621 kW	65
Figure 6.3 Emission spectrum. Flow rates: Ar- 100 sccm, CH ₄ - 8 sccm, H ₂ - 300sccm, N ₂ - 0 sccm. Pressure: 120 Torr. Input Power: 1.621 kW	66
Figure 6.4 Variation of species concentration with H ₂ flow rate. Flow rates: Ar- 600 sccm, CH ₄ - 8 sccm. Pressure: 120 Torr. Input Power: ~ 1.2 kW	67
Figure 6.4a Variation of species concentration with H ₂ flow rate. Flow rates: Ar- 600 sccm, CH ₄ - 8 sccm. Pressure: 120 Torr. Input Power: ~ 1.2 kW	68
Figure 6.5 Variation of species concentration with CH ₄ flow rate. Flow rates: Ar- 600 sccm, H ₂ - 0 sccm. Pressure: 120 Torr. Input Power: ~ 1.2 kW	69
Figure 6.5a Variation of species concentration with CH ₄ flow rate. Flow rates: Ar- 600 sccm, H ₂ - 0 sccm. Pressure: 120 Torr. Input Power: ~ 1.2 kW	70
Figure 6.6 Variation of species concentration with N ₂ flow. Flow rates: Ar- 600 sccm, H ₂ - 12 sccm, CH ₄ - 8 sccm. Pressure: 120 Torr. Input Power: ~ 1.1 kW	71
Figure 6.7 Variation of species concentration with Ar flow rate. Flow rates: H ₂ - 50-300 sccm, CH ₄ - 8 sccm. Pressure: 120 Torr. Input Power: ~ 1.4 kW	72
Figure 6.7a Variation of species concentration with Ar flow rate. Flow rates: H ₂ - 50-300 sccm, CH ₄ - 8 sccm. Pressure: 120 Torr. Input Power: ~ 1.4 kW	73
Figure 6.8 Variation of C ₂ /H _α ratio with H ₂ flow rate. Flow rates: Ar - 600 sccm, CH ₄ - 8 sccm. Pressure: 120 Torr. Input Power: ~ 1.2 kW	74
Figure 6.9 Variation of C ₂ /H _α ratio with CH ₄ flow rate. Flow rates: Ar - 600 sccm, H ₂ - 0 sccm. Pressure: 120 Torr. Input Power: ~ 1.2 kW	75
Figure 6.10 Variation of H _β /H _α ratio with H ₂ flow rate. Flow rates: Ar - 600 sccm, CH ₄ - 8 sccm. Pressure: 120 Torr. Input Power: ~ 1.2 kW	76
Figure 6.11 Variation of H _β /H _α ratio with H ₂ flow rate. Flow rates: Ar - 600 sccm, H ₂ - 0 sccm. Pressure: 120 Torr. Input Power: ~ 1.2 kW	77

Chapter 1

Introduction

1.0 Motivation

Microwave cavity plasma reactors are being used for a range of materials processing applications including the deposition of diamond thin films and the etching/surface treatment of semiconductor materials during device fabrication. The etching applications are carried out in electron cyclotron resonance (ECR) microwave cavity reactors which typically operated at low pressure below 10 mTorr. The deposition of diamond thin films use the microwave cavity reactor without the static magnetic fields and the pressure used are much higher in the range of 10-120 Torr. For all these microwave plasma processes a concise understanding of the plasma species concentration and energies are often still lacking.

For example, during the diamond deposition process the addition of small amounts (10-100 ppm) of nitrogen can significantly change the deposit film's properties and growth rate [1]. The reason for the importance of nitrogen in the deposition process is not understood. One possible explanation is that the bulk plasma species concentration or plasma temperature are changed by the nitrogen and that these bulk changes effect the deposition process. Hence a study of the various species concentration in the diamond CVD plasma with the addition of nitrogen would be helpful in understanding the role of nitrogen and how it affects the plasma parameters.

A second example where additional understanding of a plasma process would be useful is the deposition of nanocrystalline diamond using Ar-CH₄-H₂ gas mixture. For the microcrystalline and nanocrystalline diamond growth, the ratio of argon to hydrogen has been found to be a dominant factor [2]. Therefore an analysis of the species in the plasma may shed some light on their role in the plasma deposition process.

A third example for additional understanding of plasmas being of interest that is investigated in this study is the electron energy distribution function in low pressure ECR plasmas. Specifically, in a compact ECR ion source used for generating plasmas in molecular beam epitaxy machines, the excitation mechanism in the source is not fully understood. Specifically the density of high energy electrons in the excitation region needs investigation.

1.2 Objectives

The main objective of this work is to investigate microwave plasma discharges using optical emission spectroscopy(OES) in order to add to the understanding of these discharges. The specific objectives are:

1. To study the basic Ar plasma and measure the amount of doubly ionized atoms and hence high energy electrons present under various process conditions for plasmas created in a compact ECR ion source.
2. To understand the variation of the plasma parameters like gas temperature and species concentration under various process conditions for plasmas used in diamond CVD deposition. Specific issues to be studied include the gas temperature of diamond CVD

plasma, the influx of nitrogen gas addition on CH₄-H₂ diamond deposition plasmas, and the species concentration variation in CH₄-Ar-H₂ plasmas used for nanocrystalline diamond deposition.

1.3 Thesis Outline

The main part of the thesis has been divided into four chapters (Chapters 3-6) with one chapter devoted to each of the plasmas mentioned in the objectives.

Chapter 2 discusses the equipment and the plasma reactors used in the experiments. The relevant details needed to understand the experimental set up has been provided with careful attention to each instrument.

Chapter 3 explains the argon doubly ionized atom measurements carried out in the microwave ECR plasma source. The results are presented along with the discussions. Chapter 4 details the gas temperature measurements performed on the H₂-CH₄ plasma. An insight has been provided to the theoretical aspects involved. The observations are presented along with the interpretations. Chapter 5 elaborates the role of N₂ in the deposition process as a result of the study of the H₂-CH₄-N₂ plasmas. The influence of N₂ on the hydrogen, CH and CN species concentration is given importance. Chapter 6 presents the study of the Ar-H₂-CH₂-N₂ plasmas and the results obtained. The variation of the constituent species concentration with the process parameters is discussed. Chapter 7 provides the summary of the research and discusses future research work in this area.

Chapter 2

Equipment and Experimental Method

2.1 Introduction to equipment used

This chapter describes the features of the resonant cavity microwave discharge apparatus, especially those features relevant to the optical emission spectroscopy experiments. It includes descriptions of the microwave plasma reactor, spectrometer, data acquisition system and the collection optics used in the experiments.

The experiments were performed on two different types of the resonant cavities. The diamond CVD reactor measurements discussed in chapters 4, 5 and 6 were performed in a resonant cavity suited for high power and moderate pressure. The Ar⁺⁺ density measurements discussed in chapter 3 were performed in the microwave ECR plasma source [MPDR 610] suited for low power and very low pressure plasma formation. Accordingly, the set-up is described in two sections due to the different configurations of the plasma reactor.

2.2 Multipolar ECR plasma reactor system

2.2.1 Description of the Plasma Source - the MPDR 610

The Microwave Plasma Disk Reactor [MPDR] 610 is a compact coaxial electron cyclotron resonance plasma source. A sketch of the plasma source is shown in Figure 2.1. The cylindrical source is made of stainless steel, and it has an outer diameter of about 5.8 cm with an application specific overall length [3]. The vacuum seal at one end is made by

a standard 4.5 inch Conflat flange with the entire length of the source inserted into the vacuum chamber. At the other end (near the discharge), metal-to-fused quartz vacuum seals are made using specially designed ultra high vacuum compatible ring shaped Helicoflex spring loaded seals. The discharge located at this end of the plasma source has a diameter of 3.5 cm. The electromagnetic cavity excitation region consists of a coaxial coupling section which is terminated at one end with a sliding short, and at the other end, by the discharge. The region between the sliding short and the discharge is occupied by a coaxial waveguide section and an evanescent circular waveguide section. The diameter of the inner conductor comprising the coaxial section is 1.2 cm. A small loop antenna is attached to the sliding short, and this loop excites the TEM mode in the microwave cavity. Between the terminus of the center conductor and the discharge is an impedance matching circular waveguide section that has a diameter which is too small to support any electromagnetic propagating modes for the 2.45 GHz excitation frequency. The plasma is confined in a quartz discharge chamber with an inner diameter of 3.5 cm and a height of 4.7 cm. The quartz tube is surrounded by three ring shaped axially magnetized permanent magnets which provide the static magnetic flux density within the plasma chamber for plasma confinement and the 875 Gauss field strength for ECR. The magnets have an outer diameter of 4.95 cm, a height of 1.27 cm, and an inner diameter of 4.32 cm. They are aligned with like poles facing each other.

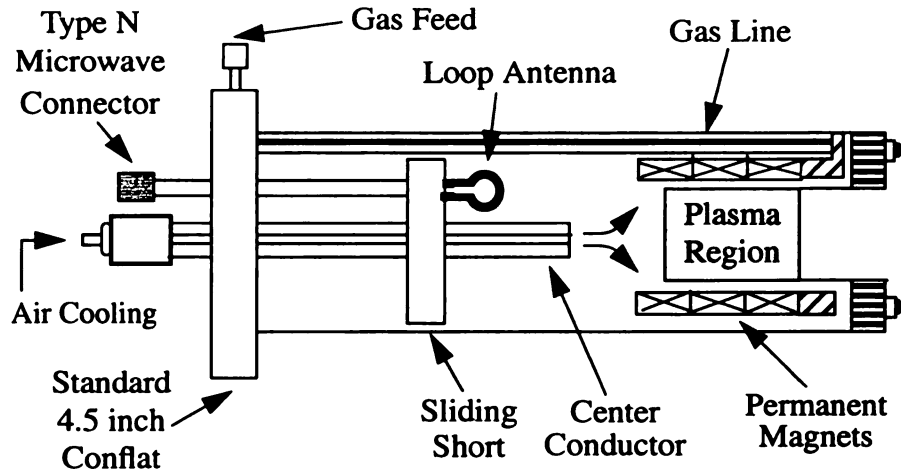


Figure 2.1 MPDR 610 Plasma Source

The quartz walls and the magnets are cooled by compressed air flowing through the center conductor and blowing onto the discharge chamber. The positions of the center conductor and the sliding short can be independently adjusted in order to match the discharge load to the input transmission line impedance. The discharge load changes as the plasma varies with input power, gas flow/pressure, gas type etc., and appropriate tuning minimizes the reflected power and ensures maximum power transfer to the plasma load.

The cylindrical stainless steel processing chamber is 10 inch high and has a diameter of 18 inches. It has four ports one each connected to the vacuum pump and the plasma source. The other two ports are used as viewing port for the optical diagnostics. The viewing ports and the port connected to the source are 8 inch in diameter. The transparent window of the viewing port has a diameter of 1.8 inches. The ports are orthogonal as shown in Figure 2.2.

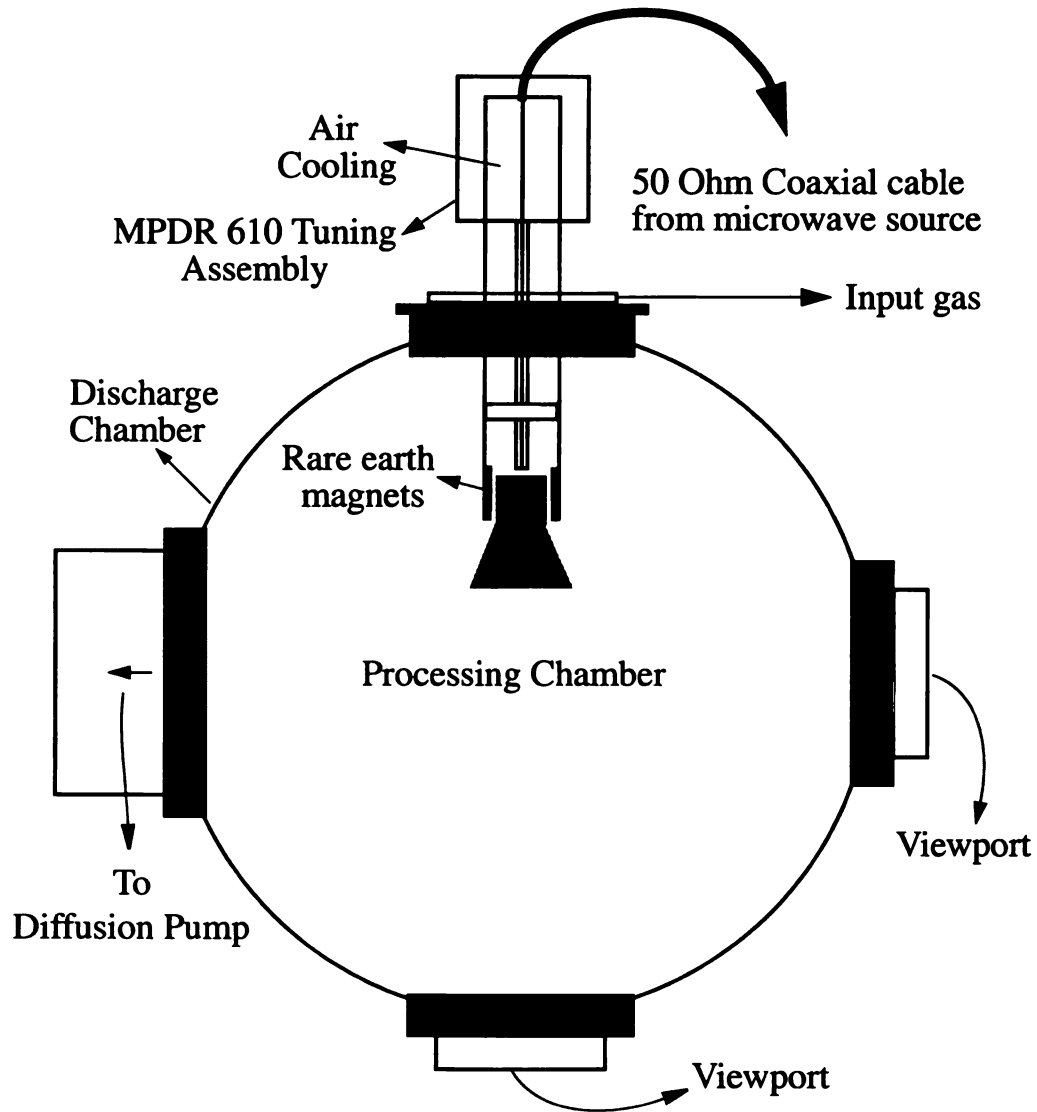


Figure 2.2 Top view of the chamber

2.2.2 The microwave apparatus

Microwave energy is supplied by a 2.45 GHz microwave power supply (Raytheon PGM10X1). The experiments described in Chapter 3 were performed with microwave power ranging from 10 Watts to 100 Watts. This power range refers to the power absorbed by the cavity which is found by subtracting the microwave power reflected by the cavity

from the power incident to the cavity. The microwave circuit includes a three port circulator and dummy load to protect the power supply and a dual directional coupler for sampling both the reflected and incident power.

A 50 ohm coaxial cable with type N connectors and a Teflon dielectric filling material transfers power from the bi-directional couplers to the plasma source. The coaxial structure of the cable is continued into the source body, terminating in the loop antenna as shown in Figure 2.1. This loop excites the TEM mode in the coaxial cavity that stretches from the end of the sliding short to the terminus of the center conductor, beyond which evanescent fields are excited in the circular waveguide section of the source.

2.2.3 Gas/vacuum systems

The vacuum system connected to the plasma reactor used for the argon doubly ionized atom identification and measurement (discussed in chapter 3) can be represented as shown in the Figure 2.3.

The vacuum chamber is connected to a 6 inch diameter oil diffusion pump and backed by a mechanical pump. A gate valve isolates the vacuum chamber from the diffusion pump stack. Between the gate valve and the diffusion pump is a gate conductance valve and a water cooled cold trap that helps in keeping stray pump oil away from the vacuum chamber. The diffusion pump is filled with a hydrocarbon-free oil [Fomblin] to allow the use of reactive gases. Normal chamber base pressures under optimal pumping conditions were about 10^{-5} Torr.

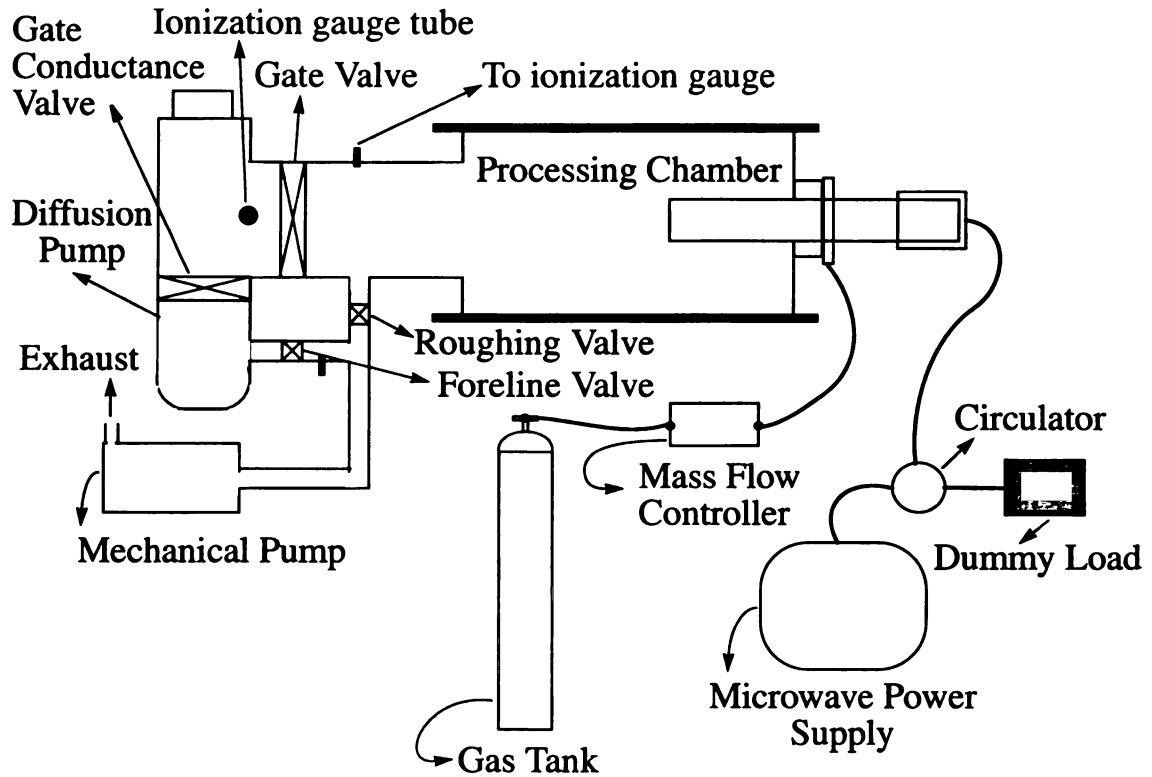


Figure 2.3 Vacuum system of the plasma source

The gate valve, roughing valve and the foreline valves are pneumatically controlled through a specially designed switch box. The pressure of the processing chamber is measured using an ionization gauge and a capacitance manometer (100 mTorr full range), while the foreline and the diffusion pump stack pressure are measured using thermocouples.

Gas flow into the MPDR is controlled through an MKS 247C four channel read-out/controller. Pressure conditions inside the vacuum chamber are controlled by a gate conductance valve. All components of this system are made of Ultra High Vacuum [UHV] compatible steel.

2.3 High power resonant cavity microwave reactor

The high power microwave cavity plasma reactor is a resonant cavity microwave discharge operating in the TM_{013} mode. The reactor includes a 7 inch inside diameter microwave cavity that can be electromagnetically tuned with a sliding short and an adjustable probe. The tuning process consists of matching the complex impedance of the cavity ($Z_{in}=R_{in}+jX_{in}$) to the transmission line impedance which carries the microwave power source to the cavity. The cavity effectively directs intense microwave energy into the plasma source region. A Cober model S6F/4503 2.45 GHz microwave power supply was used to provide 0.2-2.0 kilowatts of microwave power.

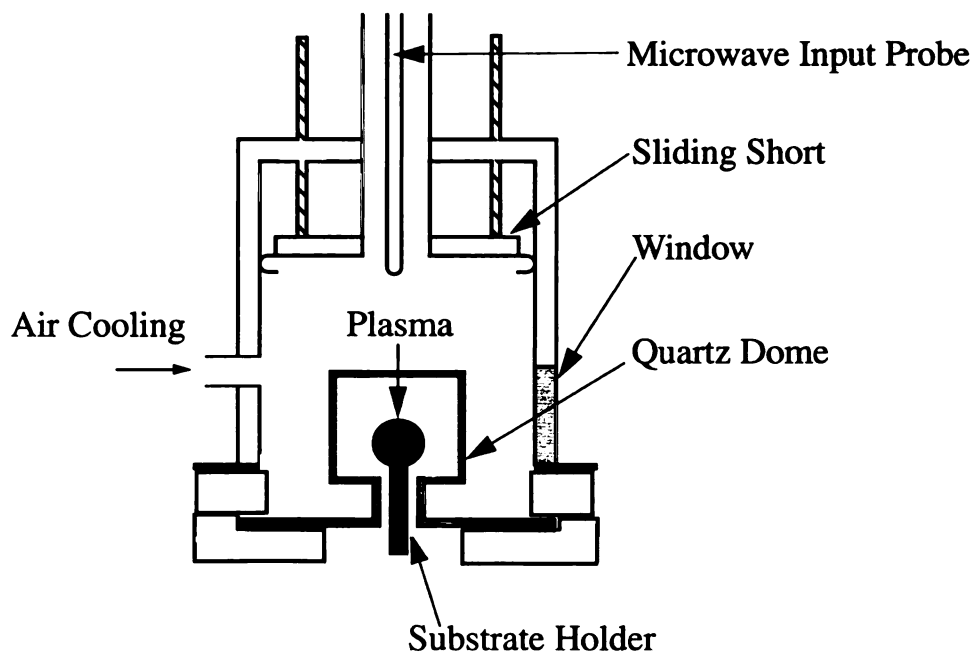


Figure 2.4 High Power Microwave Plasma Reactor

The hydrogen discharge experiments discussed in chapter 4 and 5 were performed in the same reactor as shown in Figure 2.4. The experiments discussed in chapter 6 were carried out in the reactor shown in Figure 2.5. These reactors differ in the shape of the quartz dome used and the other basic configuration remains the same. All the experiments were performed at pressures of 10-120 Torr. The MKS 247C four channel readout/controller regulates the flow of hydrogen, methane and nitrogen.

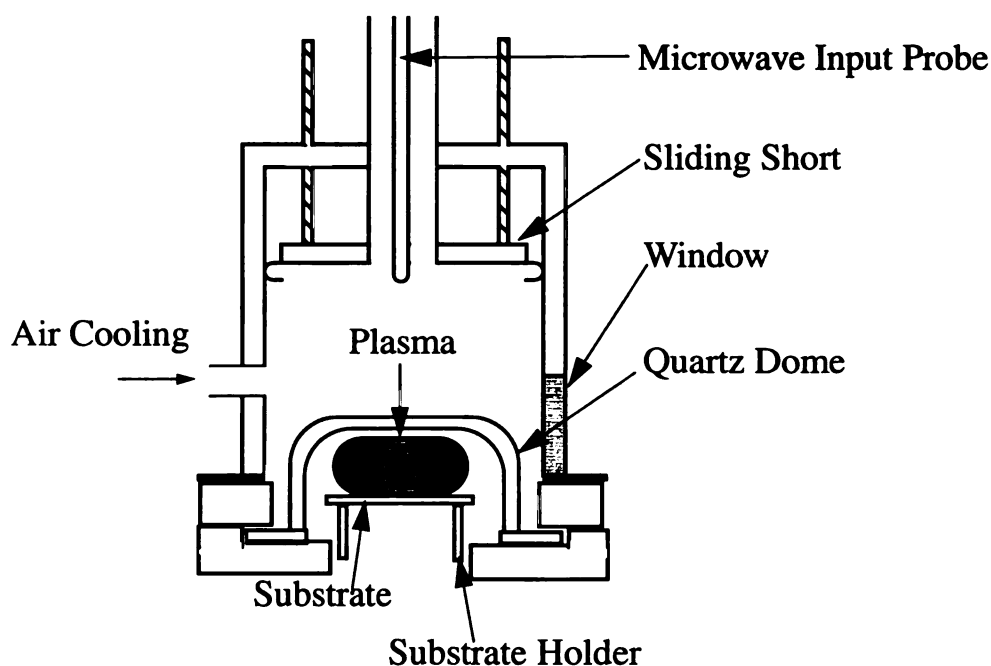


Figure 2.5 High Power Microwave Plasma Reactor

The source is designed to operate at high power and moderate pressure conditions. Hence the vacuum system is not as complex as the previous system. The chamber is directly connected to a mechanical pump. A throttle valve connected between the pump and the chamber is used for fine control of the chamber pressure. Since high powers are

involved the quartz dome gets heated. Air cooling is provided to the quartz dome by a duct with a fan connected to the other end. The heated air flows out through the mesh window, which is also used as a viewing port.

2.4 Spectrometer- system #1

The spectrometer used for some of the measurements is a McPherson Model 216.5, 0.5 meter, f/8.7, plane grating scanning monochromator. It is designed to operate in the wavelength from 1050 Å to 160,000 Å by interchanging the gratings. The 2400 grooves/mm grating can be used in the 1050 Å - 5000 Å wavelength range and the 1200 grooves/mm grating can be used in the 1050 Å - 10,000 Å wavelength range. The spectrometer has a resolution of 0.2 Å and 0.4 Å for the 2400 line/mm and 1200 lines/mm grating respectively with input and output slits of the spectrometer set at 10 μm wide. The optical system of the spectrometer consists of two concave mirrors and a plane grating.

A collimating mirror is 3" in diameter and has a 0.5 meter focal length. A focusing mirror is 6" in diameter and has a 0.5 meter focal length with a 4" focal plane. The mirrors are mounted in rigid aluminum holders. The input and the output slits are adjustable and are provided with a opening range of 10 microns to 2 mm.

A photomultiplier tube is mounted at the exit slit. The McPherson model scanning monochromator houses a EGI-GENCOM RPI QL/20 photomultiplier tube. For all the experiments a bias voltage of -800 V was applied to the photomultiplier tube in order to

get a good signal-to-noise ratio. An Oriel model 70705 photomultiplier power supply was used for this purpose.

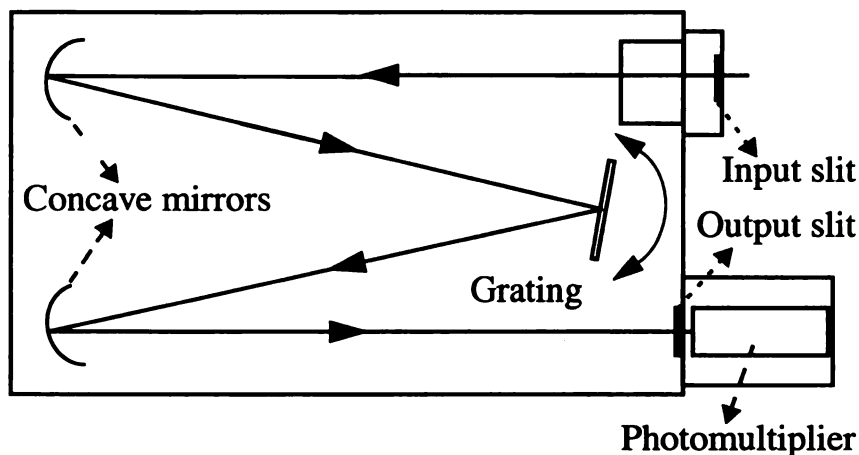


Figure 2.6 Sketch of the spectrometer

The principle used in the operation of the monochromator is diffraction. The grating in the monochromator diffracts the incoming light. The angle of diffraction varies with the wavelength. Hence at any time only the diffracted signal of a particular wavelength is collected by the concave mirror and focussed on to the photomultiplier. The wavelength scan is done by tilting the grating about its vertical axis as shown in Figure 2.6. The scanning motor has fixed speeds of 0.5, 1, 2, 10, 20, 50, 100, 200, 500, 1000, 2000 Å per minute. Usually the data acquisition system collects around 4 samples/sec. from the spectrometer. Depending on the wavelength range and accuracy desired, the speed of the scanning motor is selected.

2.5 Data acquisition and signal processing for spectrometer system #1

The data acquisition and processing were done by a semi-automated system. The spectrometer has a fixed speed motor used for scanning, that needs to be operated manually. Except for the start-up of the scanning motor of the spectrometer, the rest of the process was automated. The output current from the photomultiplier tube was read by a Keithley 485 Autoranging picoammeter. The output current was usually in the range of a few nanoamperes, depending on the intensity of the signal. The picoammeter was connected to a personal computer by a IEEE-488 interface. The IEEE-488 bus was connected to a National Instruments GPIB card in the computer. The software consisted of a Quick-BASIC program that was used to collect the data at the desired interval. The processing was done using MATLAB. The code for the software part is included in Appendix A.

2.6 Diode array detector - spectrometer system #2

The spectroscopic measurements described in chapter 6 were performed using the ORIEL Instaspec diode array detector. A spectrograph/diode array combination is a replacement for a motor driven monochromator and photomultiplier tube. The light source is reduced to a point or thin line at the entrance slit, and the spectral content of the image is measured. The dispersed spectrum is then projected as a continuous band of wavelengths onto a diode array placed at the focal plane.

The diode arrays have their own advantages and limitations compared to the photomultiplier tube. The most important difference between the photomultiplier tube and

diode arrays is the multichannel nature of the arrays. The large number of photodiodes constitute a series of detectors in close proximity, and this results in the ability to detect a number of independent events simultaneously. Thus, rather than being a single detector, the diode array is a one dimensional array of detectors. This multichannel nature of the diode array results in an increased rate of data acquisition for multiple data points and eliminates the requirement to move the image relative to the detector as in the scanning monochromator.

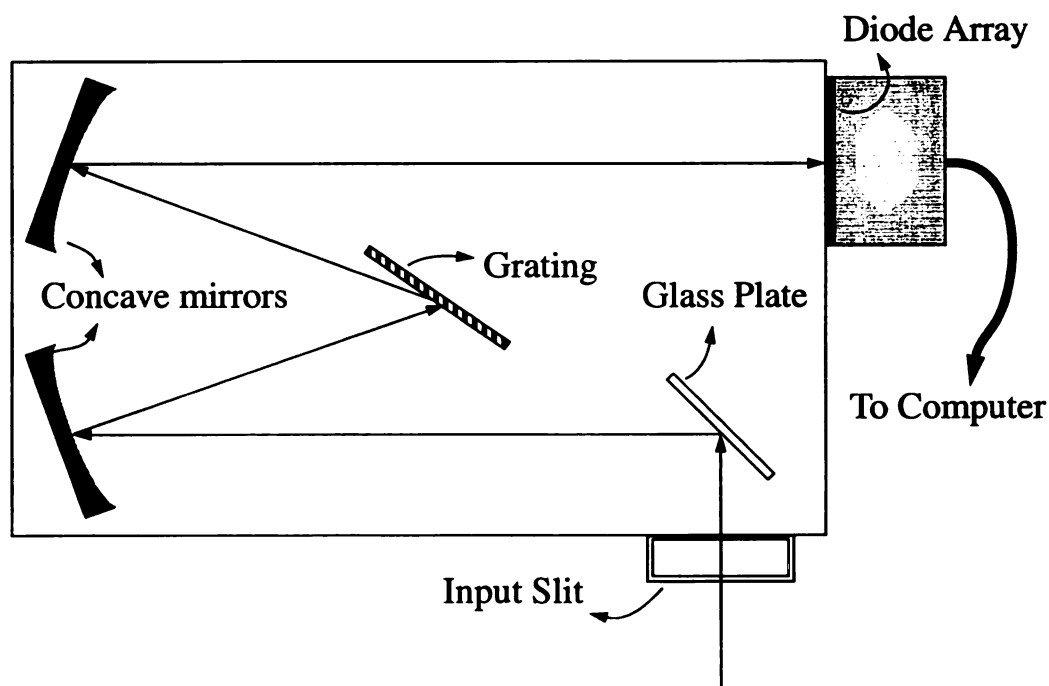


Figure 2.7 Sketch of the diode array detector

The limiting spatial resolution of a diode array is the element spacing along the detector. The wavelength resolution of the array is dependent on the dispersed wavelength range over the array and the element size. The spectroscopic wavelength resolution is

dependent on the input slit width, the total bandpass over the array and the number of elements in the array. The diode array detection system is fully automated and is controlled by the software provided by the manufacturer.

2.7 Collection Optics

The collection optics usually consisted of an arrangement of lenses of different focal lengths depending on the strength of the signal and the amount of coupling desired. Three different arrangements were used for the various experiments. For simplicity, the positioning of the lenses and the selection of the focal lengths were based on the results of the calculations obtained by considering the emission beam from the plasma source as straight rays. Fine tuning of the output was done manually by viewing the focus of the output beam on a sheet of white paper. The fiber optic cable of the spectrometer was aligned so that the focussed beam had maximum coupled to the core of the fiber. Additional focusing was not needed since the diameter of the core of the fiber optic cable was large [1-3 mm]. Since measurements were performed on the whole plasma, spatial resolution was not required. This avoided the necessity of collecting light from specific parts of the plasma. In cases where the signal was very weak, a black cloth was used to cover the entire collection optics set up to the entrance of the fiber, to prevent interference from the ambient light. The optical arrangements are presented below in the increasing order of complexity along with the necessary details.

Two types of fibers were used. One of them is an optical cable with a diameter of 3 mm and the other one consisted of a multimode fiber with a core diameter of 1 mm.

2.7.1 Arrangement #1

This arrangement is very simple and requires the direct focussing of the multimode fiber to the plasma. This arrangement was used when the plasma discharge was very bright and there was enough signal coupled through the multimode fiber.

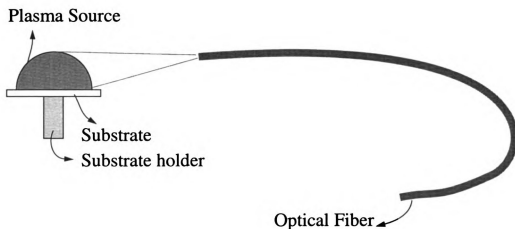


Figure 2.8 Optical set up for light collection - arrangement #1

2.7.2 Arrangement #2

This arrangement involves a single biconvex lens of diameter 5.1 cm and focal length 5 cm. The optical cable was used in this set up. The optical set up is shown in Figure 2.9. The distances S and S' and the focal length f of the lens is governed by the relation

$$\frac{1}{f} = \frac{1}{S} + \frac{1}{S'}$$

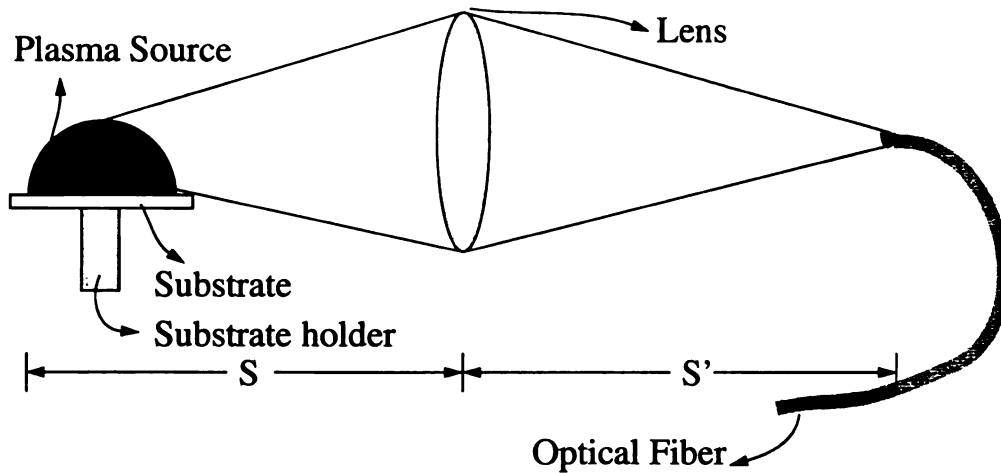


Figure 2.9 Optical set up for light collection - arrangement #2

2.7.3 Arrangement #3

This arrangement involves three biconvex lenses, two of them with diameter 6.3 cm and the third one with a diameter of 5.1 cm. They had focal lengths of 30 cm, 15 cm and 5 cm respectively. Since the signal from the plasma was weak, the collected light was directly focussed on to the input slit of the spectrometer system #1. The arrangement is shown in Figure 2.10.

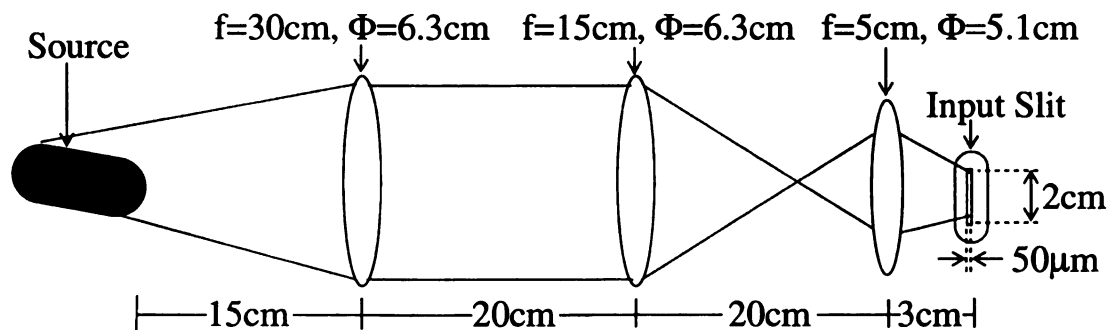


Figure 2.10 Optical set up for light collection - arrangement #3

Chapter 3

Identification and analysis of Argon Doubly-ionized atoms

3.1 Introduction

This chapter deals with the identification and analysis of the doubly-ionized Argon atoms in a microwave ECR plasma discharge. This experiment is aimed at identifying the Ar^{++} density variation and to a lesser extent the electron temperature variation with changing process parameters in a compact ECR ion source. The motivation for studying Ar^{++} emission is that higher energy electrons in excess of 27 eV are required to produce Ar^{++} emission. Hence the observation of Ar^{++} emission intensities is a relative indicator of the number of high energy electrons. The first section briefly discusses about the optical technique and the research literature used as a reference in identifying the Ar^{++} emission lines. The subsequent sections describe the experiment and the data obtained. The last section contains a discussion of the results.

3.2 Theory of the diagnostic technique

The spectroscopic radiation is emitted when a bound electron makes a transition in an atom or ion. The observed intensity of the radiation thus emitted depends on

- 1.the probability of there being a bound electron in the upper level of the transition,
- 2.the atomic probability of the transition in question, and
- 3.the probability of the photons thus produced escaping from the volume of the plasma without being reabsorbed.

The relevant atomic states of the Argon atom can be represented as shown in Figure 3.1. As it could be seen from the figure, the ionization potential of the Ar atom is 15.76 eV. By imparting 27.628 eV to the Ar^+ ion an electron from the valence shell of the Ar^+ ion can be removed resulting in an Ar^{++} ion. To cause further ionization 40.9 eV is required.

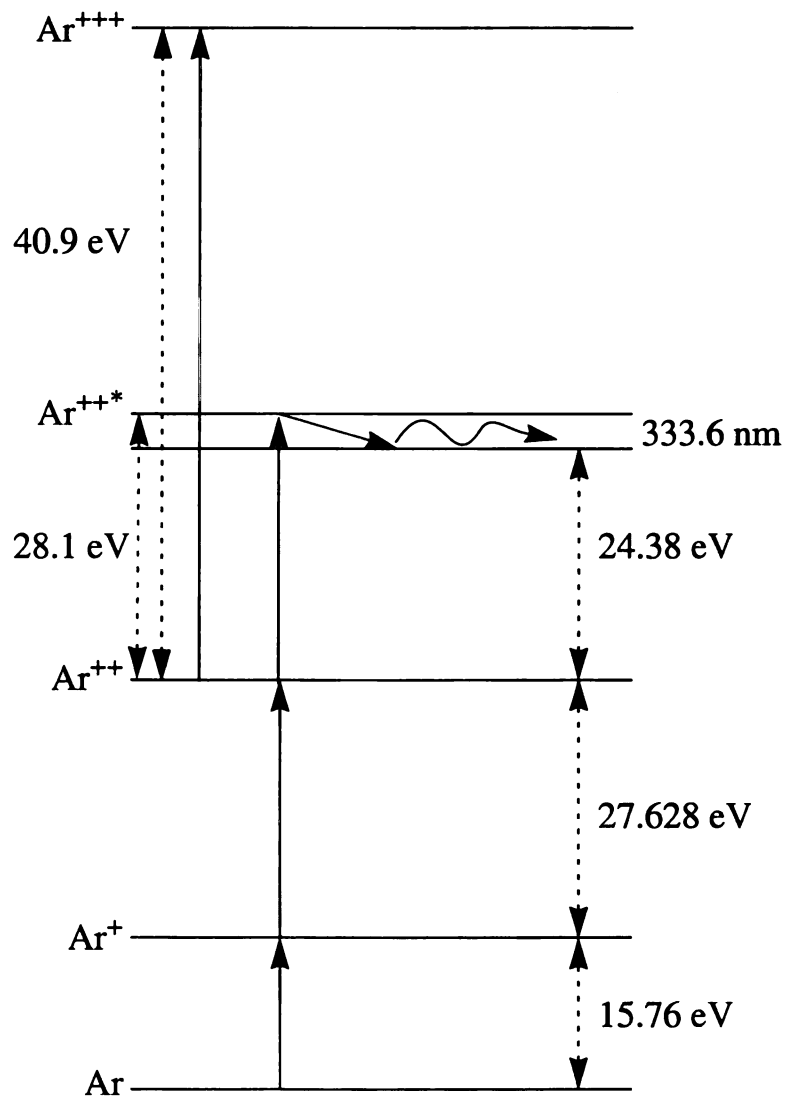


Figure 3.1 Atomic states of the Ar atom

Figure 3.1 depicts the observed 3336.13 Å transition of the excited Ar^{++*} ion. The valence electron of the Ar⁺⁺ ion is excited to an intermediate state by absorbing 28.1 eV via an electron collision. This energy state is well below the ionization potential of the valence electron of the Ar⁺⁺ ion. From this intermediate state, the electron drops spontaneously to a lower intermediate state 3.72 eV below it, simultaneously radiating the excess energy as a photon. It is this radiation which is observed as a 3336.13 Å line in the spectra. Also the energy separation between Ar⁺⁺-Ar⁺ and Ar^{++*}-Ar⁺⁺ are almost the same. This shows that the intensity of the 3336.31 Å is a good indicator of the density of the Ar⁺⁺ ions since both Ar^{++*} and Ar⁺⁺ are created by electrons of similar energy. The doubly-ionized Ar emission lines were identified using the data presented by Striganov et al. [4]. The spectral lines that are presented in this reference have been measured with an accuracy of more than 1Å.

For a better understanding of the principles involved in the measurement, let us show that the transition that is considered is indeed indicative of the doubly ionized atom density. The ion formation results due to the excitation of electrons to higher energy levels. In an atom, the energy transfer required for the excitation of the bound electrons from one energy level to the other takes place due to the collision of the free high energy electrons with the bound electrons in the lower energy level. The collision frequency of the free electrons at a given energy level is given by

$$v_{ex} = n_e \int \sigma(E) f(E) dE$$

where E is the electron energy, σ is the excitation cross section, n_e is the electron density and $f(E)$ is the free electron distribution function. For Ar⁺ to Ar⁺⁺ transition, v_{ex} can be

approximated as $v_{ex} \sim C_1 n_e(E_{ex})$, where C_1 is a constant. Hence basically the collision frequency depends on the number of electrons at or above the given energy level E_{ex} . Similarly for the Ar^{++} to Ar^{++*} transition, v_{ex} can be approximated as $v_{ex} \sim C_2 n_e(E_{ex})$, where C_2 is another constant. Thus the number of ions excited from Ar^{++} to Ar^{++*} state depends on the same set of higher energy free electrons that formed the Ar^{++} state. The 333.6 nm transition that is observed occurs due to the loss of energy of the electrons as they move from the Ar^{++*} state to another Ar^{++*} state. The observation of this transition is thus a good indicator of the density of the electrons with energy above E_{ex} and the density of Ar^{++} ions.

3.4 Experimental method

The experiments were performed using the MPDR 610 microwave plasma reactor. The optical emission from the discharge was focused to a fiber using a lens. The arrangement #2 of the collection optics shown in Figure 2.9 was used. The other end of the fiber was focussed to the input slit of the spectrometer system #1 shown in Figure 2.6. The entrance and exit slits of the spectrometer were 50 μ wide by 2 cm high. The resolution of the spectrometer used was 1 \AA with 50 μ slits. The 0.5 meter spectrometer contains a 2400 lines/mm grating. The wavelength range scanned during the experiments is 3320 \AA - 3550 \AA . The optical fiber used in the experiment allowed the signal in this wavelength range without attenuation. The experimental setup is as shown in Figure 3.2. The data acquisition system is the same as that discussed in the chapter 2.

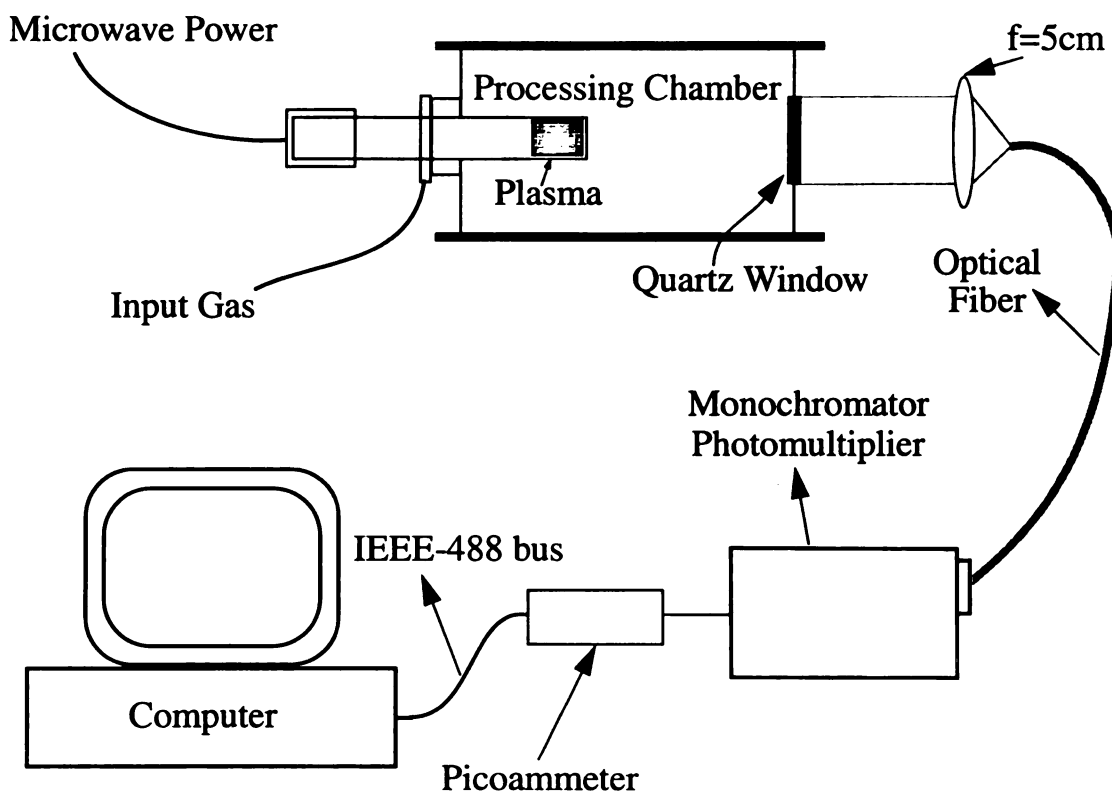


Figure 3.2 Experimental Set-up for the identification of Ar^{++} lines

3.3 Observation and measurement of the doubly ionized lines

The intensity of the doubly ionized atom emission lines gives more details about the parameters of the plasma. Ionization occurs when the high energy particles collide with an atom or ion. For double ionization to occur the energy of the charged particles needs to be particularly high. Hence the intensity of the doubly ionized lines in the spectra is a direct representation of the presence of high energy electrons in the plasma.

For the measurements at least 10 doubly ionized lines of Ar were identified initially. In order to make sure that the identified lines belonged to Ar and not any other impurity atom, argon was replaced by krypton and the same wavelength range was scanned. By comparison, more than half the number of peaks were identified as impuri-

ties. More scans with greater resolution were taken in the wavelength range of the remaining peaks to check for their presence. One such wavelength scan is shown in Figure 3.3.

Finally three lines were chosen for the Ar^{++} measurements. In the measurements, doubly ionized lines with wavelengths 3336.13 \AA ($4s' \ ^3D^0 [J=3] - 4p' \ ^3F [J=4]$), 3344.72 \AA ($4s' \ ^3D^0 [J=2] - 4p' \ ^3F [J=3]$) and 3358.49 \AA ($4s' \ ^3D^0 [J=1] - 4p' \ ^3F [J=2]$) were considered.

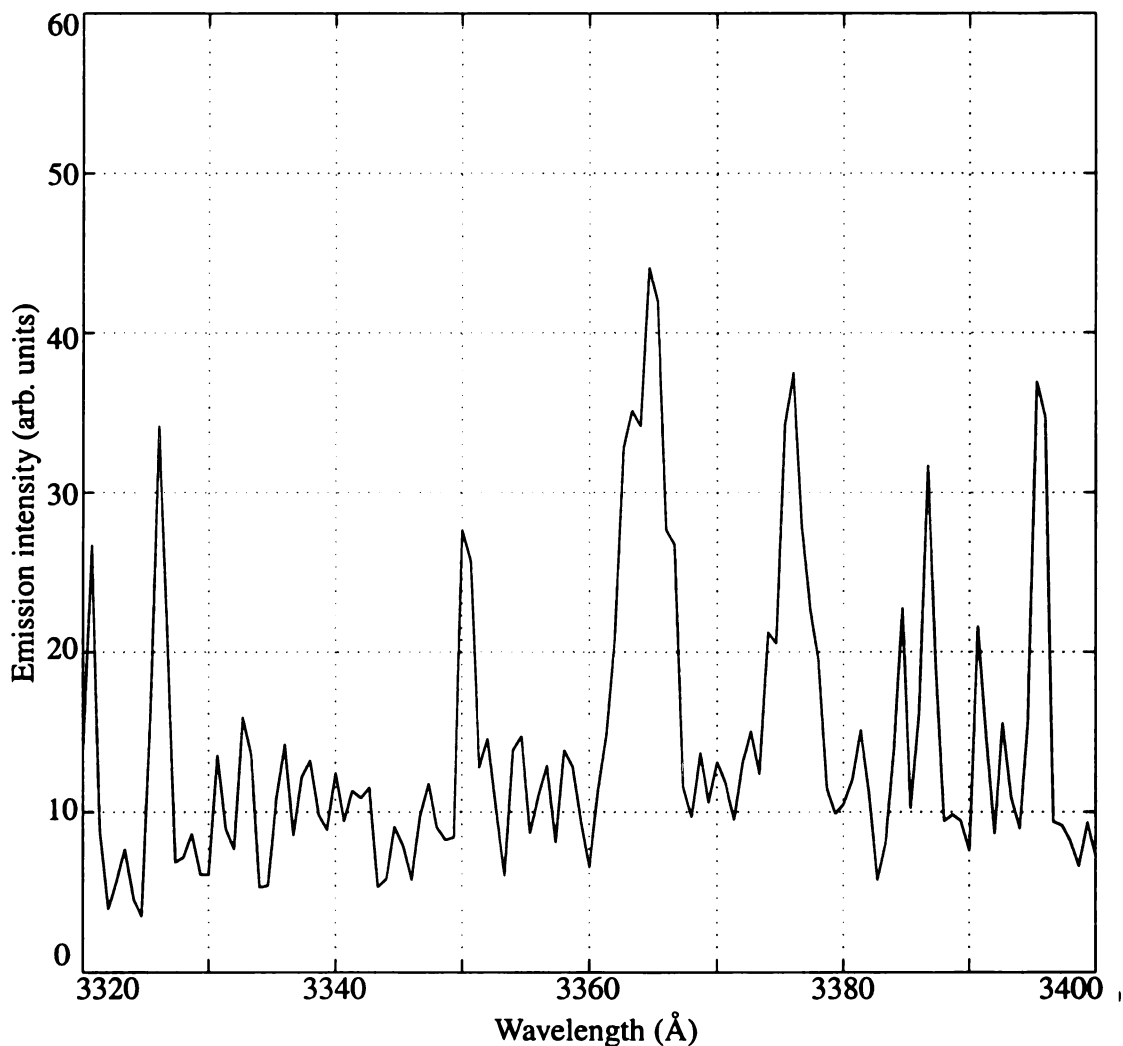


Figure 3.3 Emission spectra of krypton plasma. Pressure: 3 mT, Flow rate: 1 sccm, Input Power: 90 W.

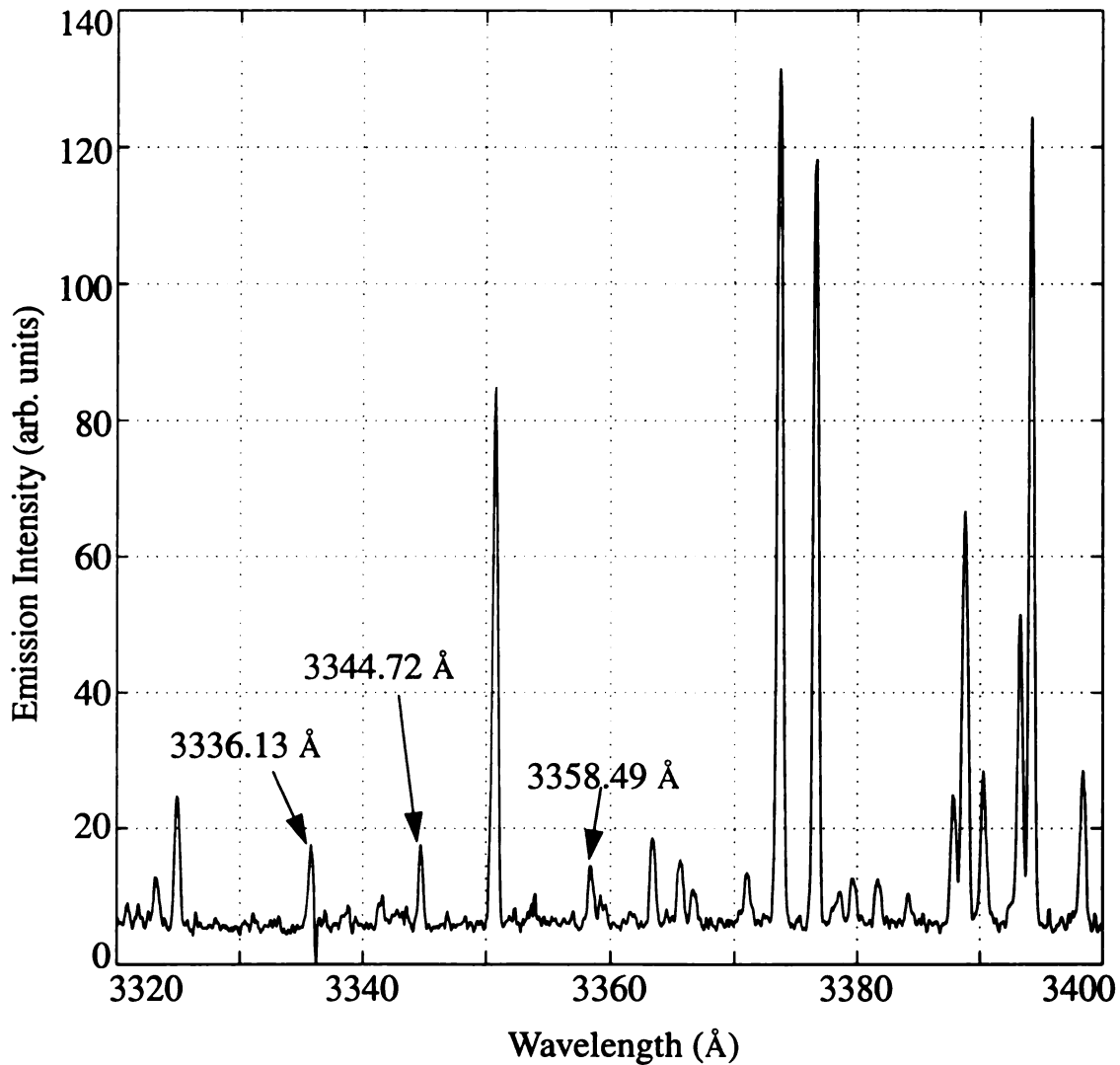


Figure 3.4 Emission spectra of argon plasma. Pressure: 0.75 mT, Flow rate: 1sccm, Input Power: 100 W.

LS (Russel-Saunders coupling scheme) notation is used here to represent the quantum states. In this scheme the quantum state of an atom is labeled in the following manner:

$$Nl^k 2S+1 L^j$$

where L is the *total orbital angular momentum quantum number*, S the *total spin quantum number*, and J the *magnitude of the total angular momentum* ($J=L+S$). $2S+1$ gives

the *multiplicity* of the quantum state. The number N denotes the *orbit number* (in the Bohr sense), and l the *angular momentum states* of the *last k active electrons*

Measurements were made for different values of incident microwave power, pressure and gas flow rates. For greater accuracy, the area under the peak was calculated, rather than the peak intensity after subtracting the background noise. The emission spectrum observed in the 3320-3400 Å range is shown in Figure 3.4. The peaks corresponding to the doubly ionized atoms are marked on the figure. For calculating the area of the peak, the trapezoidal method [In this numerical integration method, the curve is approximated by small trapezoids and the total area under the curve is obtained by adding the areas of the individual trapezoids] was used. The QBASIC code that was used to carry out these measurements is presented in Appendix C.

3.5 Results and discussion

The results of the experiments are presented in this section. The complete data obtained for the various conditions are shown in Appendix A. The various table entries show changes in Ar^{++} emissions produced by the plasma source input parameter changes. The source parameters that were analyzed included pressure, input power, and gas flow rate. The pressure was varied from 0.4 to 3.0 mTorr, the input power from 10 to 100 watts, and the flow rate from 1 to 20 sccm argon.

Figure 3.5 and 3.6 show the variation in Ar^{++} emission versus pressure. The line on these plots indicate the average intensity of the three emission lines. The higher Ar^{++} emission occur in these figures at the lower pressures. This is consistent with the electron temperature increasing at low pressure. Basically, the increased electron temperature have more electrons with 28 eV or more of energy. It is these electrons that are needed to pro-

duce Ar^{++} and Ar^{+++} as shown earlier in Figure 3.1. Figure 3.5 is at a power of 40 watts. The Ar^{++} emissions at this power are seen to drop by a factor of 6 when the pressure changes from 0.4 mTorr to 3 mTorr. Figure 3.6 is at a higher power of 100 watts. The Ar^{++} emission is seen at this power to drop by a factor of about 2 when the pressure changes from 0.4 mTorr to 3 mTorr.

Figure 3.7 shows the influence of microwave power on the Ar^{++} emission. The flow rate was 1 sccm and the pressure was 0.9 mTorr for the data shown in this figure. The Ar^{++} emission is seen to rise with input power to about 40-50 watts and then the emissions appear to saturate. This implies that for input power levels of 50-100 watts the Ar^{++} density is not changing significantly.

The last figure shown is Figure 3.8. The Ar^{++} emission is plotted versus argon flow rate at a power of 40 watts and a pressure of 0.9 mTorr. The Ar^{++} emission and hence its density drops at the higher flow rates. The effect is quite substantial with the emission dropping by an average factor of 8 when the flow rate changes from 1 sccm to 20 sccm.

The typical behaviors expected from a plasma are: 1) As the pressure is reduced the electron temperature increases, and 2) as the input microwave power increases the ion density Ar^+ increases. The variation in the argon Ar^{++} emission follows the expected pressure dependence. Specifically, Ar^{++} production requires high electron temperatures, and the higher Ar^{++} emission at low pressures in Figure 3.5 and 3.6 support the presence of more high energy electrons at low pressure. The data in Figure 3.7 shows that the Ar^{++} density is increasing with input power from 10-50 watts. This is as expected since more power increases Ar^+ and hence more Ar^+ can be ionized to Ar^{++} . For the higher micro-

wave power, the Ar^{++} emission appears to saturate versus microwave power increases. This effect is a deviation from the expected behavior and further, future investigation would be needed to clarify the cause of this effect.

The data of Ar^{++} emission versus argon flow rate in Figure 3.8 shows a strong variation. It can be concluded from the data that at the large flow rates, the Ar^{++} density is reduced. Two mechanisms could be possible explanations of the observed data. Mechanism 1 is that at high flow rates the residence time of the plasma particles in the plasma source region is reduced. The reduction is enough that Ar^{++} ions do not have time to be created and excited. The second mechanism is that at the low flow rates, strong neutral gas heating occurs which reduces the electron collision frequency. The reduced electron collisions raises the average electron energy making Ar^{++} density and emission larger. Further experimentation such as gas temperature measurements would help to clarify the responsible mechanism.

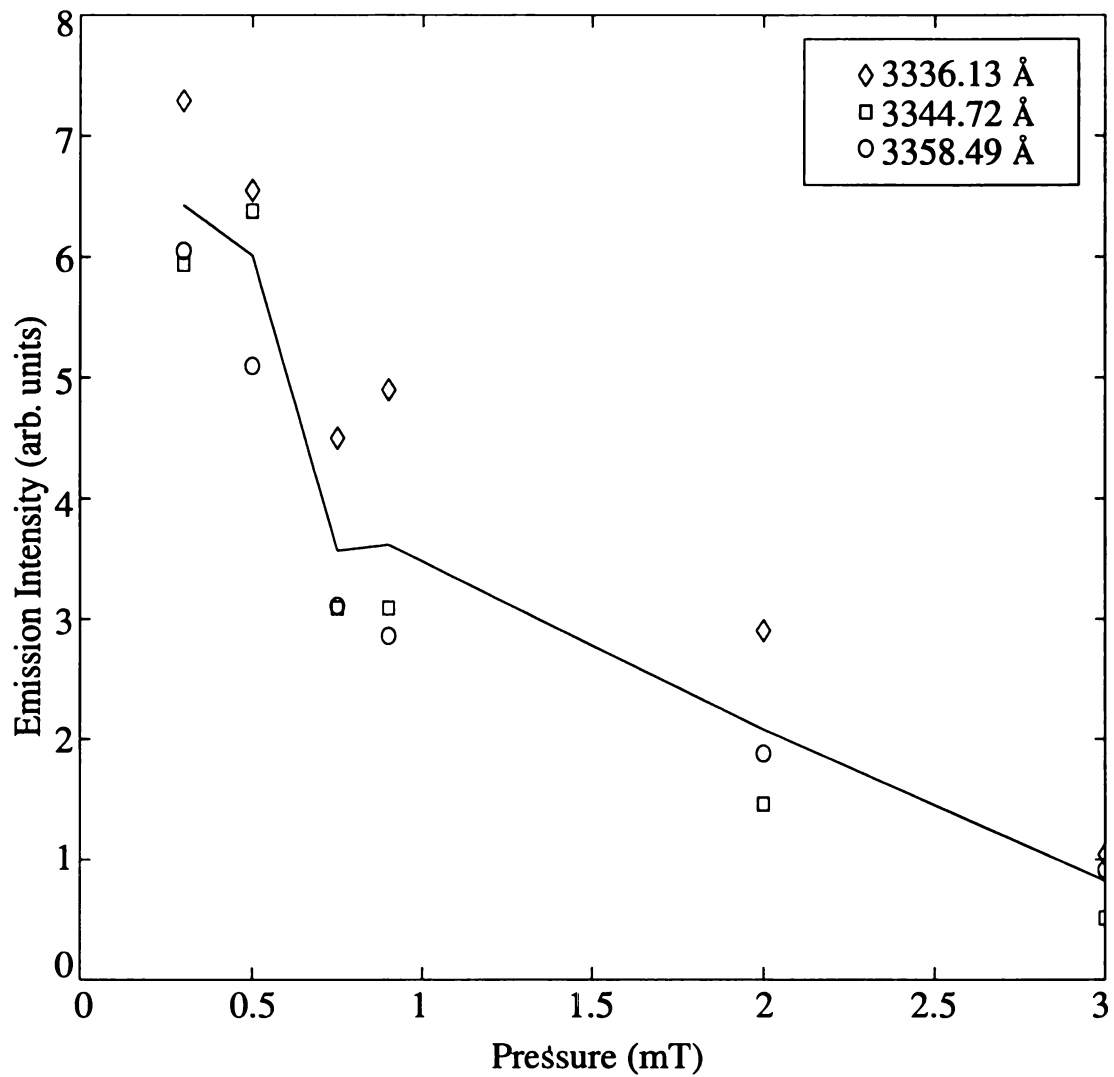


Figure 3.5 Variation of Ar^{++} density with pressure for argon plasma. Flow rate:

1sccm. Input power: 40 W

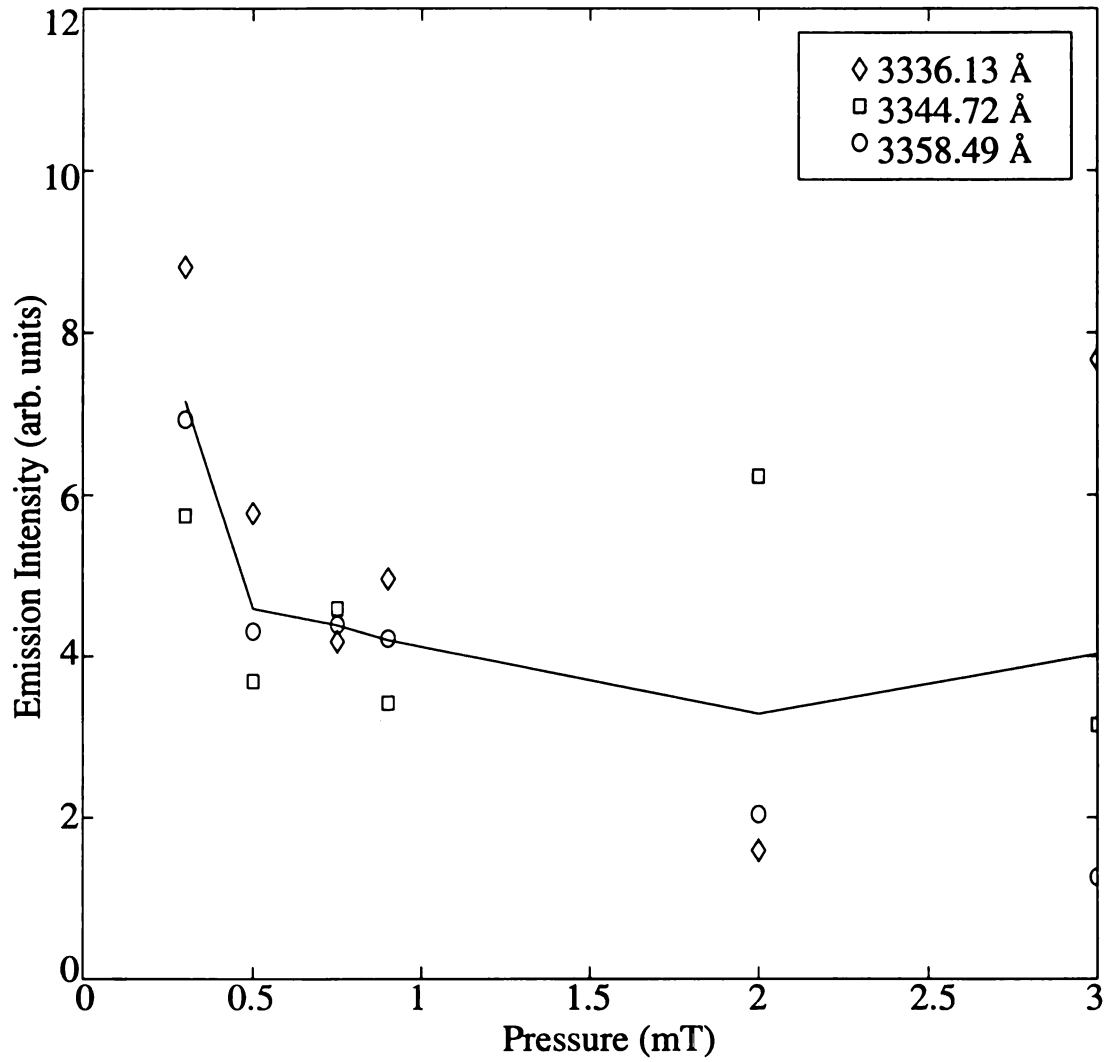


Figure 3.6 Variation of Ar^{++} density with pressure for argon plasma. Flow rate:

1sccm. Input power: 100 W

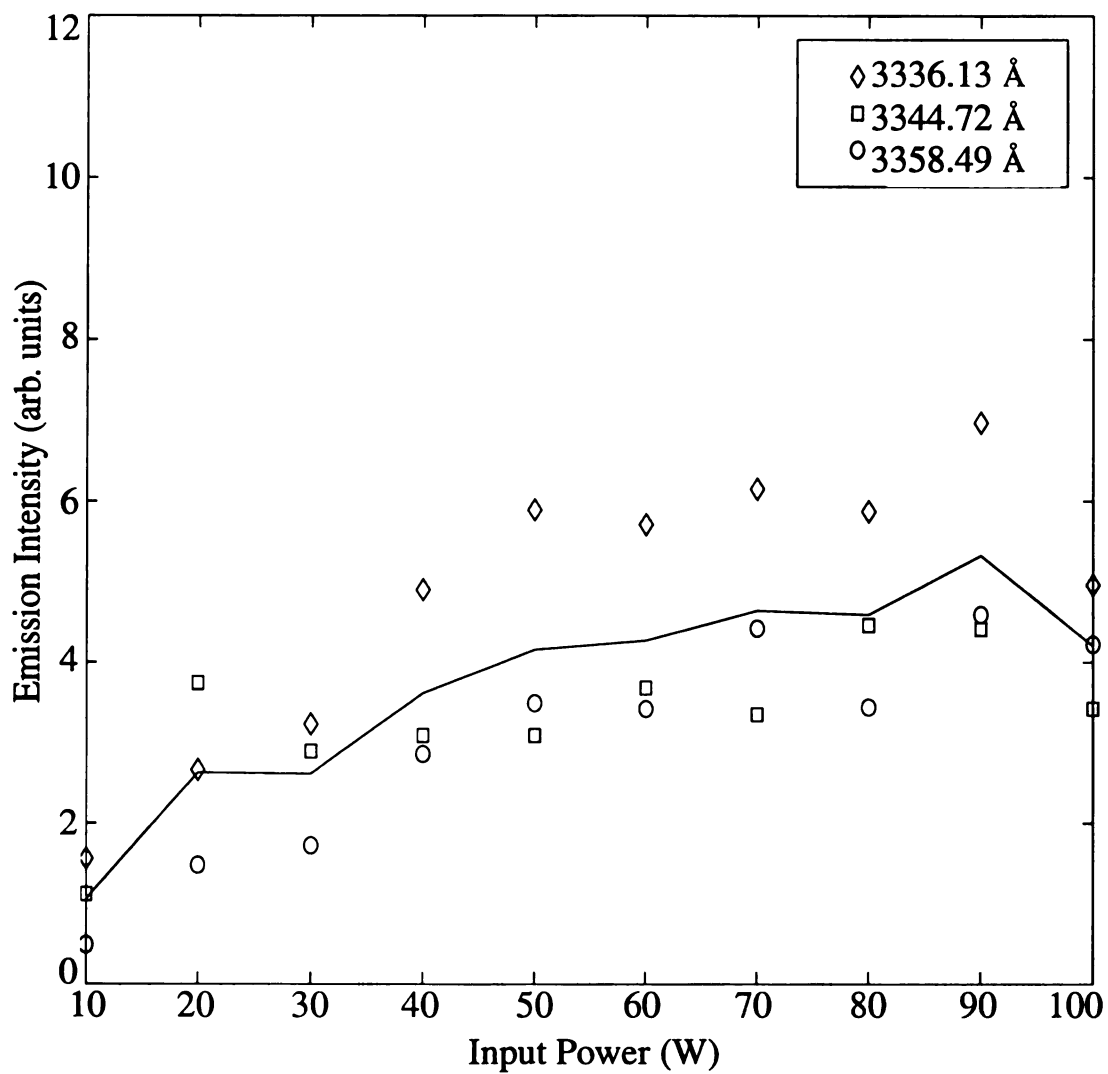


Figure 3.7 Variation of Ar^{++} density with input power for argon plasma. Flow rate:

1 sccm. Pressure: 0.9 mT.

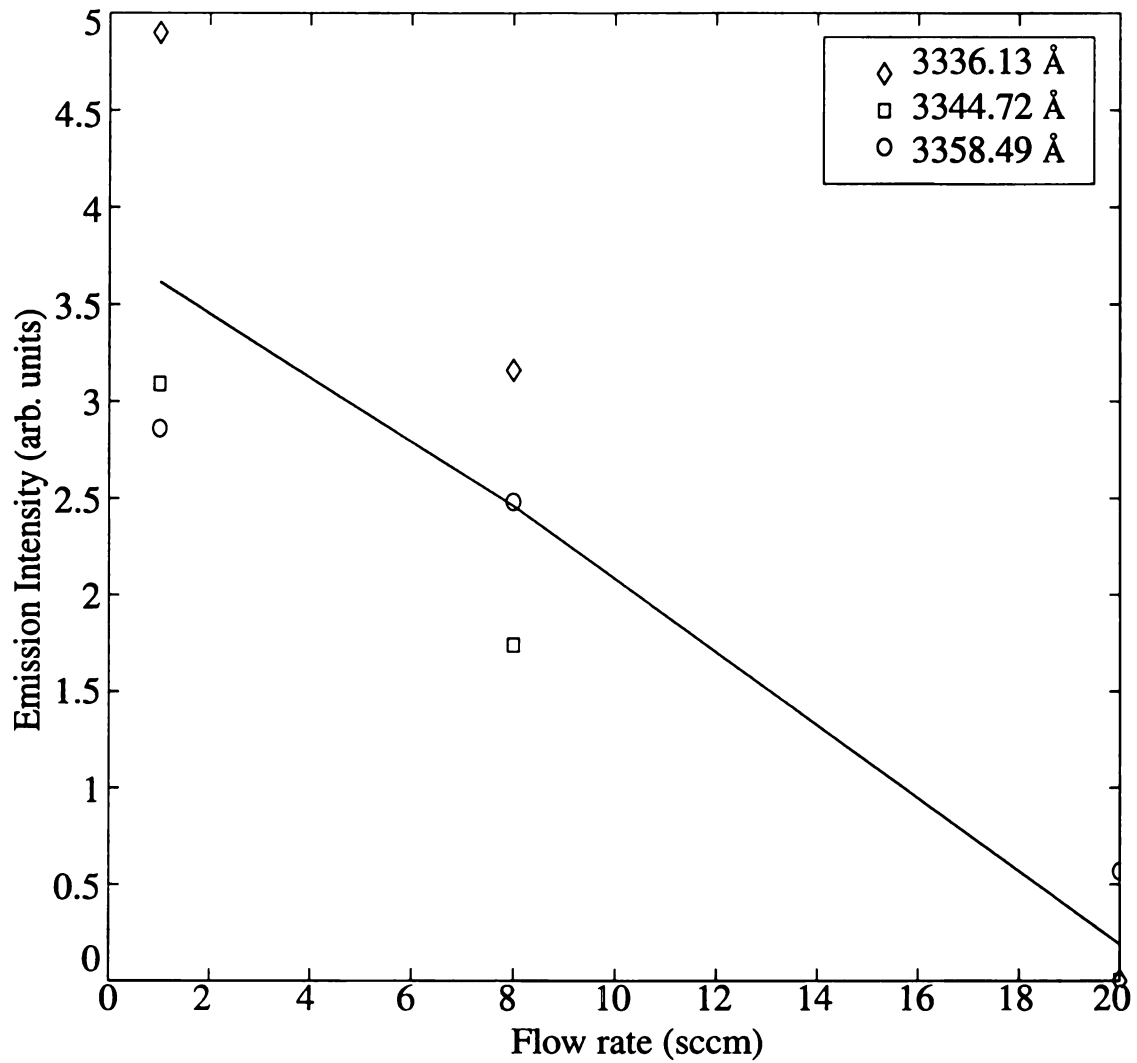


Figure 3.8 Variation of Ar^{++} density with flow rate of Ar for argon plasma. Pressure: 0.9 mT. Input power: 40 W

3.6 Conclusion

The experiments have shown the dependence of Ar^{++} emissions on the process parameters. It confirms the presence of Ar^{++} ions in the system. Also the Ar^{++} ion density has a large dependence on the flow rate and the pressure. Both low flow rates and low pressures produce larger Ar^{++} emissions. The results obtained presents data for helping to understand the Ar^{++} density variation and high energy electron density variation in the 610 compact ion source.

Chapter 4

Gas Kinetic Temperature of H₂ - CH₄ Microwave Plasma

4.1 Introduction

This chapter introduces the experimental set-up used to carry out the diagnostic experiments on H₂-CH₄ plasma gas temperature and then describes the experimental results. For both the growth rate and quality of the diamond films the optimum temperature is between 1100 and 1300 K [5]. It is likely that the deposition process is sensitive to the gas kinetic temperature. The gas temperature helps determine the concentration of various radicals, because many gas-phase reaction rates are strongly dependent on the gas kinetic temperature. The first section details the theory of optical emission spectroscopy used in the gas temperature measurement. The subsequent sections describe the specific details of the experimental setup. Finally the results obtained are discussed.

4.2 Gas kinetic temperature measurement theory

Optical emission spectroscopy (OES) is used to measure the rotational temperature of H₂ neutral species. The energy separations between rotational levels in a given vibrational and electronic state are typically small compared with the thermal translational energy. Nearly all gas kinetic collisions produce a change in the rotational quantum number, whereas collisions producing a change in the vibrational or electronic quantum numbers usually occur much less frequently. Consequently, the relative rotational population distribution in a sufficiently long-lived vibrational state has a Boltzmann distribution and the rotational temperature reflects the gas kinetic temperature [6]. The rotational tempera-

ture is derived from measurement of the relative intensities of rotational lines within a single vibrational band. The relative rotational line intensities I of a Boltzmann distribution are described by [7]

$$I = K\nu^4 S_{J',J''} \exp\left(-\frac{B_{\nu} J'(J'+1)hc}{kT_r}\right) \quad 4.1$$

where K is a constant for all lines originating from the same electronic and vibrational level, ν is the frequency of the radiation, $S_{J',J''}$ is the appropriate **Hönl-London factor**, B_{ν} is the **molecular rotational constant** for the upper vibrational level, J is the **rotational quantum number**, h is the **Planck's constant**, c is the **speed of light**, k is the **Boltzmann's constant** and T_r is the **rotational temperature**. Quantum numbers associated with the upper level of a transition are indicated with a prime, those corresponding to the lower level with a double prime. If the variation in ν^4 across the vibrational band is negligible, then a Boltzmann plot of $\ln[I/(S_{J',J''})]$ versus $B_{\nu} J'(J'+1)$ produces a line of slope $-hc/(kT_r)$ from which the rotational temperature is determined. The above assumes that the radiative decay rates for various rotational levels are the same. If a given vibrational-rotational level is mixed with a different vibrational-rotational level then the radiative decay rate of that level may be altered and the intensity of the line may be unusually strong or weak in comparison with those of others in the band.

Equation 4.1 can be represented in a simplified form by

$$\frac{I}{S} = \exp\left(-E_{upper} \frac{hc}{kT_r}\right) \quad 4.2$$

where E_{upper} represents the energy level of the upper electronic state.

Under typical operating conditions, the plasma with a neutral gas density of around 10^{17} cm^{-3} is far from local thermodynamic equilibrium. However we can expect that, at this pressure, the collision rate is high enough to equilibrate the rotational modes of the long lived electronic excited states of H_2 with the heavy particles kinetic one [8]. In this case, the plasma heavy particle temperature can be determined from the rotational bands of the radiative excited states of H_2 . The temperature was determined using the *R* branch of the $G^1 \Sigma_g^+ \rightarrow B^1 \Sigma_u^+ (0,0)$ electronic transition, where $G^1 \Sigma_g^+$ and $B^1 \Sigma_u^+$ denote the upper and lower electronic levels involved in the transition. The (0,0) symbol represents a band of transitions occurring between the levels with 0 vibrational quantum number in the upper electronic state and the levels with 0 vibrational quantum number in the lower electronic state.

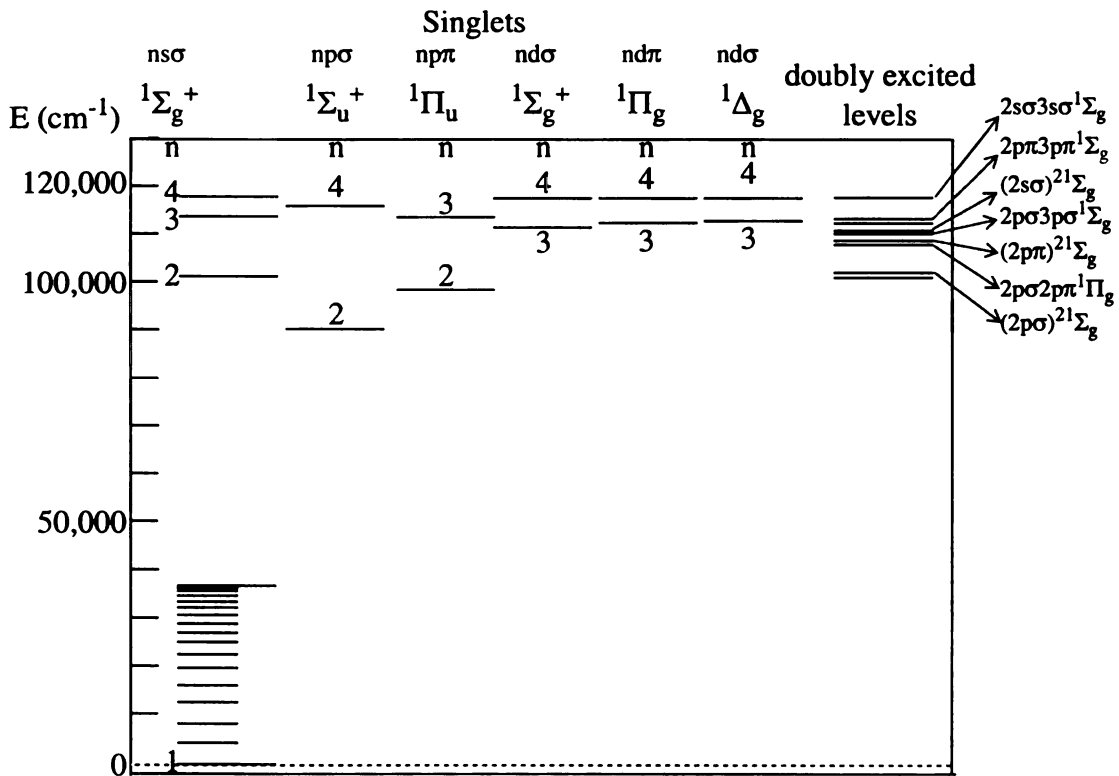


Figure 4.1 Diagram of the Observed Electronic States of the H_2 Molecule

The electron configuration for this transition is $1s\sigma 3d\sigma$. The observed electronic states of the H_2 molecule is shown in Figure 4.1. According to the selection rule for electronic transition, if both the upper and lower electronic state involved in the transition have zero electronic angular momenta, only the transitions with $\Delta J = \pm 1$ are allowed, where ΔJ is the change in the rotational quantum number. The $\Delta J = +1$ transition gives rise to the R branch and $\Delta J = -1$ transition gives rise to the P branch. Since the electronic angular momentum of a Σ state is zero, the $G^1 \Sigma_g^+ \rightarrow B^1 \Sigma_u^+ (0,0)$ electronic transition has the R and P branches as shown in Figure 4.2

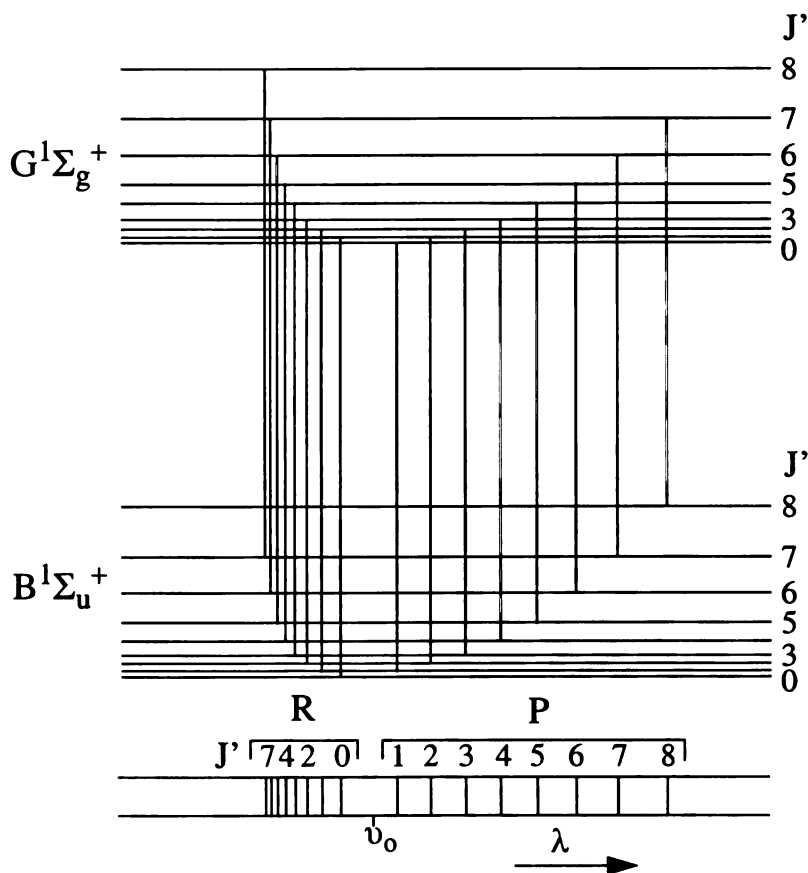


Figure 4.2 Energy Level Diagram for a Band with P and R Branches

The $B^1\Sigma_u^+$ level is well described by Hund's limiting case *b* approximation [A brief discussion about the Hund's coupling cases is included in Section 4.2.1]. This is not the case for the $G^1\Sigma_g^+$ level which is intermediate between the Hund's limiting cases *b* and *d* [9,10]. Then, the rotational energy is no longer a linear function of $J(J+1)$. Therefore, the exact numerical values of the rotational energy levels in the temperature Boltzmann plot has to be considered [11,12]. Although these levels are perturbed by the high vibrational levels of the $EF^1\Sigma\{g\}^+$, the strength of most of the *R* branch rotational lines can be well described by the Hönl-London formulae, i.e. $S_k=(J+1)/2$.

Only ten emission lines (R_0 -- R_{10}) were identified. The R_1 , R_4 and R_2 , R_3 lines are not resolved and were not used in the Boltzmann plot.

4.2.1. Hund's Coupling Cases

The influence of rotational and electronic motions on each other is given by the Hund's coupling cases *a* to *e*. The different angular momenta in the molecule - ***electron spin S, electronic orbital angular momentum L or Λ , angular momentum of nuclear rotation N*** - form a resultant that is designated *J* [13]. If *S* and Λ are zero, as in the $^1\Sigma$ state, the angular momentum of nuclear rotation is identical with the total angular momentum *J*.

In Hund's case *a* it is assumed that the interaction of the nuclear rotation with the electronic motion (spin as well as orbital) is very weak, whereas the electronic motion itself is coupled strongly to the line joining the nuclei. The ***total electronic angular momentum about the internuclear axis Ω and the angular momentum N of nuclear rotation*** form the resultant *J*.

Case *b* describes the condition when $\Lambda = 0$ and $S \neq 0$, the spin vector S is not coupled to the internuclear axis at all. Sometimes, particularly for light molecules, even if $\Lambda \neq 0$, S may be only very weakly coupled to the internuclear axis. In this case the angular momenta Λ and N form a designated K , where K is the ***total angular momentum*** apart from spin.

Case *c* discusses certain cases like heavy molecules, where the interaction between L and S may be stronger than the interaction with the internuclear axis. In this case L and S first form a resultant J_a which is then coupled to the internuclear axis with a component Ω . Ω and N then form the ***resultant angular momentum J***.

Case *d* arises if the coupling between L and the internuclear axis is very weak while that between L and the axis of rotation is strong. In this case the angular momentum of nuclear rotation which is called R (rather than N) is quantized. The ***angular momenta R*** and L are added vectorially, giving the total angular momentum apart from spin, designated by K .

Case *e* occurs when L and S are strongly coupled. L and S form a resultant J_a which is combined with R to form J .

Hund's coupling cases represent idealized limiting cases. Nevertheless they do often represent the observed spectra to a good approximation. However, small or even large deviations from these limiting cases are observed. These deviations have their origin in the fact that interactions which were neglected or regarded as small in the idealized coupling cases really have an appreciable magnitude, and particularly that the relative magnitude of the interactions changes with the increasing rotation. Therefore, sometimes, with increasing rotation, a transition takes place from one coupling case to another.

4.3 Experimental setup

The measurements were performed in the high power microwave cavity plasma reactor shown in Figure 2.4. The collection optics arrangement #3 was used to focus the optical emission from the discharge to the spectrometer system#1 described in chapter 2. A spectrometer with a resolution of 0.2 \AA for a slit width of 10 \mu m was used for the measurements. The entrance and exit slits of the spectrometer were set to 50 \mu m wide by 2 cm high in order to get the optimum spectral resolution and signal intensity.

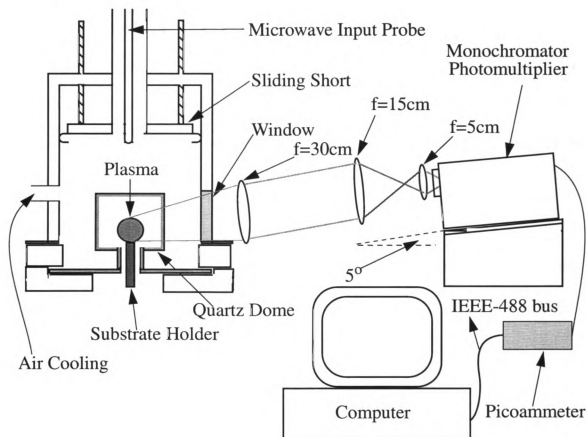


Figure 4.3 Experimental Set-up for the measurement of rotational temperature of

H_2

The optical emission spectroscopy experiments were carried out using a McPherson 0.5 m, plane grating scanning monochromator with a 2400 grooves/mm grating and a EGI-GENCOM RPI QL/20 photomultiplier tube. A voltage of -800 V was applied to the photomultiplier tube. The output of the photomultiplier tube was connected to the Keithley 485 Autoranging picoammeter, which was interfaced to a computer using the IEEE-488 interface. The data acquisition and processing were performed by the computer. The complete source code of the QBASIC program used in the processing is included in Appendix C.

4.4 Hydrogen rotational temperature

A series of experiments were performed using pure H₂, a mixture of H₂ and CH₄ and a mixture of H₂, CH₄ and N₂. The parameters that were varied include input power, pressure and flow rate of the gases. The monochromator was scanned in the range of 4530 Å to 4650 Å, corresponding to the R0-R10 rotational band of H₂ molecule.

4.4.1. Estimation of the rotational temperature

The calculation involved in the determination of the rotational temperature is outlined below for the H₂-CH₄ plasma operated at 30 Torr pressure, 200 sccm flow rate [H₂], 4 sccm flow rate [CH₄] and a microwave input power of 400 W. The microwave input power means the resultant power input to the system, i.e. the difference between the incident power and the reflected power. Figure 4.4 shows the emission spectrum obtained for the above said operating conditions. The various rotational lines are marked on the plot. As it could be seen, the R1, R4 and R2, R3 lines are not resolved. Hence they are not used in the calculations.

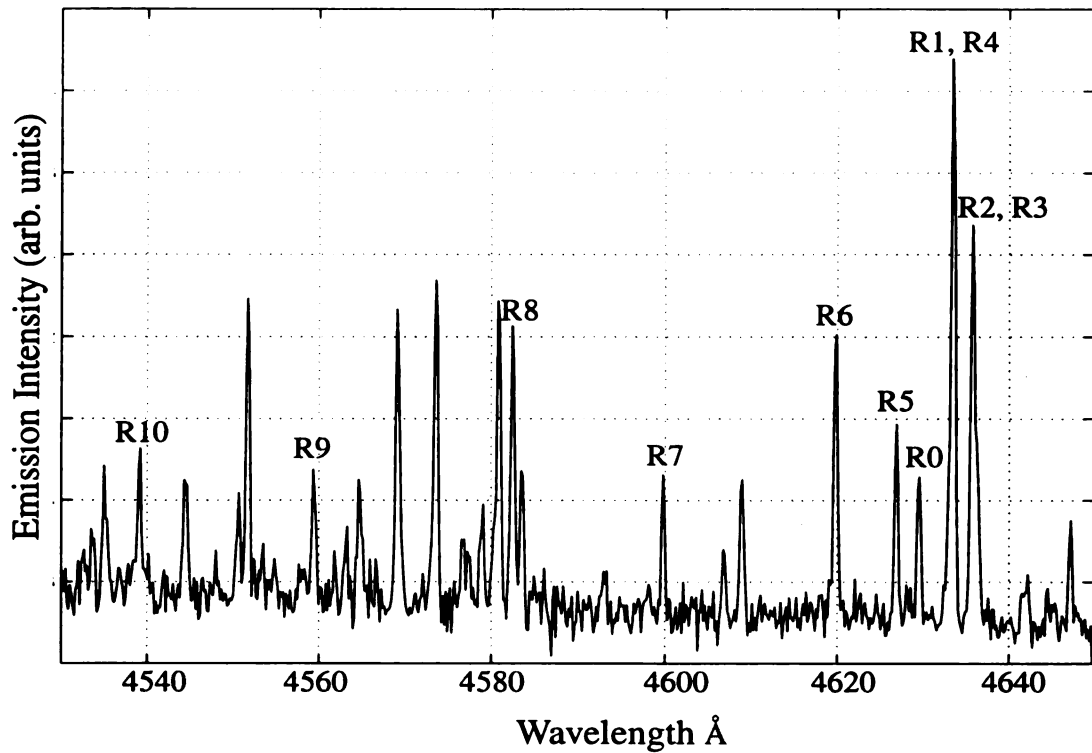


Figure 4.4 Emission Spectra of the *R*-Branch rotational lines of H_2

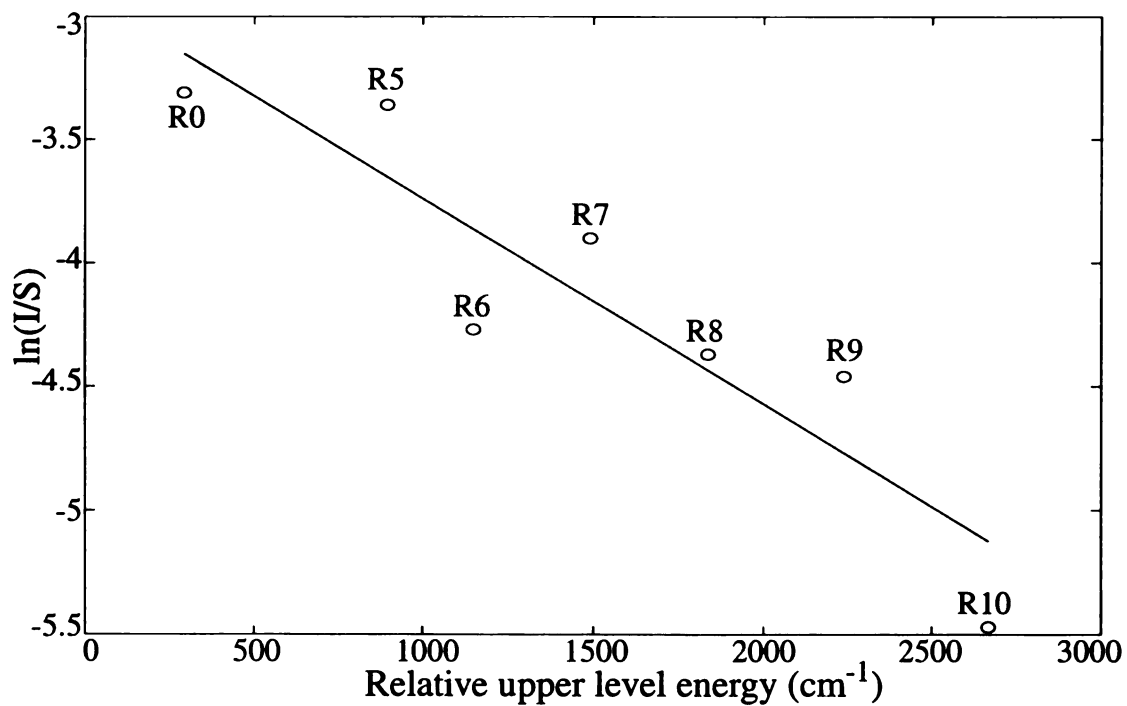


Figure 4.5 Boltzmann plot for the lines R0 and R5-R10

Table 4.1: Energy level for the R-branch rotational lines

Rotational Line	Wavelength Å	Relative upper level energy cm ⁻¹	S
R0	4627.5	292.86	60.01
R5	4624.7	895.24	86.17
R6	4618.4	1150	315.83
R7	4598.1	1490.48	113.09
R8	4581.3	1835.71	356.69
R9	4557.4	2238.1	199.34
R10	4537.9	2666.67	642.39

Table 4.1 shows the upper energy level for the R-branch rotational lines and the corresponding value of S , the Hönl-London factor. The value of $\ln(I/S)$ is calculated and plotted against the upper level energy, as shown in Figure 4.5. The line of best fit is

obtained for the plot. The slope of this line corresponds to $-\frac{hc}{kT}$, where c is the speed of light in cm/s. From the value of the slope, the rotational temperature of H₂ is obtained.

4.5 Rotational temperature results

The experimental results for the rotational temperature are presented below. The accuracy of rotational temperature determined using this method is found to be within ± 200 K. This is estimated from the reproducibility of the data obtained.

From Figure 4.6 it is seen that the rotational temperature T_r of H₂ increases with pressure. The temperature ranges from 1200-2000 K. Also from Figure 4.7 it can be observed that T_r of H₂ in H₂-CH₄ mixture is higher than that of a pure H₂ plasma dis-

charge. Figure 4.8 shows the increase in T_r with increase of input power. As more power is fed to the system, i.e. more energy is used to heat the gas and hence the kinetic energy of the gas molecules increases resulting in the increase of T_r .

When the flow rate of the gas through the system was varied with the other parameters held constant, a slight decrease in T_r was observed with increasing flow rate, especially at the lower rates below 100 sccm. With higher flow rate the amount of time that a gas molecule spends in the active region of the plasma decreases as more molecules flow through the system. Consequently, the molecules do not gain as much kinetic energy as compared to the case when the flow rate is less, wherein the gas molecules remain in the active region of the plasmas for a longer time. Hence the rotational temperature T_r decreases slightly as shown in Figure 4.9.

Since the presence of nitrogen plays a major role in the diamond deposition process [14], it is interesting to determine its effect on the rotational temperature of the gas. Nitrogen was introduced into the gas mixture and its flow rate was varied a small amount as compared to the total flow rate present in the actual diamond deposition system. As seen in Figure 4.10, there is no significant change in T_r , indicating the absence of influence of 0.1-1% nitrogen in determining the rotational temperature of the given gas mixture.

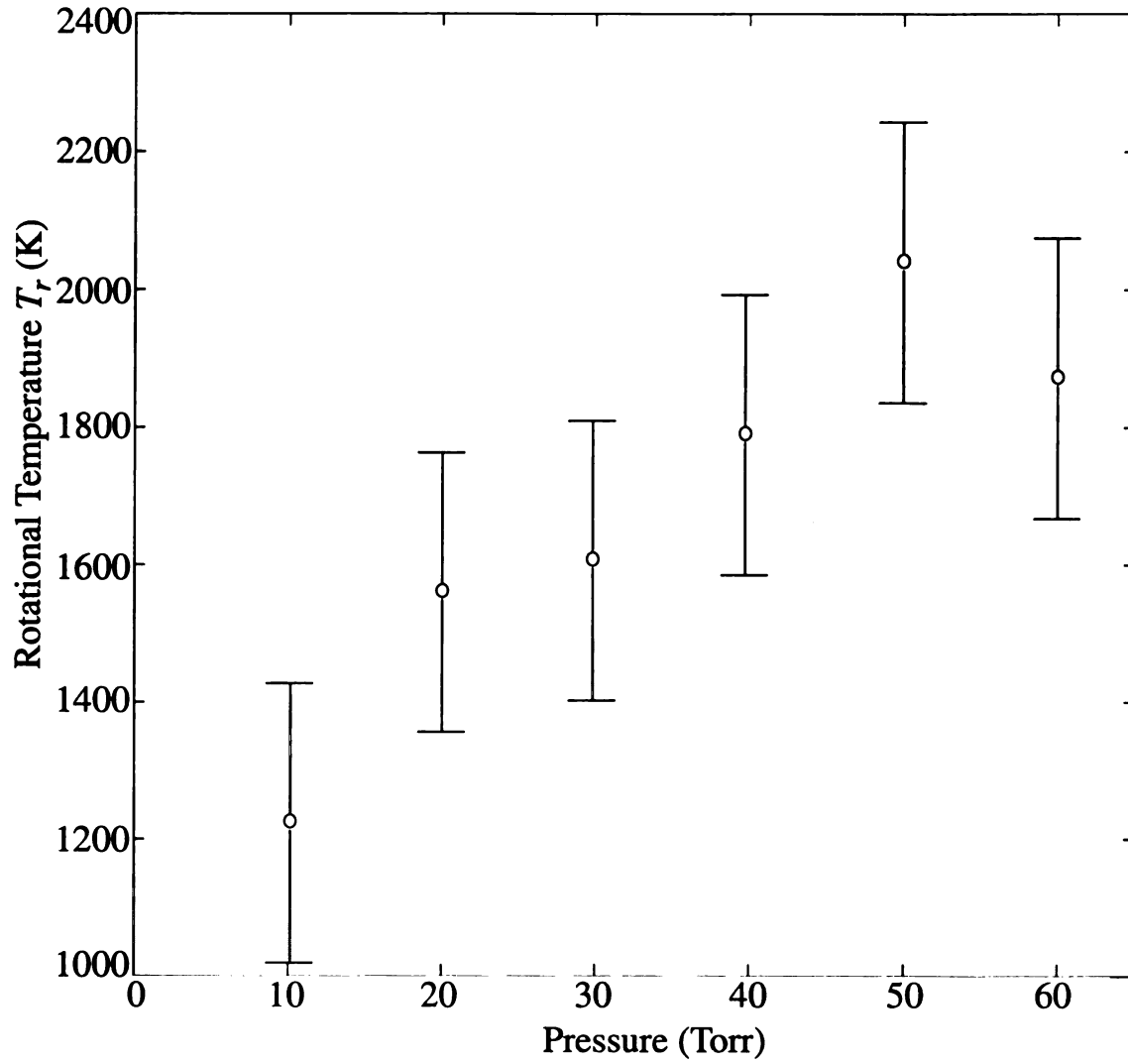


Figure 4.6 Variation of rotational temperature of H_2 with pressure for H_2 plasma.

Flow rate: H_2 -200 sccm. Input power: 400 W

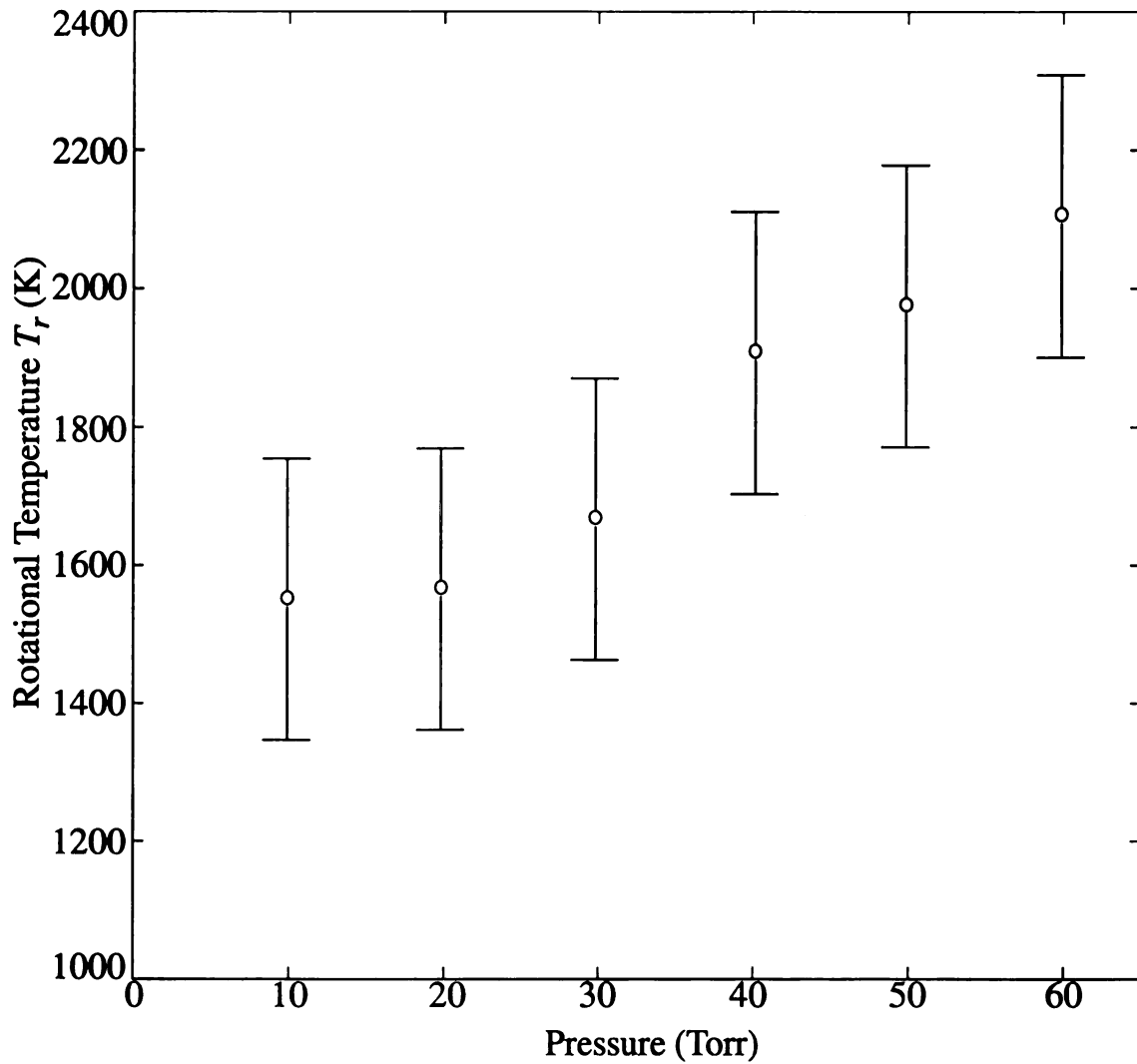


Figure 4.7 Variation of rotational temperature of H_2 with pressure for H_2-CH_4

plasma. Flow rate: H_2 -200 sccm, CH_4 -4 sccm. Input power: 400 W

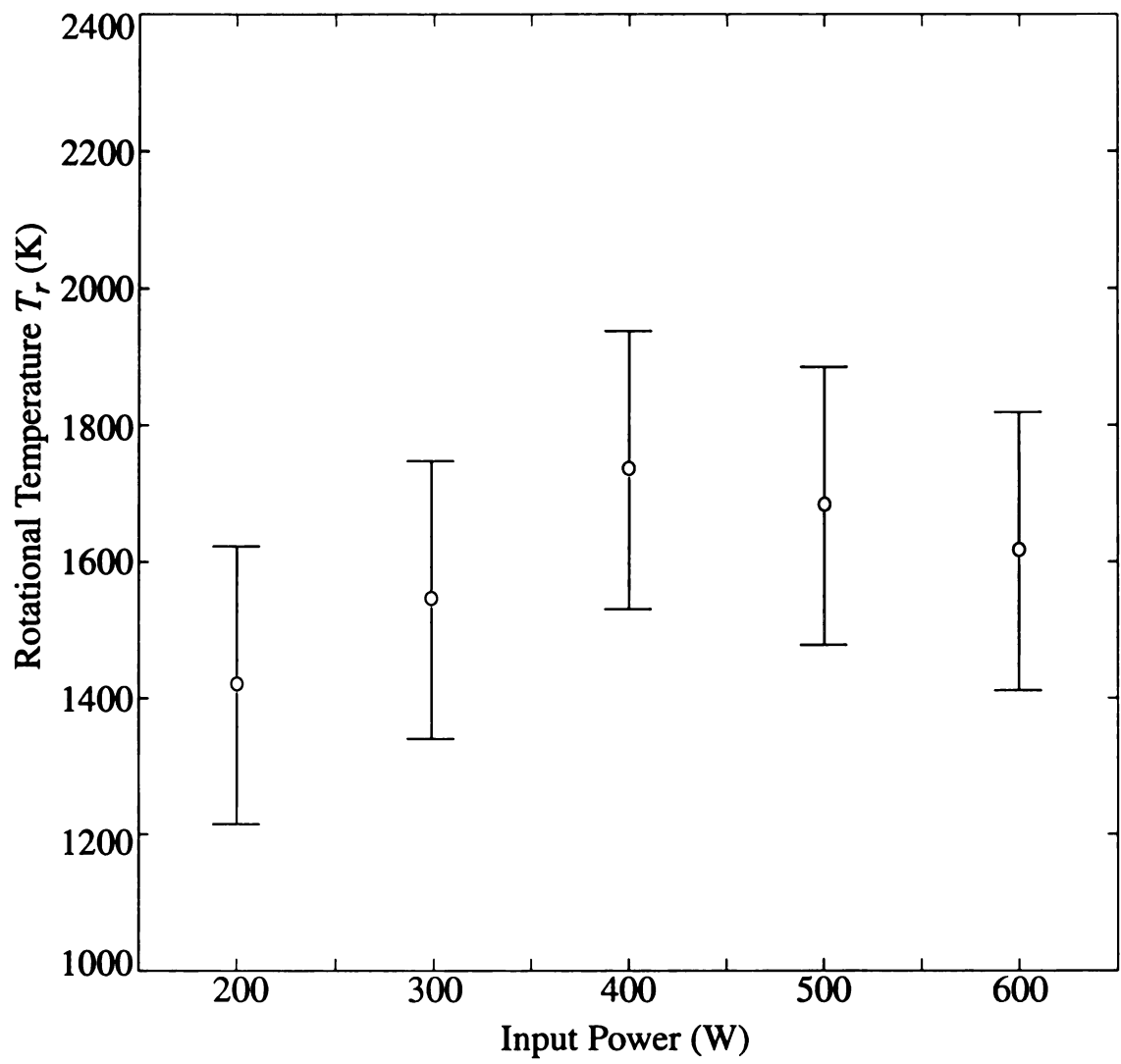


Figure 4.8 Variation of rotational temperature of H_2 with input power for H_2-CH_4 plasma. Flow rate: H_2 -200 sccm, CH_4 -4 sccm. Pressure: 30 Torr

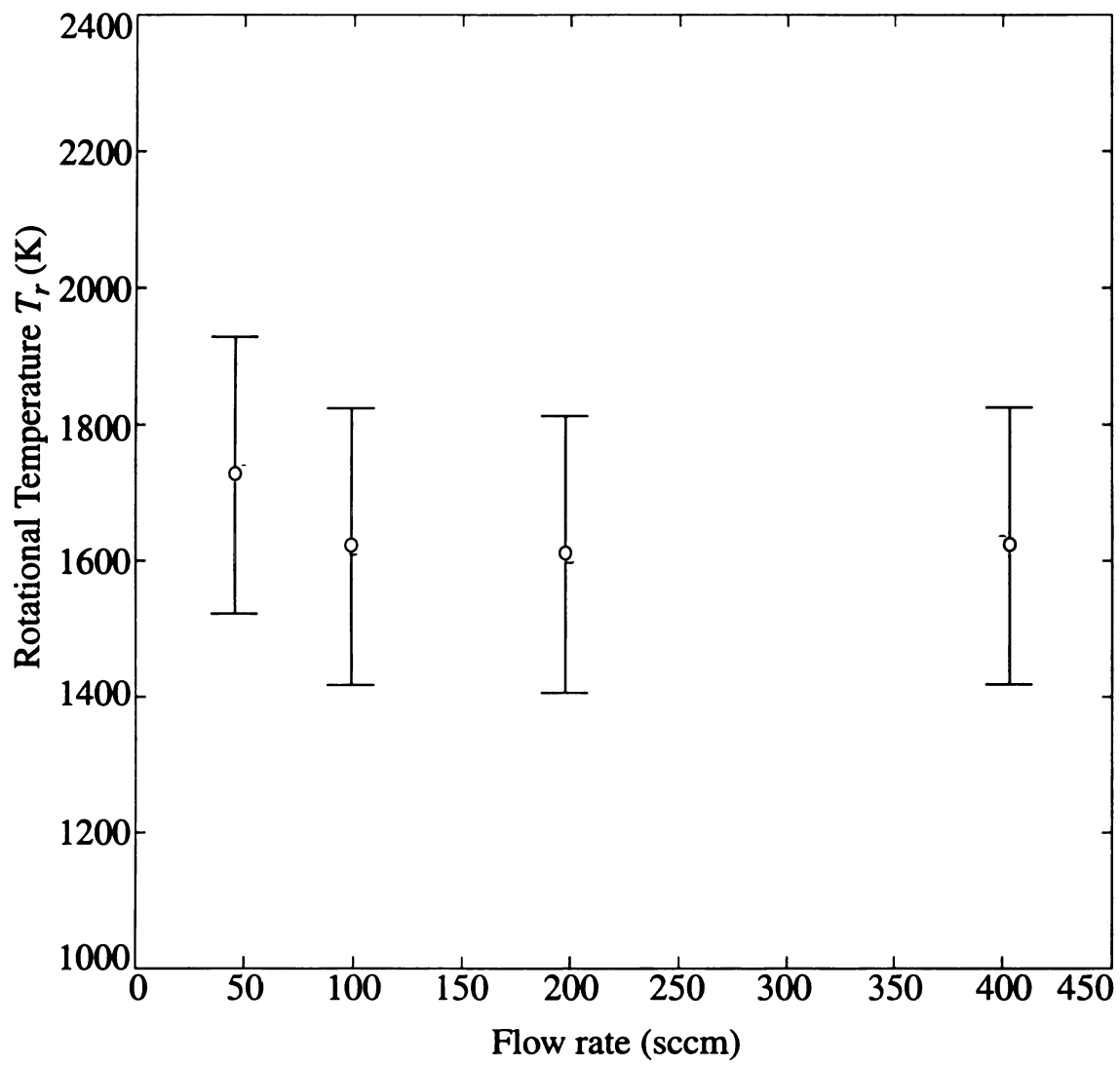


Figure 4.9 Variation of rotational temperature of H_2 with flow rate for H_2 plasma.

Pressure: 30 Torr. Input power: 400 W

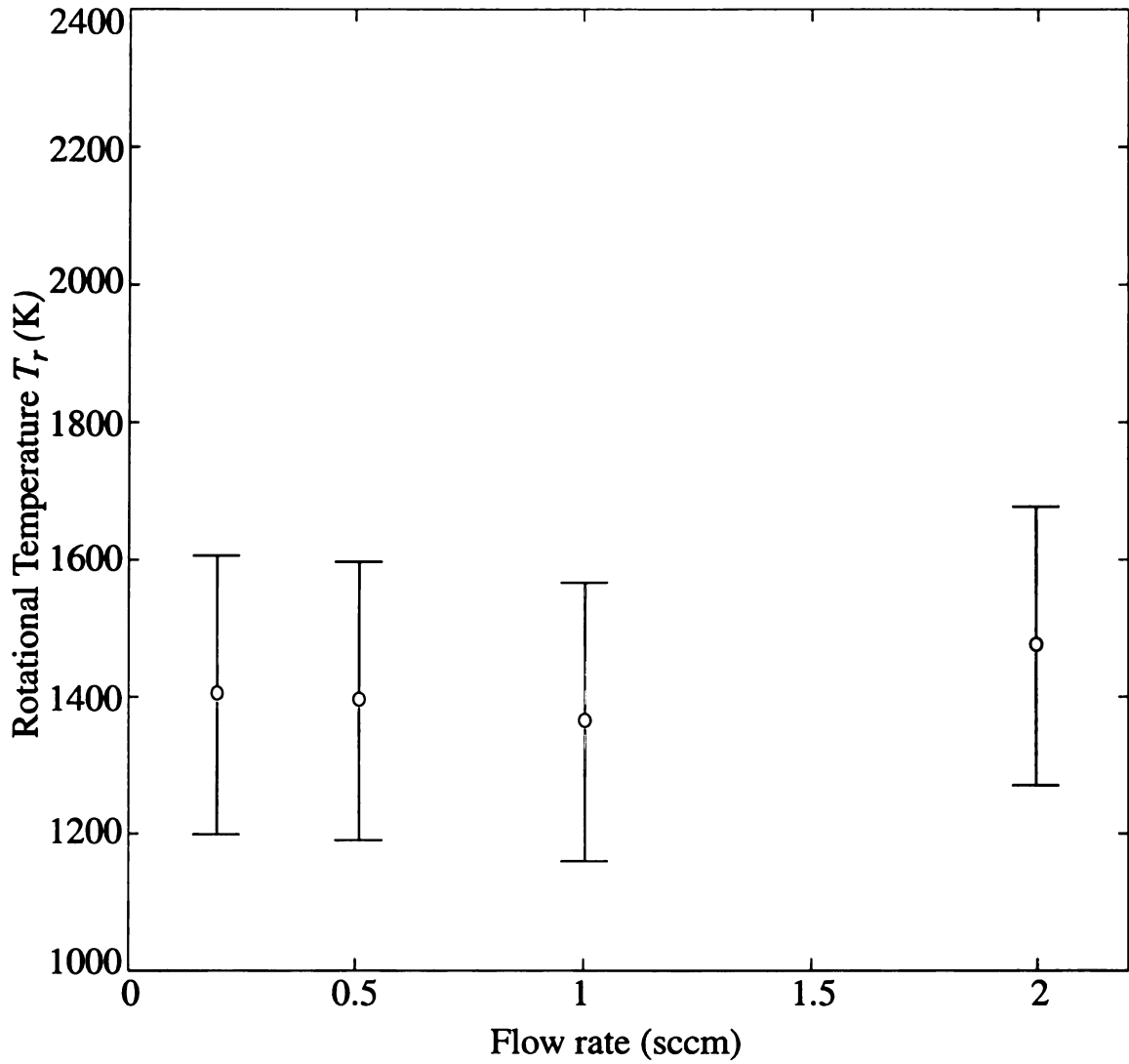


Figure 4.10 Variation of rotational temperature of H_2 with flow rate of N_2 for H_2 - CH_4 - N_2 plasma. Flow rate: H_2 -200 sccm, CH_4 -4sccm. Pressure: 30 Torr. Input power: 400

W

4.6 Conclusion

The rotational temperature of H_2 , $\text{H}_2\text{-CH}_4$ and $\text{H}_2\text{-CH}_4\text{-N}_2$ microwave plasma discharge were measured. The temperature was measured to an accuracy of ± 200 K. The results showed that both increase in pressure and increase in microwave input power increase the temperature.

The results also showed that the rotational temperature varies only slightly with the gas flow rate. The variation in the rotational temperature with nitrogen concentration was of particular interest, since small amount of nitrogen [0-25 ppm] present in the gas mixture has been found to enhance the growth rate in CVD diamond deposition [15]. But with the 0.1 - 1% addition of nitrogen no change in the rotational temperature was observed. This concludes that either the change in rotational temperature due to N_2 concentration was within the error limit, or there was no change at all.

Chapter 5

Study of H₂ - CH₄ - N₂ Microwave Plasma

5.1 Introduction

This chapter measures using OES the influence of nitrogen on H₂-CH₄ diamond deposition plasmas. The changes in various species emissions from the plasma are measured as nitrogen of controlled amounts is added. The motivation for this set of measurements is that in the plasma-assisted chemical vapor deposition of diamond films, the addition of small amounts of nitrogen changes the deposition rate and the characteristics of the diamond film [1, 14, 15]. The reason for this strong influence is as yet not understood. One possible influence of the N₂ addition is it produces changes in the bulk plasma properties and another reason is the nitrogen has a deposition surface influence. The measurements taken here by OES is directed at looking for bulk plasma species changes. In the previous chapter the influence of N₂ addition to diamond deposition plasma gas temperature was measured. The result was that no detectable gas temperature change was observed as nitrogen was added in small amounts (less than 2%). The first section of this chapter gives a brief detail of the experimental setup. The second section presents the results and a discussion of the results. The results are summarized in the concluding section.

5.2 Experimental Setup

The experiments were performed in the high power microwave cavity reactor as shown in Figure 2.4. The 0.5 meter spectrometer with 1200 lines/mm grating was used. The optical emission from the discharge was collected using a lens arrangement as shown

in Figure 4.3. Three lenses were used to focus the optical emission from the discharge on to the entrance slit of the spectrometer. The lens arrangement is shown in detail in Figure 4.4. The entrance and exit slits of the spectrometer were set to 50 μm wide by 2 cm high. The setup is identical to that used in chapter 4.

For the H_{α} and the H_{β} measurements, the spectrometer was not scanned over the wavelength range, as was done in other experiments. Instead, the spectrometer was set to the wavelength corresponding to the peak of the H_{α} line at 656.28 nm (486.13 nm for H_{β}). With the spectrometer fixed at this position the flow rate of N_2 was varied to give N_2 concentration of 0-5%. The corresponding variation in the intensity of the signal from the picoammeter was recorded by the computer and plotted. The CH and CN intensity measurements were obtained by scanning over a range of 3800 to 4400 \AA . The CH band at 4300 \AA and the CN band at 3880 \AA were used for the measurements are shown in Figure 5.4.

5.3 Results and discussions

From Figures 5.1 and 5.2 it is observed that the intensity of the atomic hydrogen (H_{α} and H_{β}) increases with the percentage of N_2 in the gas mixture. The increase in the H_{α} and H_{β} emission is by a factor of greater than 3 as the amount of N_2 is increased from 0 to 5%. The increase in the H_{α} and H_{β} emissions could occur due to either an increase in the atomic hydrogen concentration $[H]$ or an increase in the plasma electron temperature. A higher electron temperature in the plasma would mean that a larger portion of the electrons are capable of exciting the atomic hydrogen to the $H(n=3)$ and $H(n=4)$. These are the states that the H_{α} and H_{β} emissions originate from.

The ratio of H_{β}/H_{α} for different percentage of N_2 as shown in Figure 5.3 gives an idea of the change in electron temperature with N_2 flow. The H_{β} line involves the transition of electrons from the $n=4$ to $n=2$ state and the H_{α} line involves the transition of the electrons from the $n=3$ to $n=2$ state. Hence an intense H_{β} line is indicative of the presence of high temperature electrons in the gas. The electron temperature shows only a small change as indicated by the ratio H_{β}/H_{α} changing less than 4%. Hence, the strong changes in H_{α} and H_{β} emissions is believed to be due to increases in atomic hydrogen concentration as the N_2 is added, rather than a change of the electron temperature.

A typical CN and CH emission spectrum is shown in Figure 5.4. The CH line intensity shows a dependence similar to that exhibited by the hydrogen lines versus N_2 concentration as shown in Figure 5.5. However the dependence is not linear or as large as shown by the hydrogen lines. The CH emission intensity increases by a factor of approximately 2 as the N_2 concentration changes from 0-5%. The CN line intensity shows a larger variation with N_2 compared to the other species. The CN radicals as shown in Figure 5.6 tend to be promoted by adding nitrogen to the reactant gases. This could be attributed to the reactions of nitrogen with methane and carbon atoms in the gas phase, which formed the CN radicals. Alternatively, atomic nitrogen may remove carbon atoms from the growing surface and thus produce CN radicals [16]. The plots of CH and CN show that the addition of N_2 to the plasma in amounts of less than 1% produce changes in the CH and CN concentrations in the plasma.

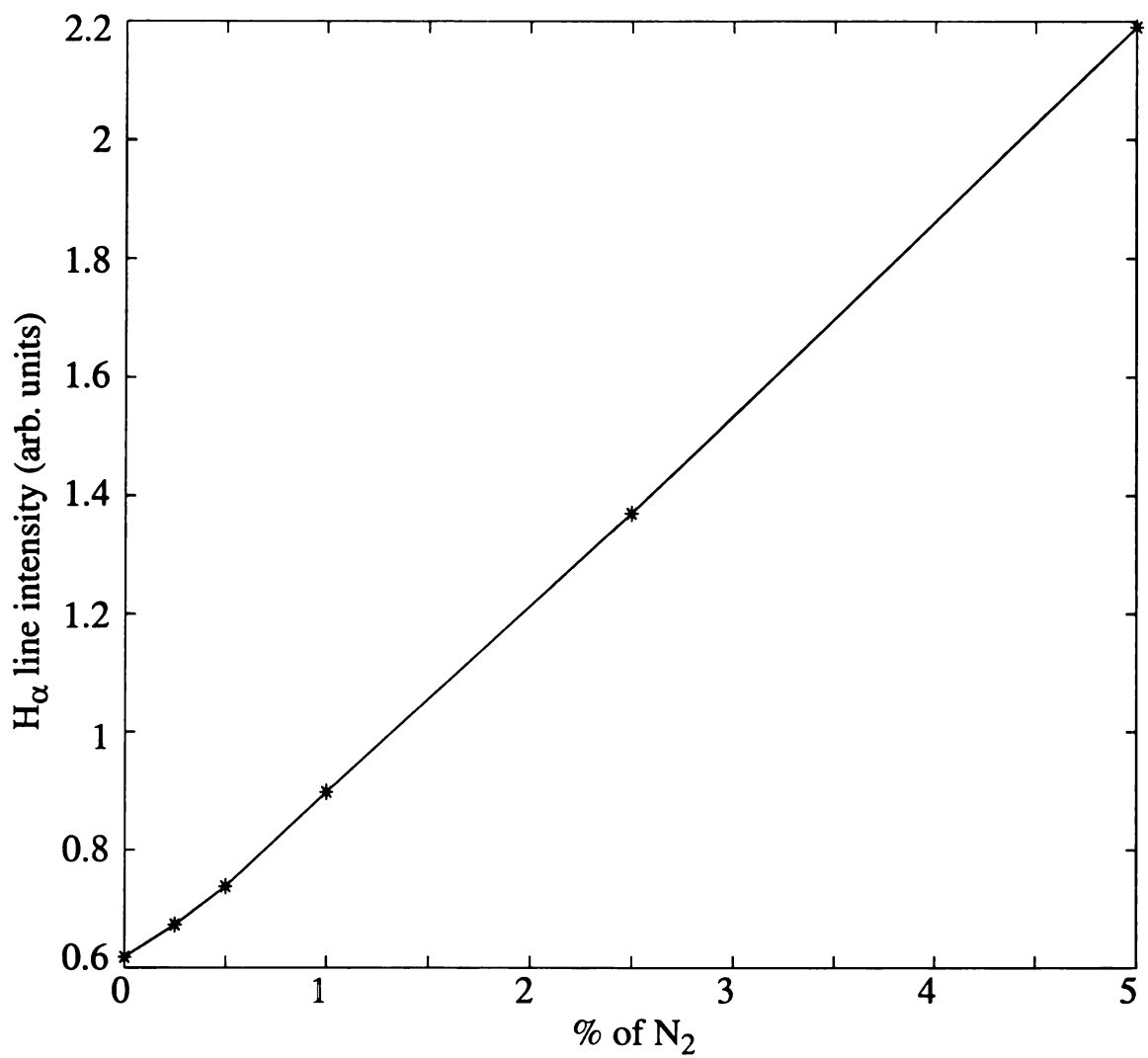


Figure 5.1 Variation of H_α line intensity with N₂ concentration. Flow rates: CH₄-4 sccm, H₂-200 sccm. Pressure: 30 Torr. Input Power: 0.8 kW

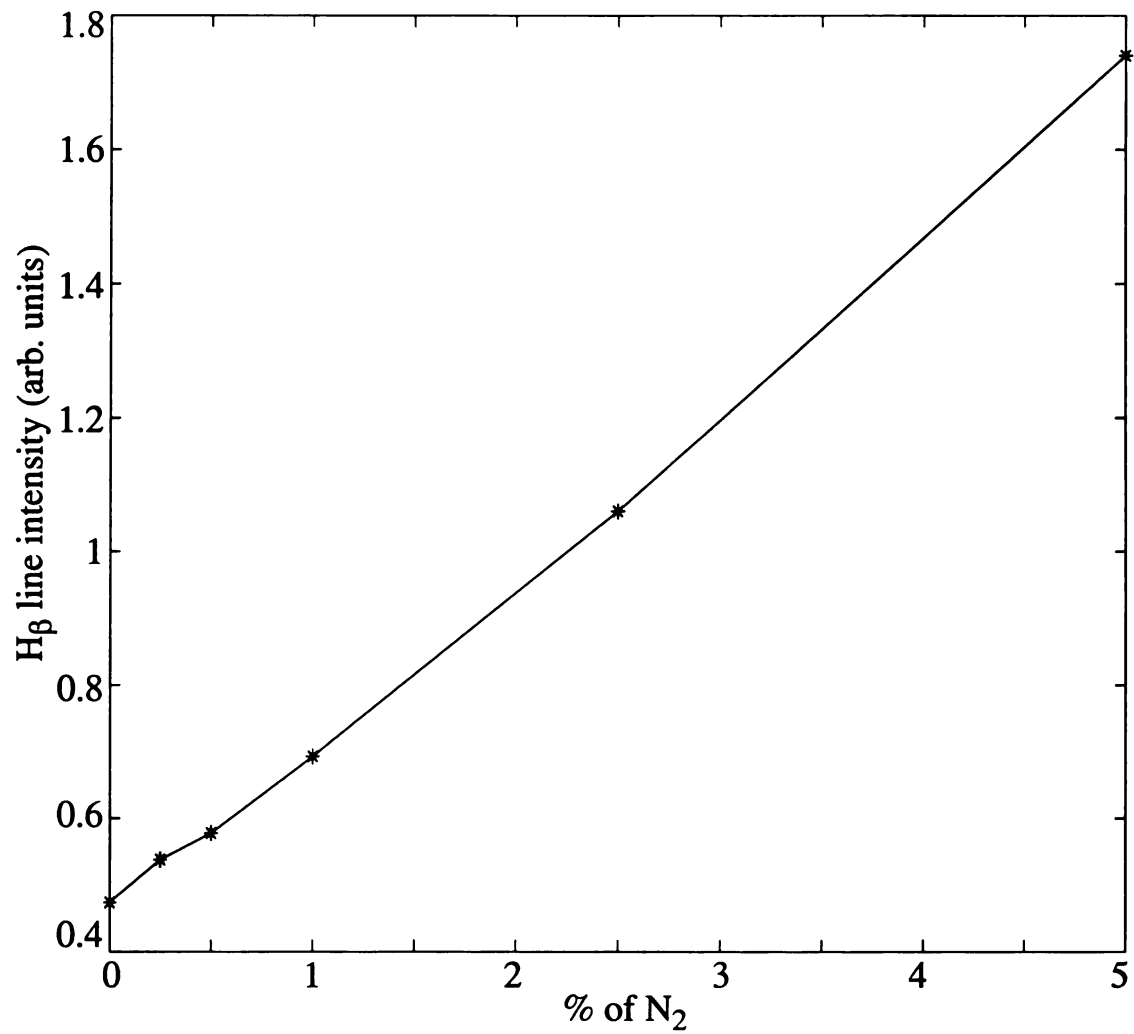


Figure 5.2 Variation of H β line intensity with N $_2$ concentration. Flow rates: CH $_4$ -4 sccm, H $_2$ -200 sccm. Pressure: 30 Torr. Input Power: 0.8 kW

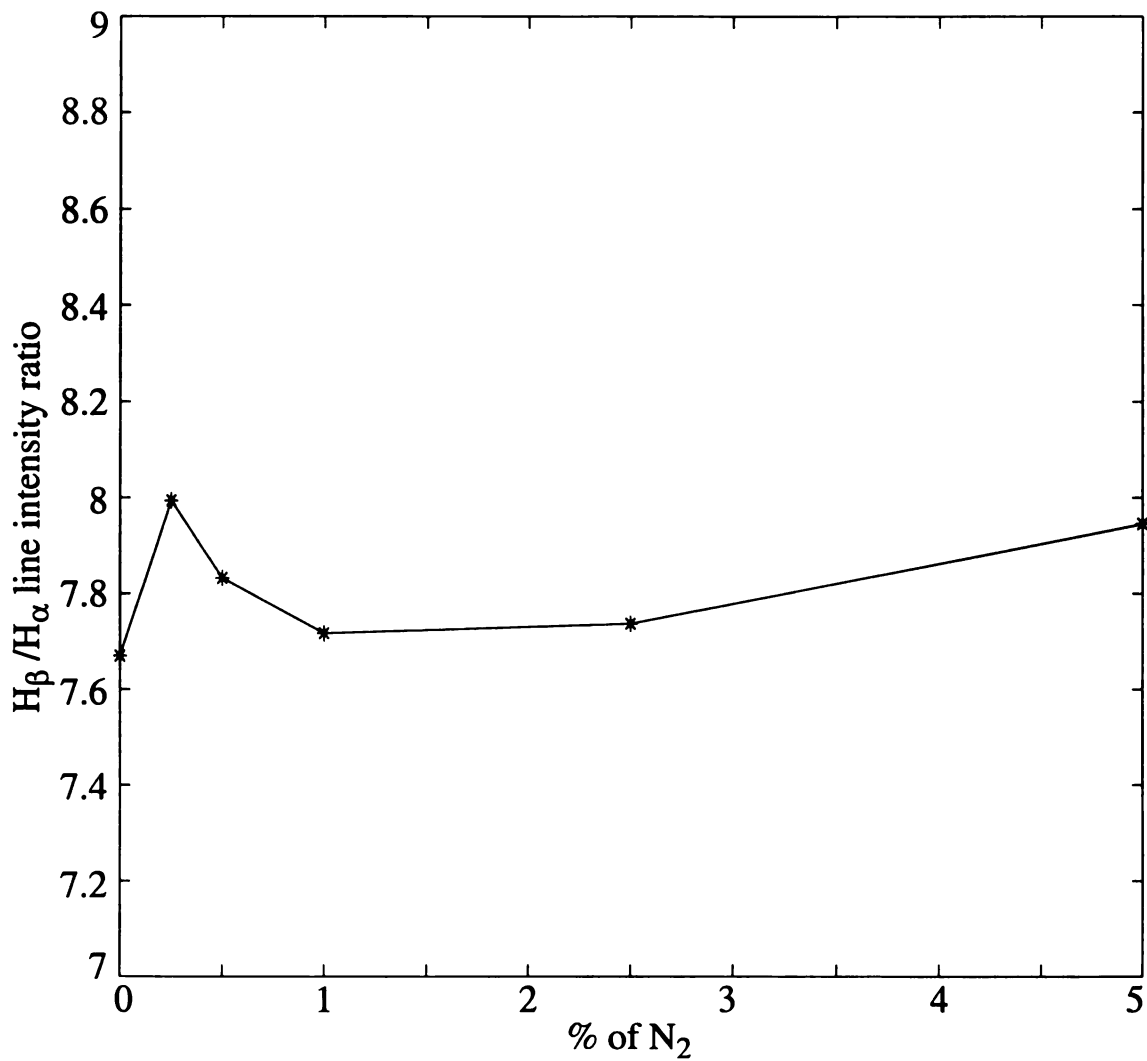


Figure 5.3 Variation of H_β / H_α ratio with N₂ concentration. Flow rates: CH₄-4 sccm, H₂-200 sccm. Pressure: 30 Torr. Input Power: 0.8 kW

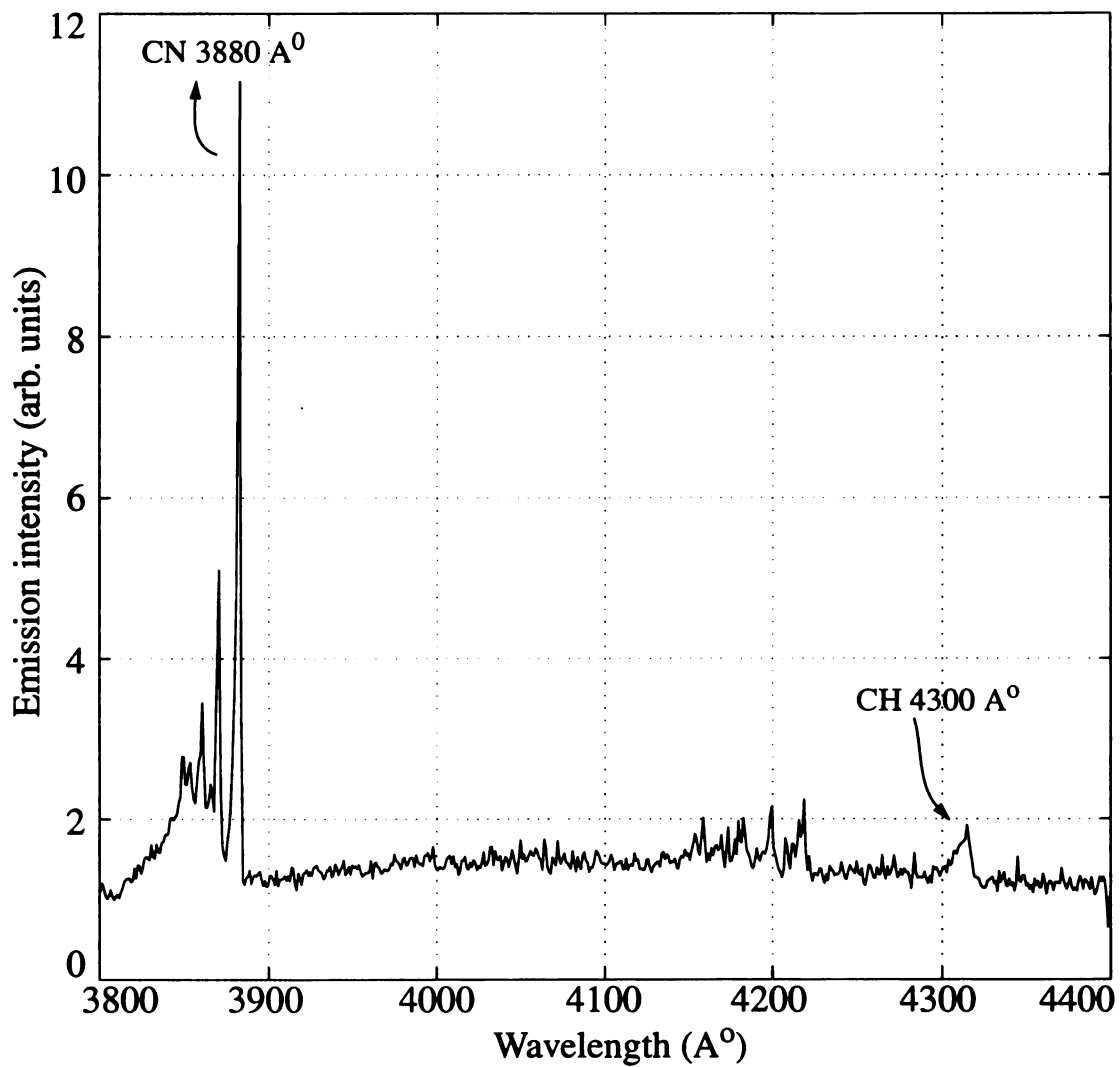


Figure 5.4 Emission spectrum of $H_2-CH_4-N_2$ plasma. Flow rates: CH_4 -7.2 sccm, H_2 -144 sccm, N_2 -0.5 sccm. Pressure: 30 Torr. Input Power: 0.8 kW

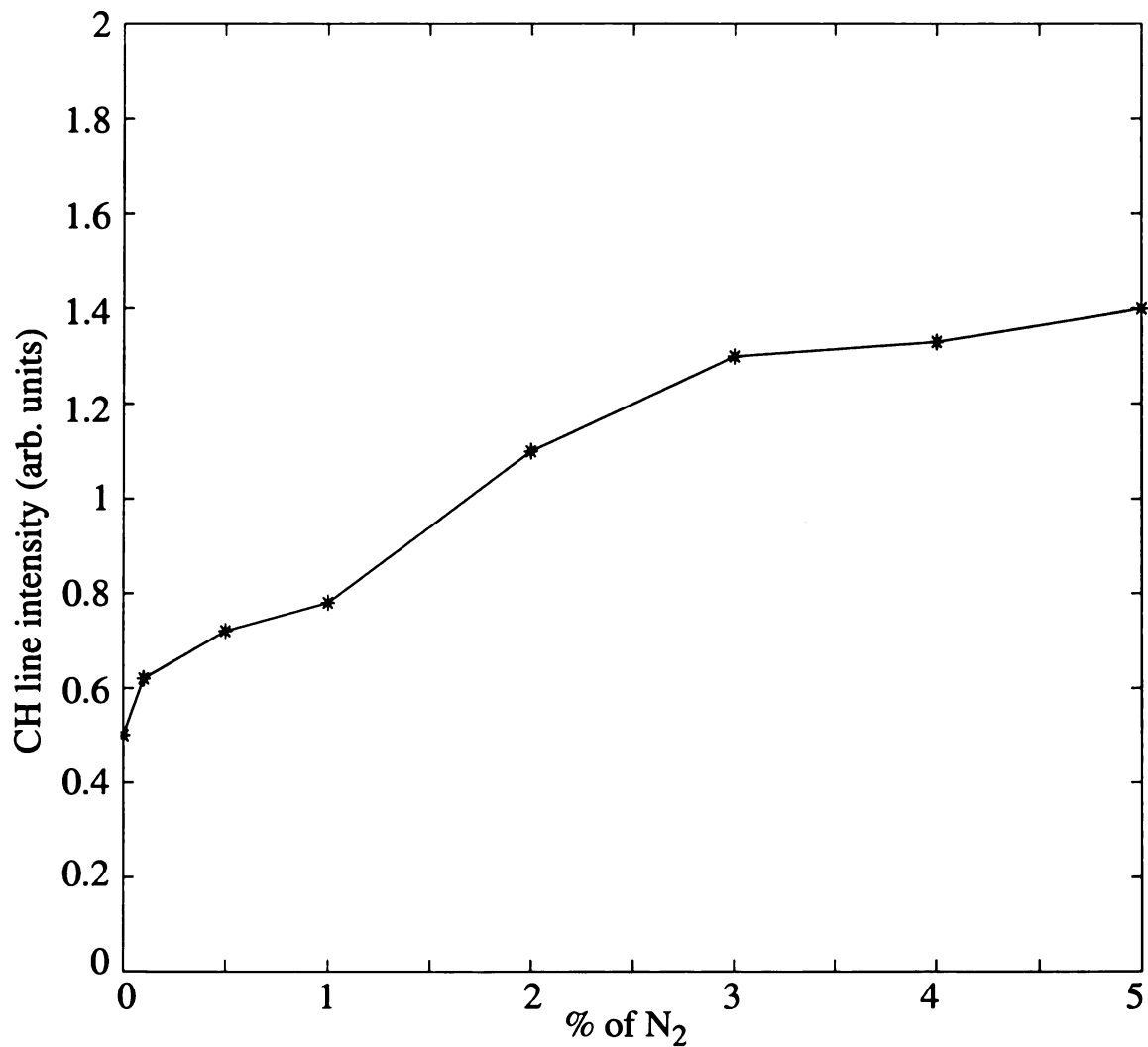


Figure 5.5 Variation of CH line intensity with N₂ concentration. Flow rates: CH₄-

7.2 sccm, H₂-144 sccm. Pressure: 30 Torr. Input Power: 0.8 kW

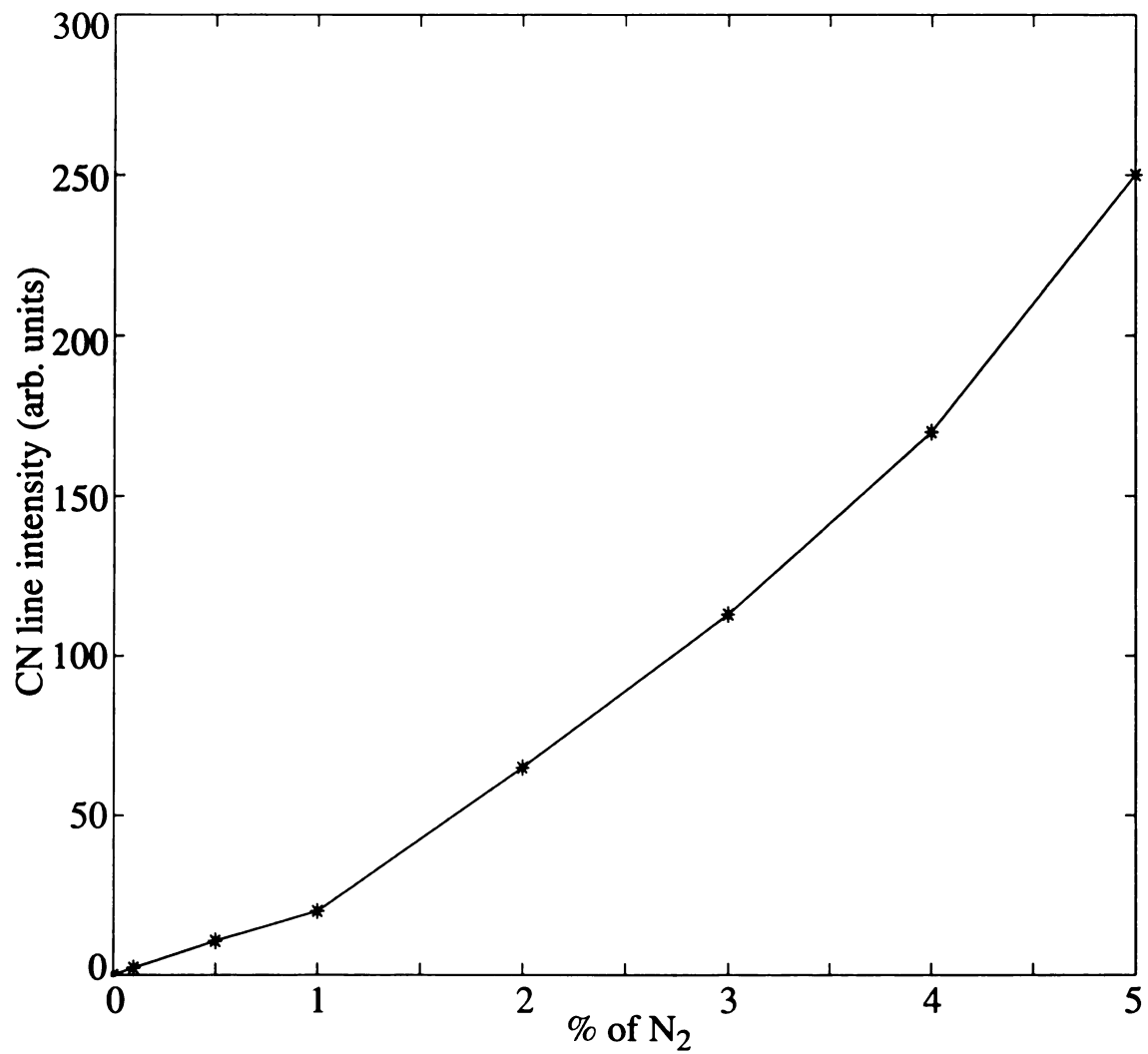


Figure 5.6 Variation of CN line intensity with N₂ concentration. Flow rates: CH₄-

7.2 sccm, H₂-144 sccm. Pressure: 30 Torr. Input Power: 0.8 kW

5.4 Conclusion

The results presented above show a strong dependence of H_{α} , H_{β} , CH and CN emissions on the N_2 concentration. An increase in the amount of atomic hydrogen is observed with increase of nitrogen. Since it is believed that atomic hydrogen plays an important role both in the gas phase and on the growing surface during diamond deposition, our observation shows that N_2 does change the bulk plasma properties. The H_{β}/H_{α} ratio shows no significant change in the electron temperature as the nitrogen is added to H_2 - CH_4 plasma. The variation of CH shows a similar trend as that of the atomic hydrogen.

Chapter 6

Study of Ar - H₂ - CH₄ - N₂ Microwave Plasma

6.1 Introduction

This chapter extends the analysis presented in chapter 5 to Ar - H₂ - CH₄ - N₂ plasmas used to deposit diamond. The addition of noble gases such as Ar has been found to influence the growth rate of diamond, and they were found to have a profound effect on the plasma chemistry, including ionization and dissociation [16]. This experiment is aimed at studying Ar - H₂ - CH₄ plasmas and the effect of nitrogen on Ar - H₂ - CH₄ plasmas. The motivation for studying this plasma stems from the fact that the surface morphology, the grain size and the growth mechanism of the diamond film can be controlled by varying the Ar/H₂ ratio in the Ar - H₂ - CH₄ plasma [2, 17]. The results of chapter 5 show that the addition of nitrogen varies the amount of atomic hydrogen in the plasma. Hence it would be interesting to observe the effect in the Ar - H₂ - CH₄ - N₂ plasmas. The first section gives an overview of the experimental setup. The subsequent section describes the results and presents a discussion of them. The concluding section highlights the significant results obtained.

6.2 Experimental setup

The experiments were carried out in the high power microwave reactor shown in Figure 2.5. This system is semi-automated so that the flow of the gases and the pressure are monitored and controlled by a computer. Microwave power used in the experiment is in the range of 1-1.7 kW. This resulted in the formation of a very bright plasma, which eliminated the need for any optical arrangement to focus the emission into the core of the

fiber. The optical arrangement #1 shown in Figure 2.8 was used. The signal was detected using the spectrometer system #2 shown in Figure 2.7. The input slit width was set to 0.4 mm. The exposure time of the diode array detector was varied to prevent saturation of the detector. The maximum exposure time needed was 0.328 - 4 seconds. The center wavelength was varied by turning the grating of the diode array detector manually.

6.3 Results and discussion

The emission from the plasma was scanned at three regions, whose center wavelengths are 410, 485 and 650 nm. The main emission lines that were observed are CH, CN, C₂, H_α and H_β. In the case of CN and C₂, a band was observed due to the presence of various rotational and vibrational levels associated with the molecules. Since the exposure time of the diode array detector was varied throughout the experiment to prevent the saturation of the detectors, the results presented here are normalized to an exposure time of 1 second. For the CN and C₂ molecules, both the peak intensities and the area under the band are presented after taking background noise into consideration. The species identified and their wavelengths are as follows: CN (383 nm), CH (430 nm), C₂(472 nm, 516 nm), H_β (486 nm) and H_α (656 nm), same as those studied by Clay et al. [18]. The C₂ bands at 472 nm and 516 nm are labeled as C_{2-a} and C_{2-b} respectively. For area measurements, the suffix “area” is attached to the species name. 2% nitrogen gas was used in the experiments. The process values and the associated data file names are provided in Appendix B.

The source parameter that was analyzed included the gas flow rate of H₂, CH₄, N₂ and Ar. The Figures 6.1, 6.2 and 6.3 show the emission spectrum with center wavelengths of 410, 485 and 650 nm. Figures 6.4 and 6.4a show the variation of the various species

concentrations with hydrogen flow. The concentration of all the observed species tend to decrease with increase in flow of H_2 . Although at high H_2 flow rates H_β and CH increase slightly, CN radical concentration was observed to decrease by a factor of 4 as H_2 flow rate varies from 0-100 sccm. This is followed by the C_2 which decreased by a factor of 3 for the same flow rate range. The presence of CN radical in the spectrum though nitrogen was not added to the gas mixture, can be attributed to the impurity present in the input gases or in the chamber. The result suggest that a lower amount of CH_4 dissociates to form C_2 or CH with increased flow of H_2 .

Figures 6.5 and 6.5a represent the variation of H_α , H_β , CN and C_2 with methane flow. H_α , H_β , CN and C_2 increases with the increase in flow of CH_4 , with C_2 and CH increase being more prominent. This result agrees with the general expectations of an increased carbon species with an increased flow of methane.

Figure 6.6 indicate the variation of CN and CH with the concentration of nitrogen. CH remains unaffected by the changes in N_2 while CN shows a linear increase by a factor of 20 with increase in concentration of N_2 by a factor of 10. Nitrogen forms CN readily with increased flow, while not affecting the amount of CH in the system. This is in agreement with the results of the work done by Clay et al. [18] in a CH_4/N_2 plasma. The CN spectral lines are readily seen in the spectrum due to its low activation energy.

The influence of argon on the concentration of the other species is shown in Figures 6.7 and 6.7a. C_2 and H_α increase by a factor of 3.5 and 1.5 respectively with increase in Ar concentration from 24- 92%. CN, H_β and CH show slight increase with the Ar concentration.

In addition to the above plots, the ratios of C_2 and H_β with H_α are plotted in Figures 6.8-6.11. The C_2/H_α ratio decreases with increase in H_2 flow and increases with increase in CH_4 flow. The ratio of H_β/H_α gives some information about the electron temperature of the system. With increase in the flow of H_2 , the H_β/H_α ratio decreases. The H_β/H_α ratio increases steadily with the flow of CH_4 , suggesting a large increase in the electron temperature with increase in methane concentration.

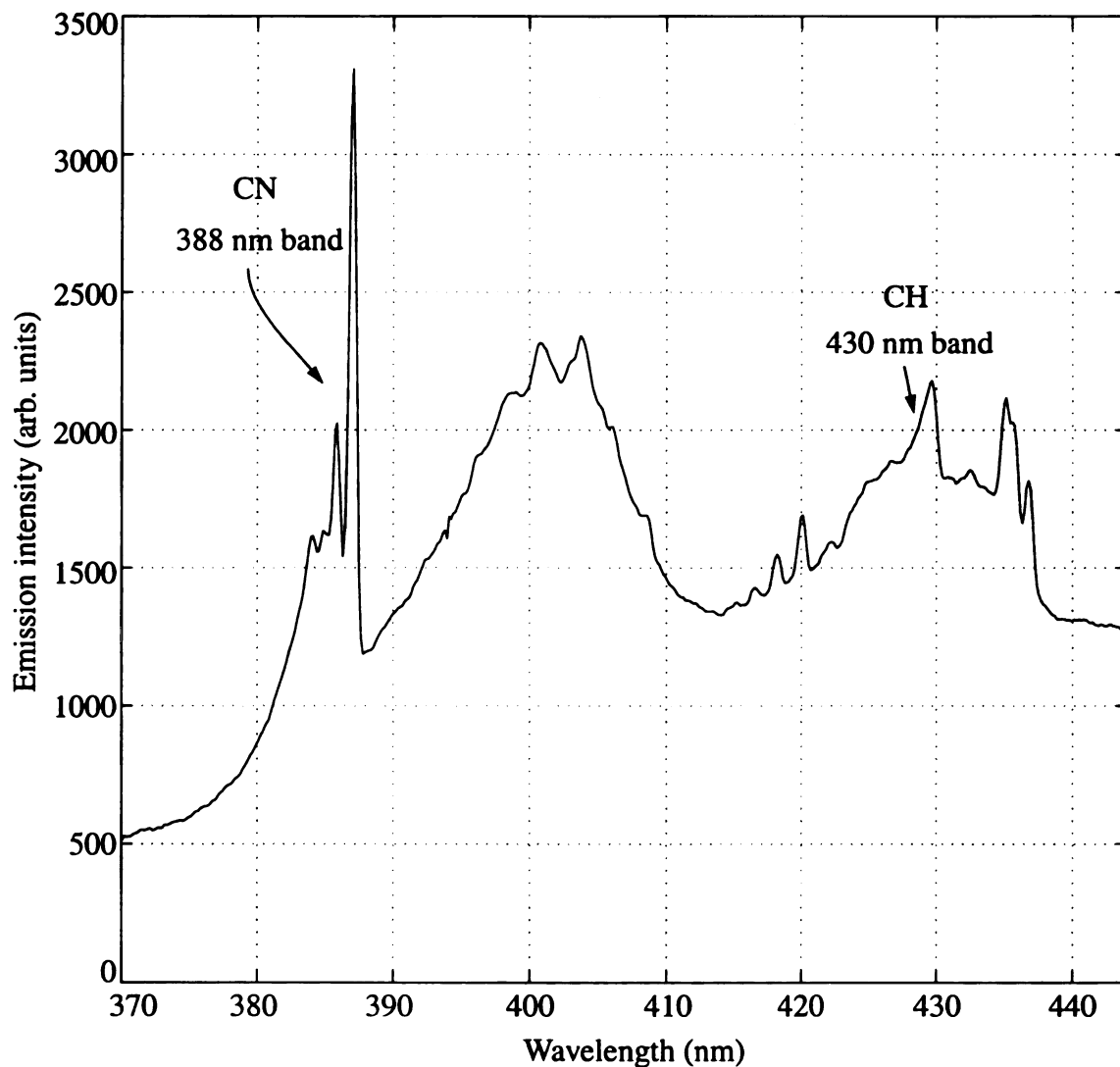


Figure 6.1 Emission spectrum. Flow rates: Ar- 600 sccm, CH_4 - 3 sccm, H_2 - 12sccm, N_2 - 3 sccm. Pressure: 120 Torr. Input Power: 1.09 kW

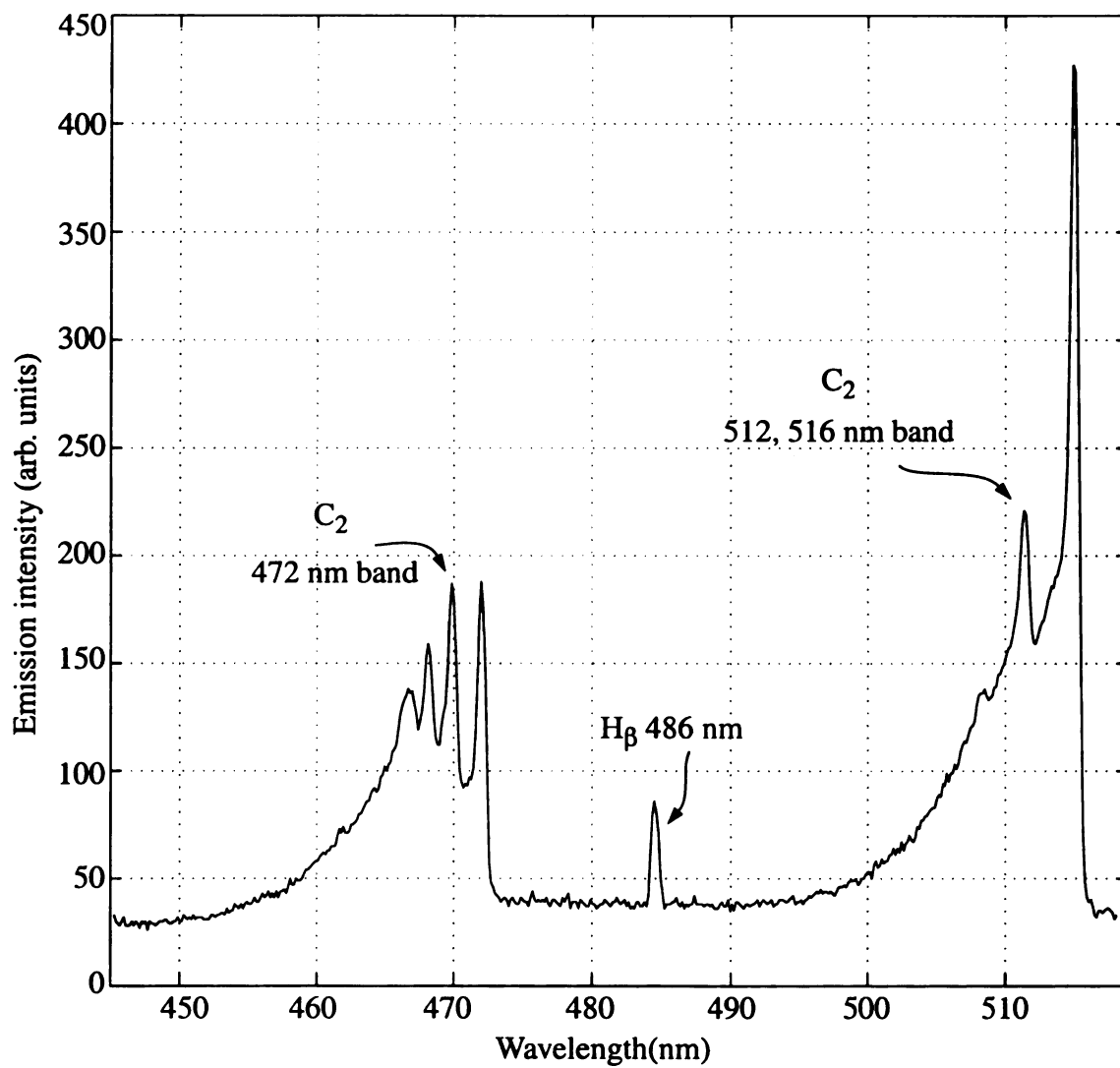


Figure 6.2 Emission spectrum. Flow rates: Ar- 100 sccm, CH₄- 8 sccm, H₂- 300sccm, N₂- 0 sccm. Pressure: 120 Torr. Input Power: 1.621 kW

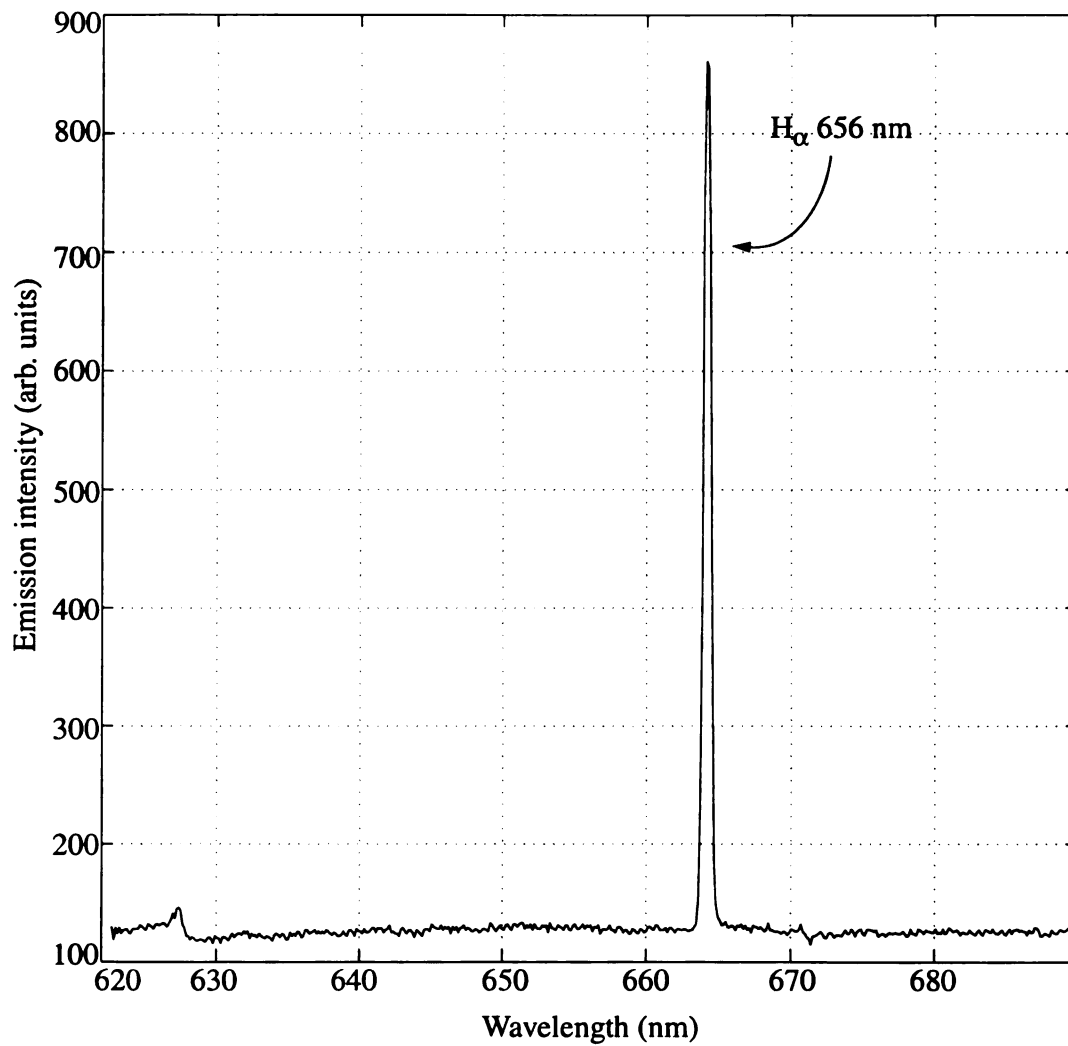


Figure 6.3 Emission spectrum. Flow rates: Ar- 100 sccm, CH₄- 8 sccm, H₂- 300sccm, N₂- 0 sccm. Pressure: 120 Torr. Input Power: 1.621 kW

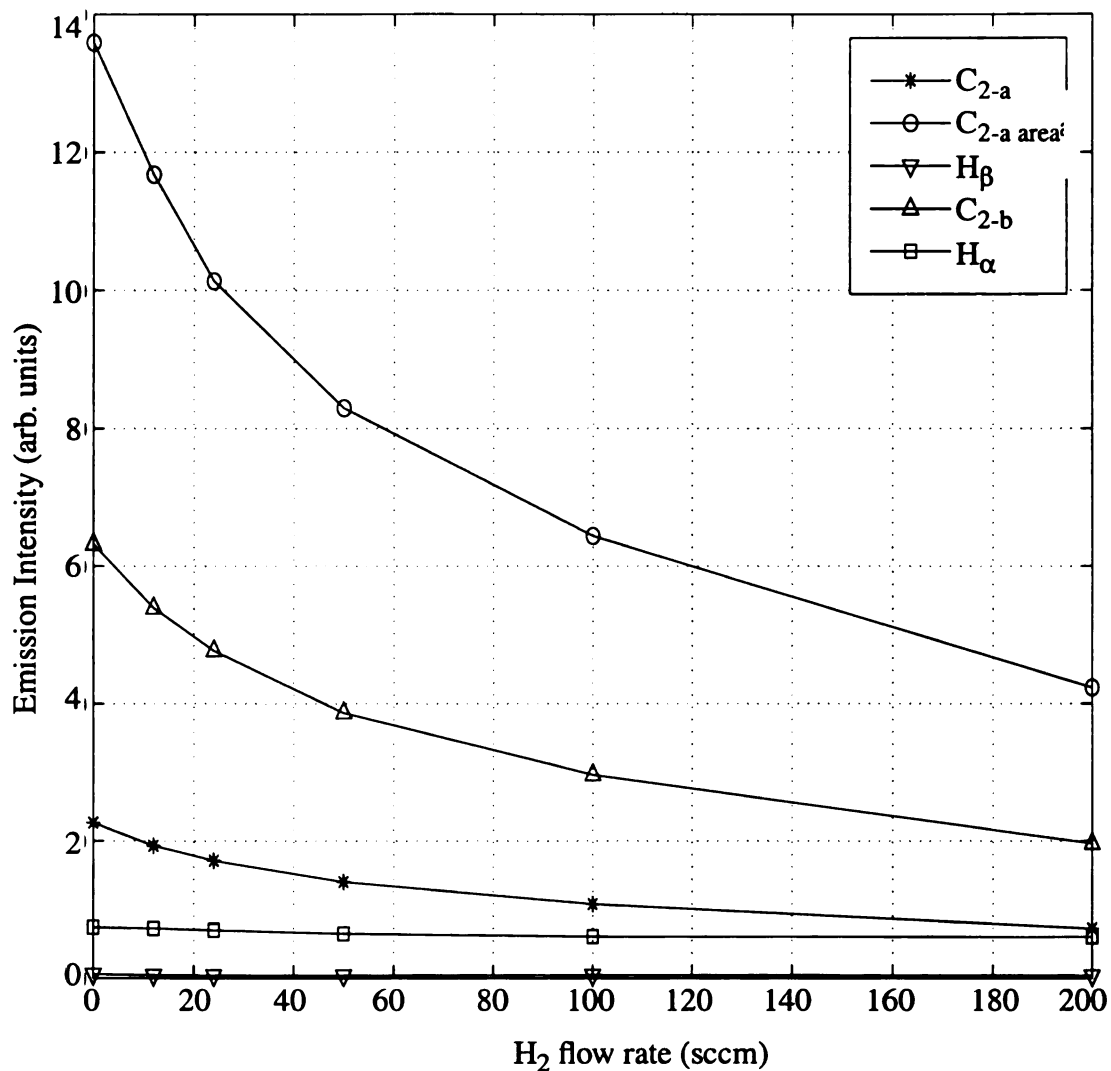


Figure 6.4 Variation of species concentration with H₂ flow rate. Flow rates: Ar-600 sccm, CH₄- 8 sccm. Pressure: 120 Torr. Input Power: ~ 1.2 kW

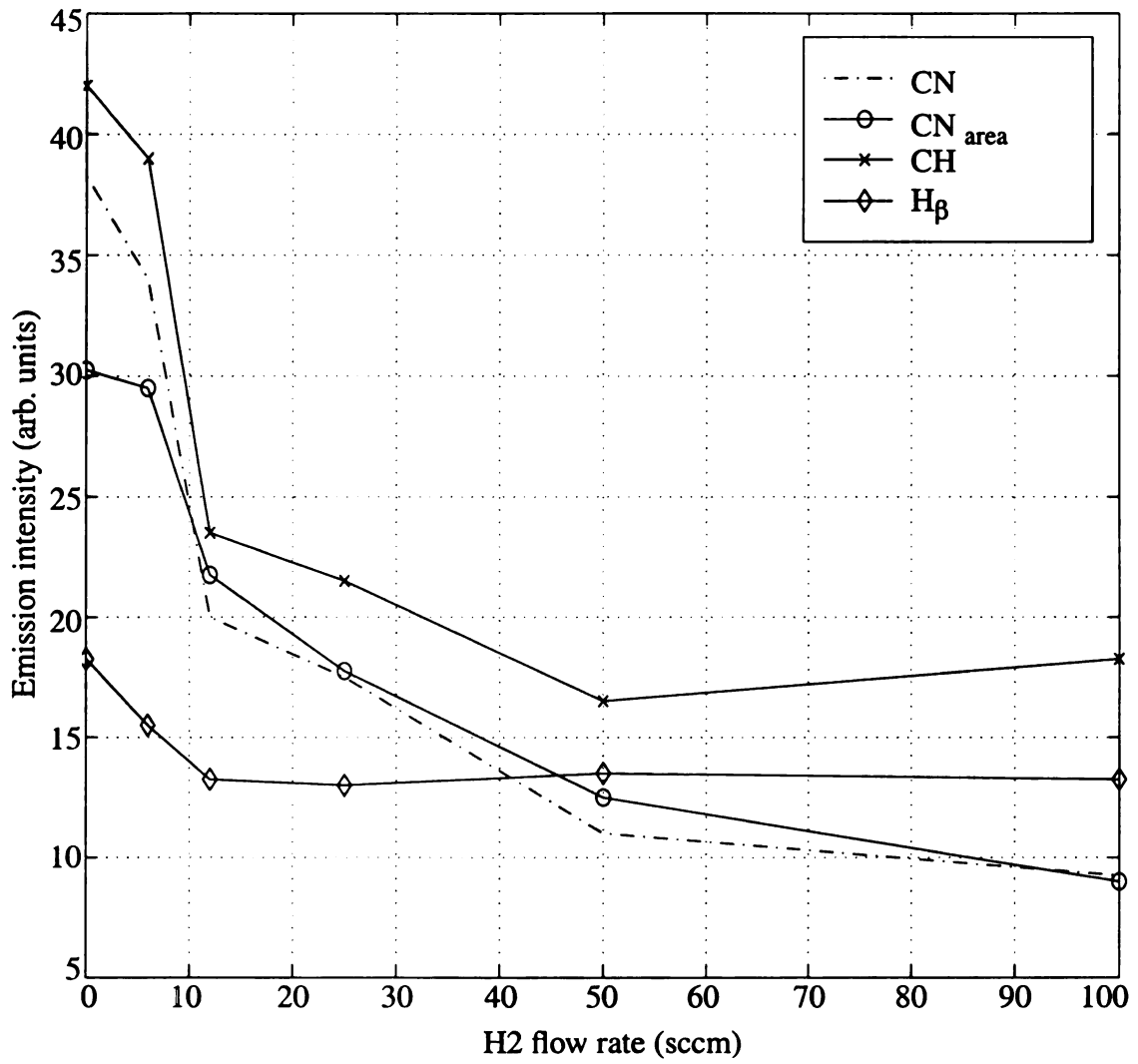


Figure 6.4a Variation of species concentration with H₂ flow rate. Flow rates: Ar-600 sccm, CH₄- 8 sccm. Pressure: 120 Torr. Input Power: ~ 1.2 kW

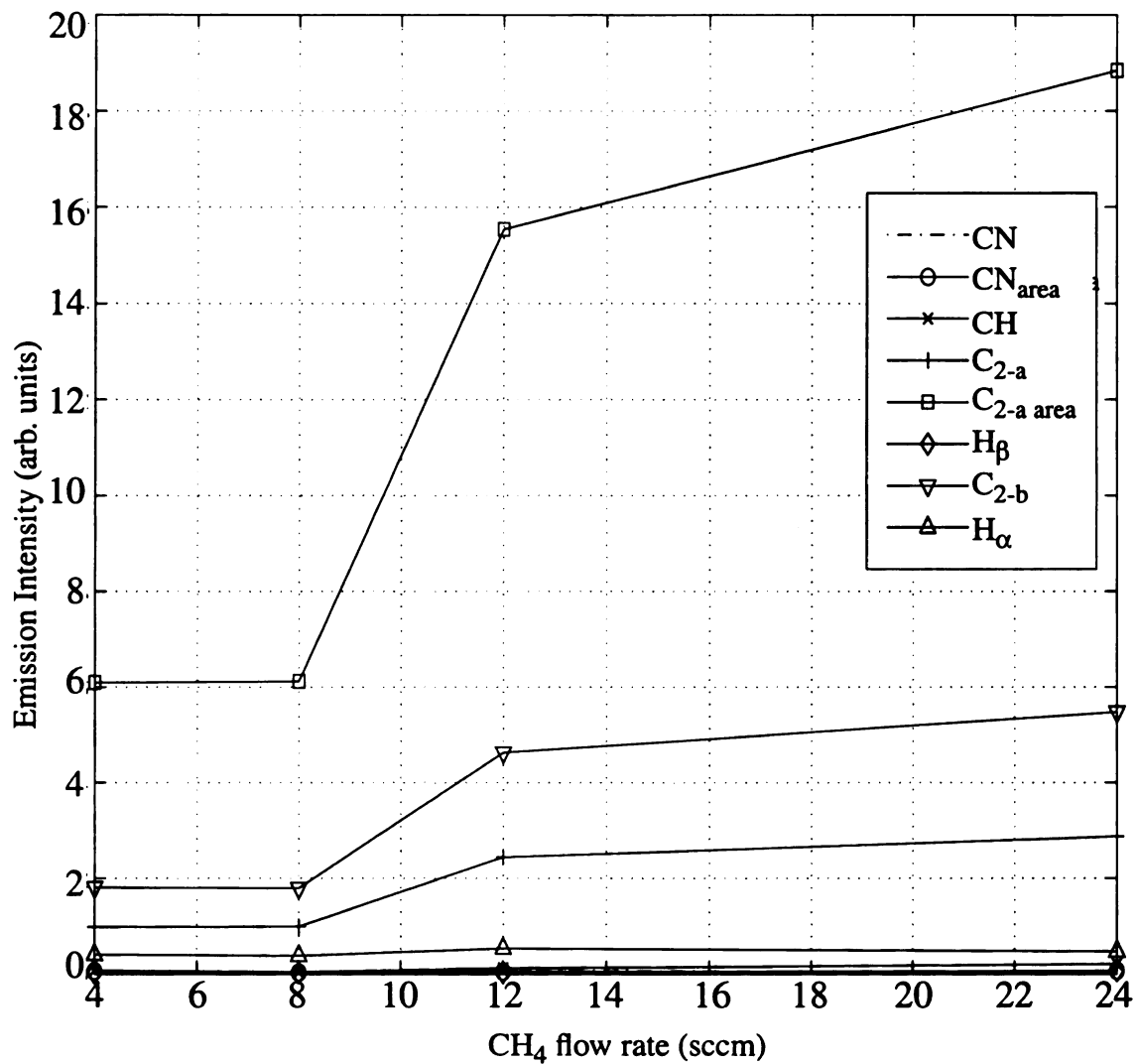


Figure 6.5 Variation of species concentration with CH₄ flow rate. Flow rates: Ar-600 sccm, H₂- 0 sccm. Pressure: 120 Torr. Input Power: ~ 1.2 kW

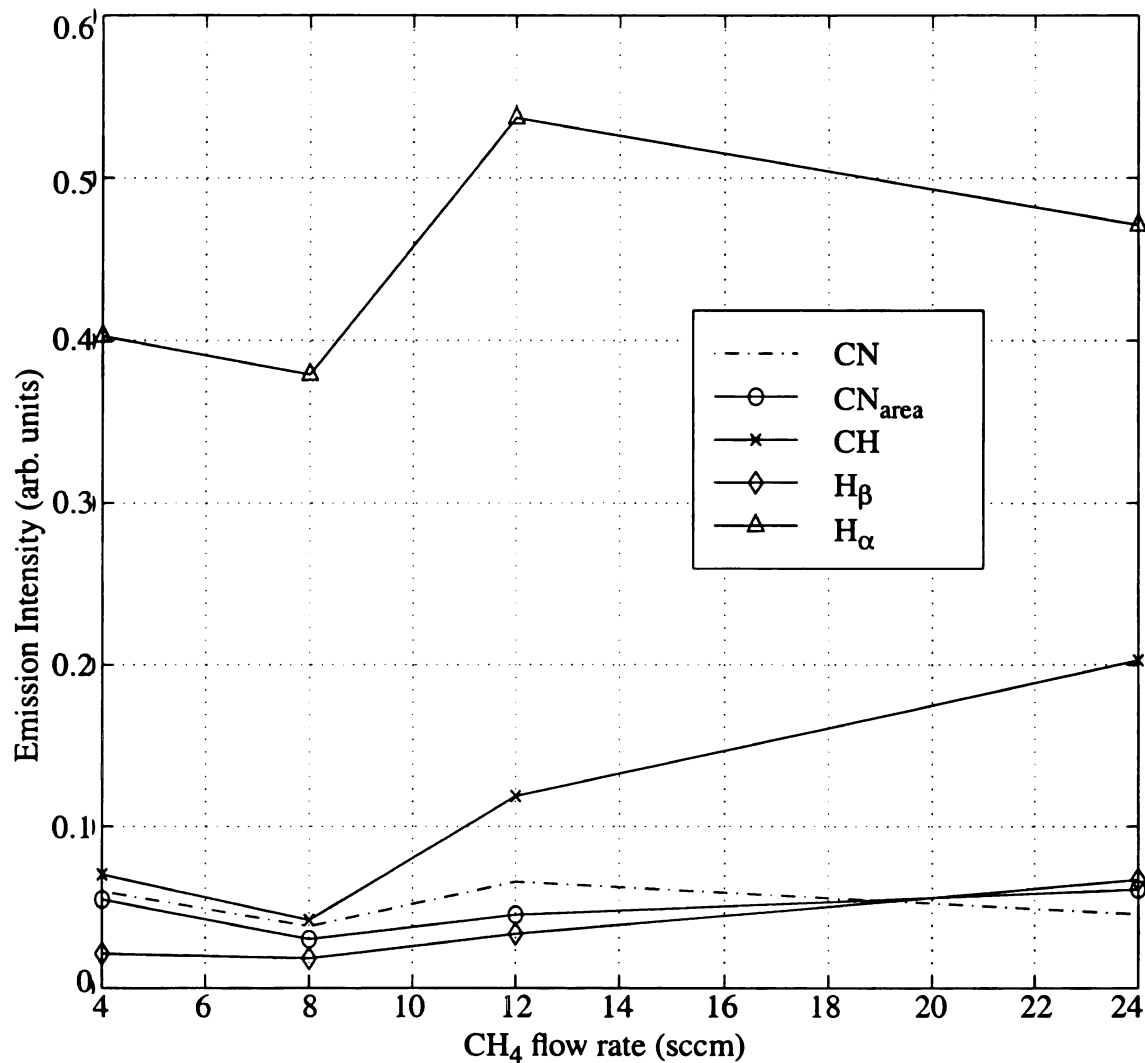


Figure 6.5a Variation of species concentration with CH₄ flow rate. Flow rates: Ar-600 sccm, H₂- 0 sccm. Pressure: 120 Torr. Input Power: ~ 1.2 kW

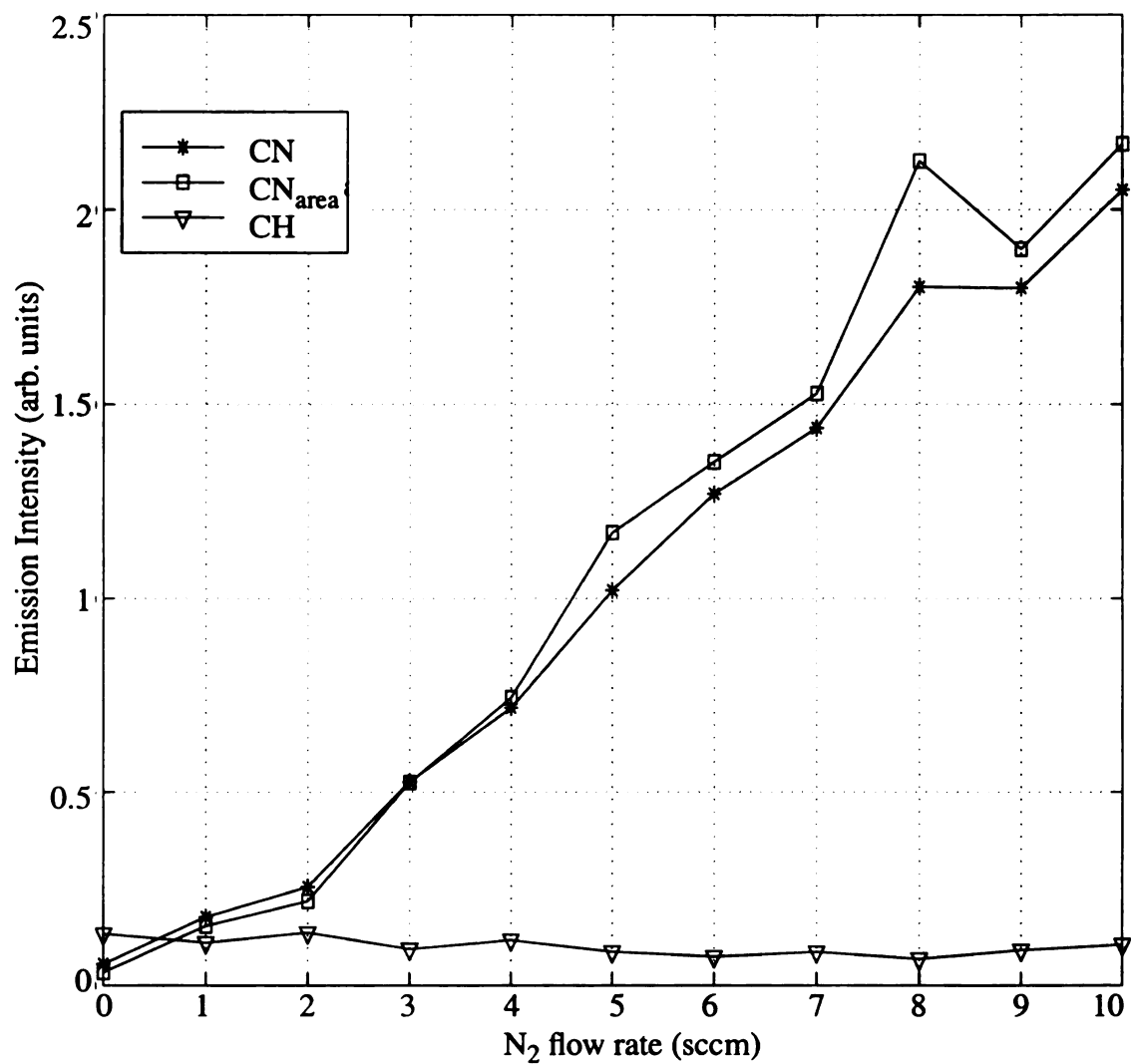


Figure 6.6 Variation of species concentration with N₂ flow. Flow rates: Ar- 600

sccm, H₂- 12 sccm, CH₄- 8 sccm. Pressure: 120 Torr. Input Power: ~ 1.1 kW

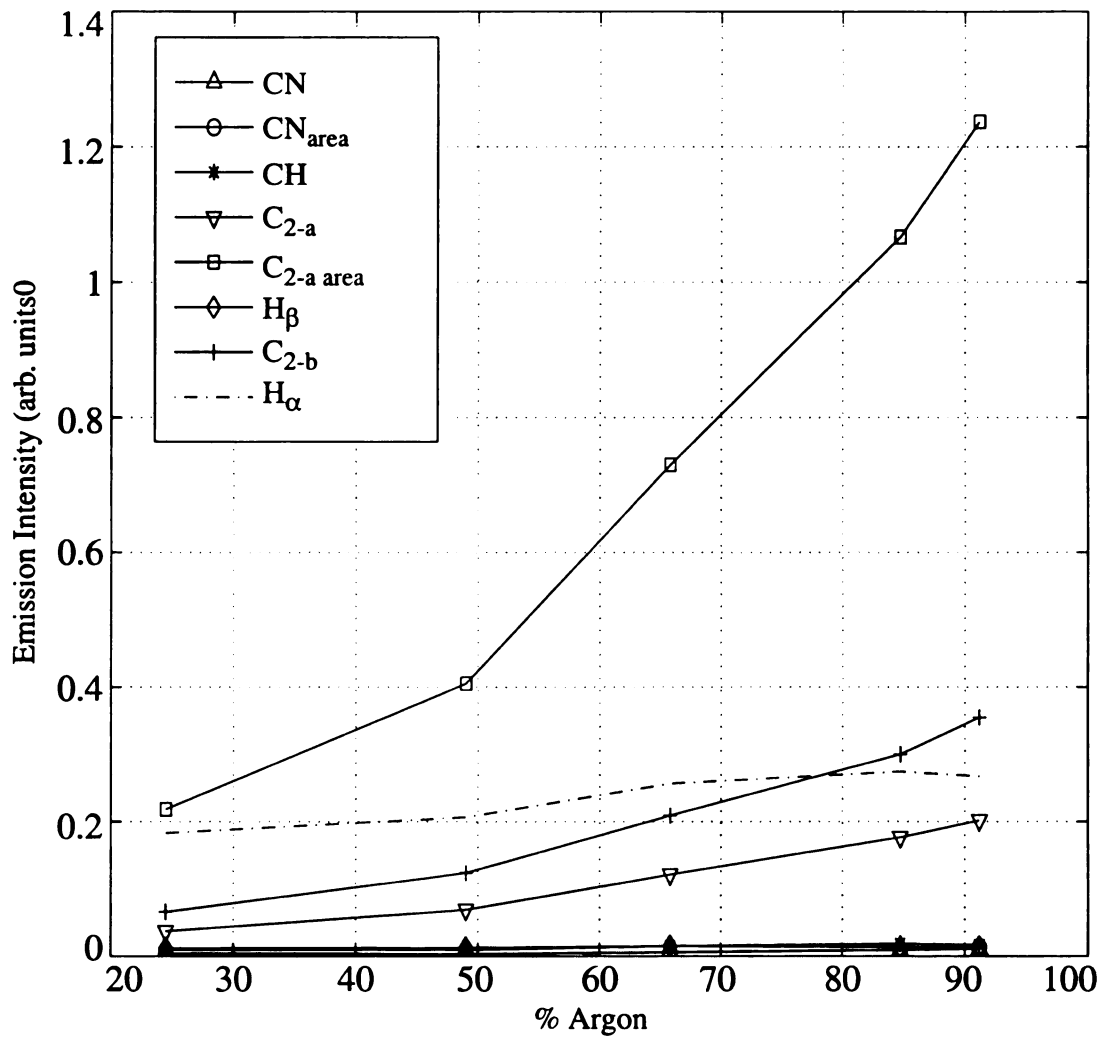


Figure 6.7 Variation of species concentration with Ar flow rate. Flow rates: H₂ - 50-300 sccm, CH₄- 8 sccm. Pressure: 120 Torr. Input Power: ~ 1.4 kW

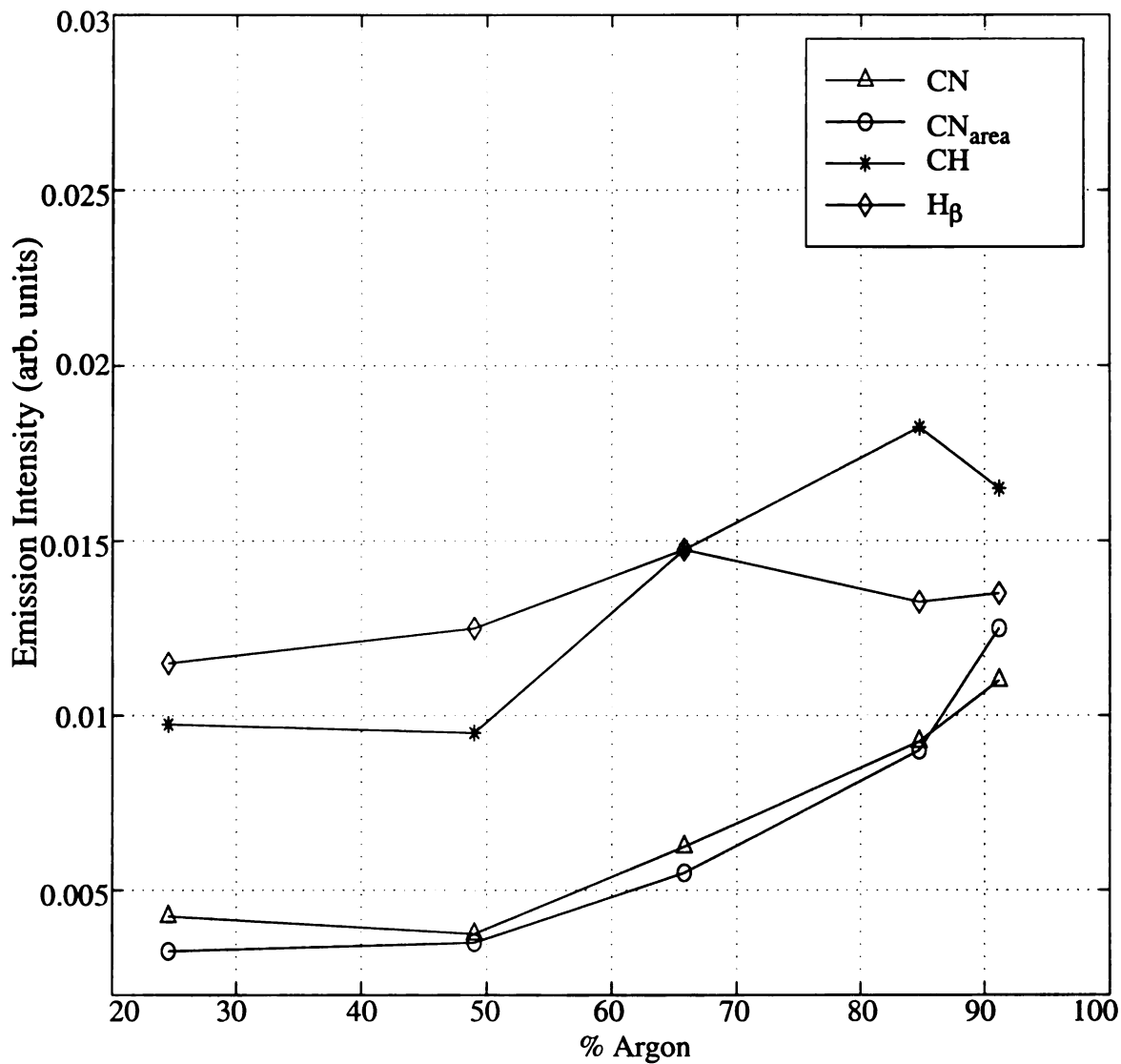


Figure 6.7a Variation of species concentration with Ar flow rate. Flow rates: H₂ -

50-300 sccm, CH₄- 8 sccm. Pressure: 120 Torr. Input Power: ~ 1.4 kW

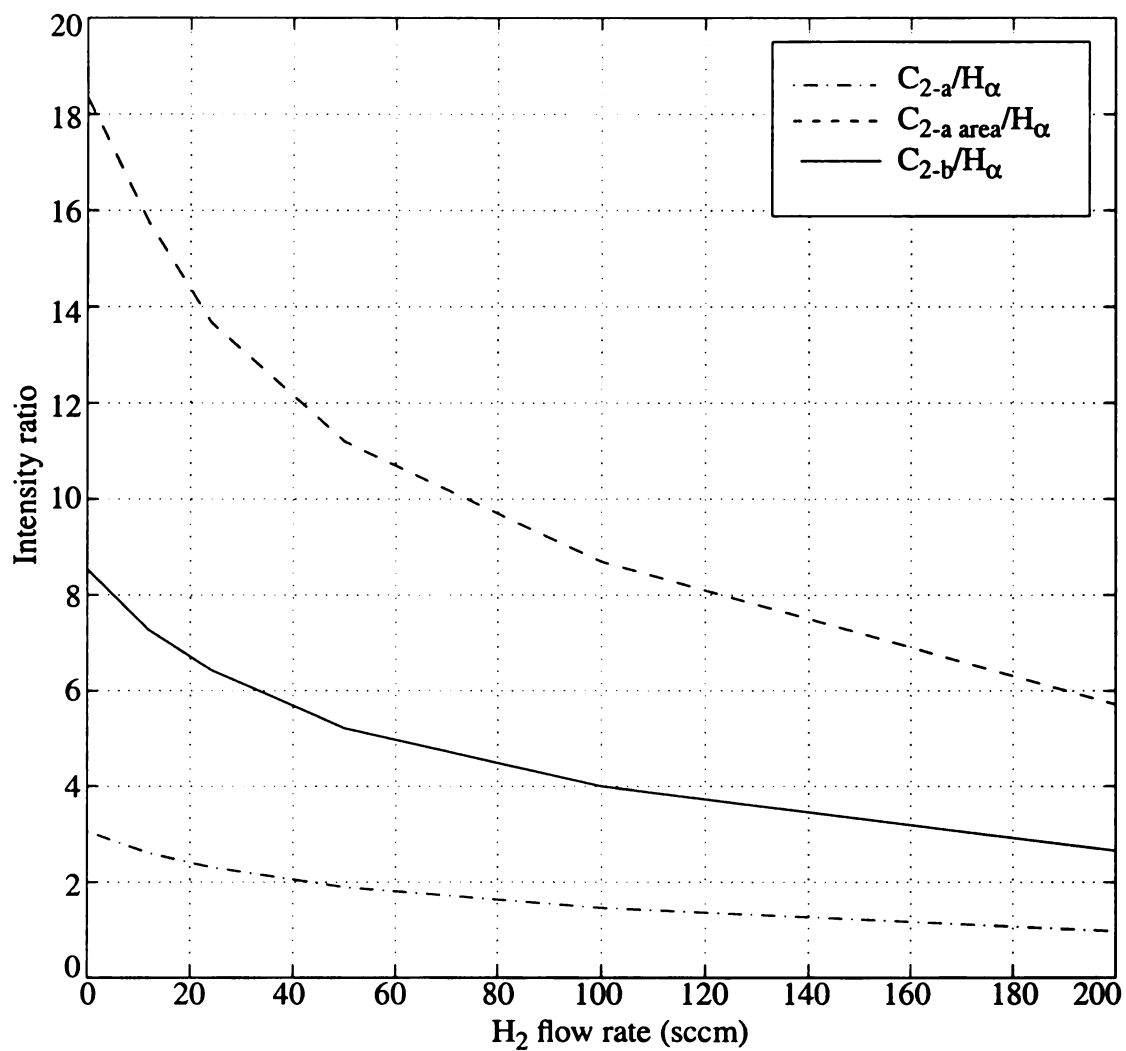


Figure 6.8 Variation of C₂/H_α ratio with H₂ flow rate. Flow rates: Ar - 600 sccm, CH₄- 8 sccm. Pressure: 120 Torr. Input Power: ~ 1.2 kW

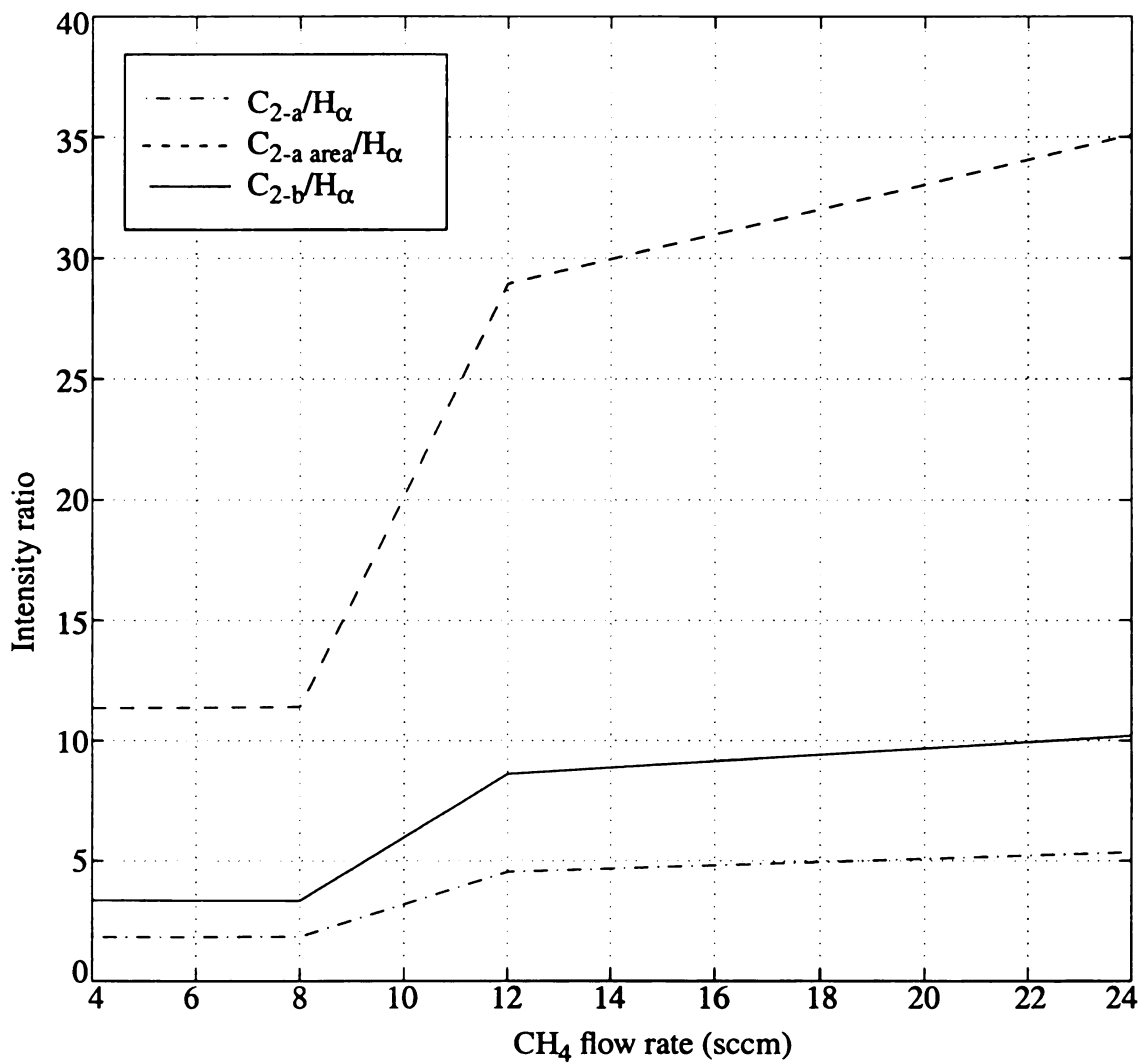


Figure 6.9 Variation of C₂/H_α ratio with CH₄ flow rate. Flow rates: Ar - 600 sccm, H₂- 0 sccm. Pressure: 120 Torr. Input Power: ~ 1.2 kW

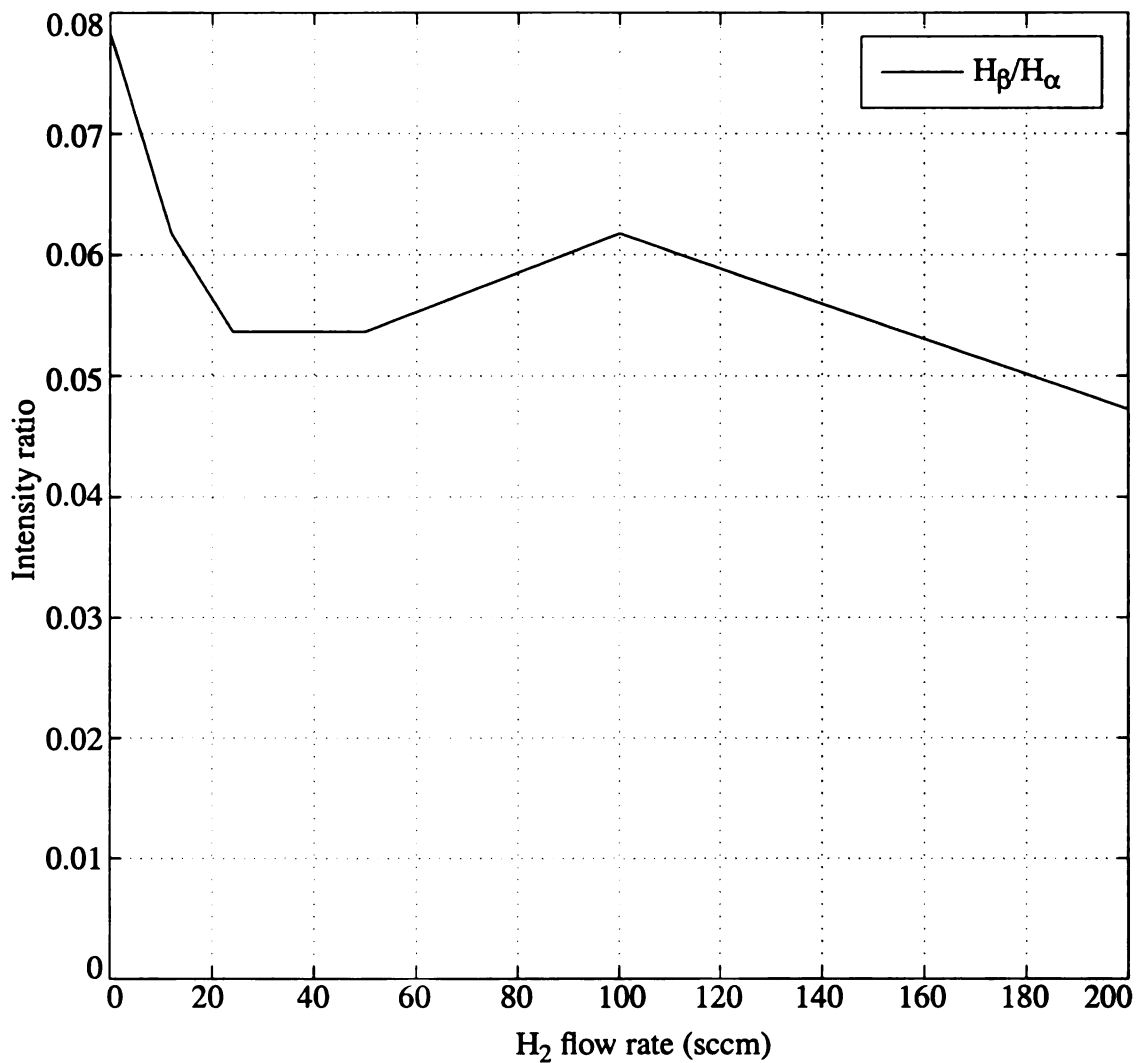


Figure 6.10 Variation of H_{β}/H_{α} ratio with H_2 flow rate. Flow rates: Ar - 600 sccm, CH_4 - 8 sccm. Pressure: 120 Torr. Input Power: ~ 1.2 kW

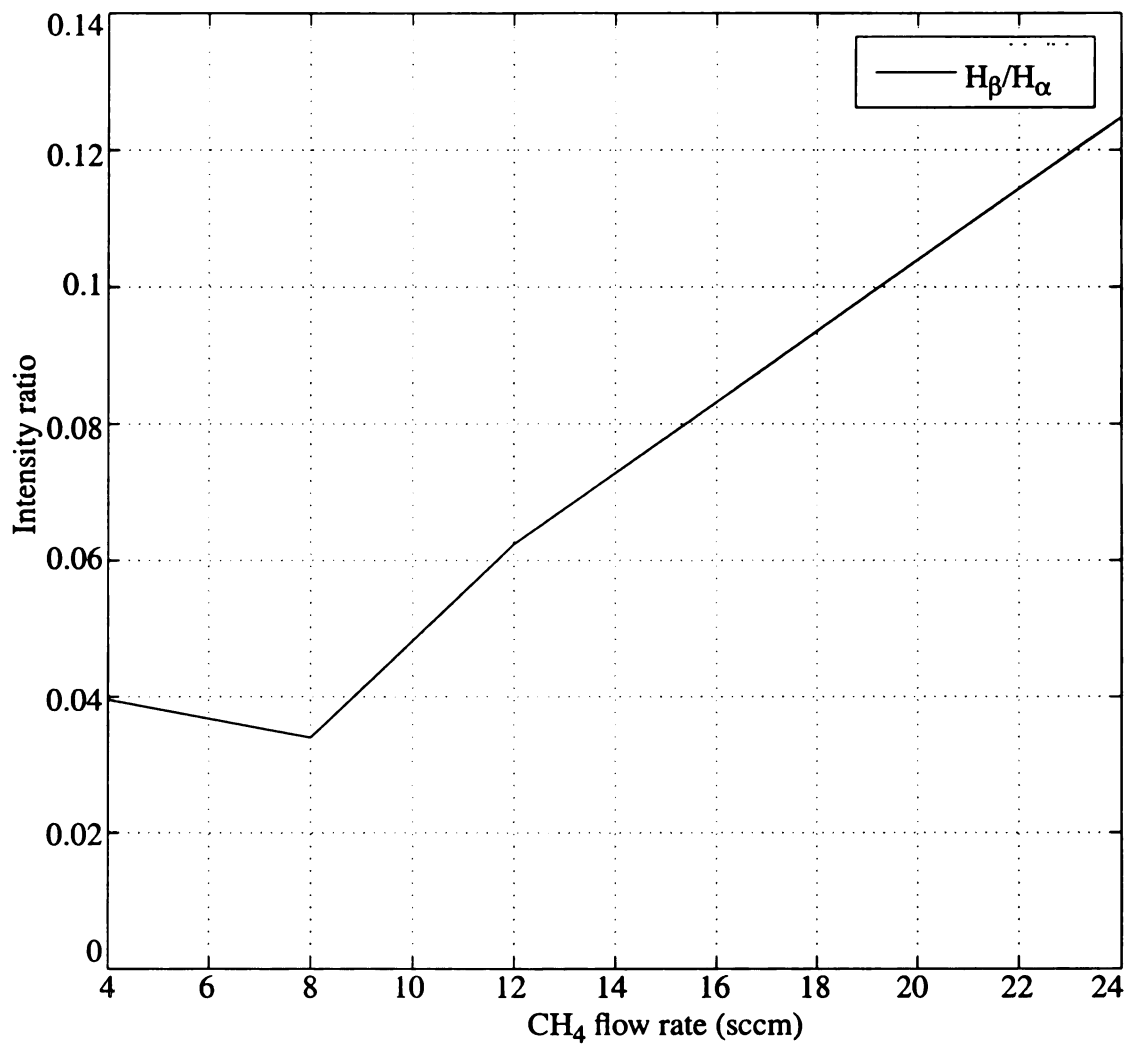


Figure 6.11 Variation of H_{β}/H_{α} ratio with H_2 flow rate. Flow rates: Ar - 600 sccm,

H_2 - 0 sccm. Pressure: 120 Torr. Input Power: ~ 1.2 kW

6.5 Conclusion

The emissions from several species including H, CH, CN and C₂ were measured versus variation in source operating parameter including input gas flow composition. The results indicate that in Ar-H₂-CH₄ plasmas the increase in argon flow percentage produces more C₂ species in the plasma. The C₂ species is important since it is believed to be a key precursor for nanocrystalline growth [2]. The amount of argon was found to affect the atomic hydrogen emission.

The influence of nitrogen on the Ar-H₂-CH₄ plasmas was also examined. The amount of N₂ added was 0-300 ppm. As expected the CN emission was seen to depend strongly on the N₂ concentration. The CH emission was not affected by nitrogen concentration.

Chapter 7

Summary of results

7.1 Conclusions

The experiments were performed in accordance with the objectives, which is to investigate the microwave plasma discharges using optical emission spectroscopy. The work was started with the aim of studying the Ar plasma and measuring the amount of doubly ionized atoms, and studying the variation of gas temperature of H₂ - CH₄ microwave plasma and the effect of N₂ addition to the plasma. The above objectives were realized by performing various experiments as discussed in the preceding chapters. This chapter presents a brief summary of all the results obtained and how they have helped in the realization of the goals set forth in chapter 1.

7.1.1 Argon Doubly-ionized atoms measurements

The experiments were carried out in a compact ion source. The results confirmed the presence of Ar⁺⁺ ions in the compact ion source. Experiments to determine the dependence of the Ar⁺⁺ emission on the source operating conditions were performed. The Ar⁺⁺ ion density was found to increase as the flow rate and the pressure decreases. The results presented gives an idea of the Ar⁺⁺ density variation in a compact ion source. And, it provides a relative indication of the high energy (>28eV) electron density.

7.1.2 Gas Kinetic Temperature of H₂ - CH₄ Microwave Plasma

The gas temperature measurements are important in understanding the plasma since the gas temperature helps determine the concentration of various radicals. The gas temperature was obtained from the rotational temperature, which was derived from the measurement of the relative intensities of rotational lines within a single vibrational band. The temperature obtained ranges from 1200-2000 K. The rotational temperature is found to vary slightly with the gas flow rate. The rotational temperature tends to increase with the pressure of the gas mixture. Interestingly, the 0.1 - 1% addition of nitrogen did not change the rotational temperature by an observable value.

7.1.3 Study of H₂ - CH₄ - N₂ Microwave Plasma

The experiments were performed in conditions similar to that of an actual diamond deposition system. Typical values of input power, pressure and flow rates were 0.8 kW, 30 Torr and 200 sccm, 4 sccm and 0-5 sccm for H₂, CH₄ and N₂ respectively. Basically the variation of H_α, H_β, CH and CN emissions produced by N₂ concentration variations was observed.

The results show a strong dependence of the observed species on the N₂ concentration. An increase in the amount of atomic hydrogen is observed with increase of nitrogen. The H_β/H_α ratio shows almost no change in the electron temperature of the mixture with the inclusion of N₂. The variation of CH shows a similar trend as that of the atomic hydrogen.

7.1.4 Study of Ar-H₂ - CH₄ - N₂ Microwave Plasma

The Ar-H₂ - CH₄ - N₂ microwave plasma is used in the deposition of nanocrystalline and microcrystalline diamond thin films. The experiments were carried out in the high power microwave reactor. The typical values of power, pressure and the flow rates of H₂, Ar, CH₄ and 2% N₂ in H₂ are 1.8 kW, 120 Torr, 0-300 sccm, 600 sccm, 3-24 sccm and 0-10 sccm respectively. Some significant results that were obtained are mentioned here.

The increase in the argon flow produces more C₂ in the plasma. The C₂ species is important since it is believed to be a key precursor for nanocrystalline growth. The amount of argon was also found to affect the atomic hydrogen emission. Unlike the previous experiments the CH emission was not affected by the nitrogen concentration change in the 0-300 ppm range.

7.2 Recommendations for future work

This study has contributed to the understanding of a few plasmas used in diamond deposition and low pressure plasma processing of materials. The results obtained were within our expectations. But some anomalies are found to exist, which need further careful study. One such example is the variation of Ar⁺⁺ density with power. Even though, the Ar⁺⁺ density was supposed to increase with power, it tends to saturate at higher power as shown by the experiments. Another study of interest would be the comparison of the temperature measurements with other methods like doppler broadening. An attempt was made to measure the same using a Fabry-Perot cavity, but due to inadequate signal, the measure-

ments were not carried out. For a more complete understanding of the plasma species concentration, the plasma can be modeled theoretically and the plasma parameter variations predicted by the model can be used to compare the validity of the experimental results. For example, the plasma parameters in the low pressure source are found to exhibit a large dependence on the flow rate of the process gases. A theoretical model should be able to help explain this dependence. Also to understand the variation of species concentration and the plasma parameters with time, the OES experiments can be performed in an actual diamond deposition process. This would also facilitate the study of the characteristics of the deposited diamond film under the various processing conditions.

APPENDICES

APPENDIX A

Table : A Identification and analysis of argon doubly ionized atoms

Expt. #	Input Power (W)	Pressure (mT)	Flow rate (sccm)	Intensities (arbitrary units)		
				3336.13Å	3344.72Å	3358.49Å
1	40	0.3	1	7.29e-11	5.94e-11	6.05e-11
2	40	0.5	1	6.55e-11	6.38e-11	5.10e-11
3	40	0.75	1	4.50e-11	3.09e-11	3.11e-11
4	40	0.9	1	4.90e-11	3.09e-11	2.86e-11
5	40	0.9	8	3.16e-11	1.74e-11	2.48e-11
6	40	0.9	20	0	0	5.68e-12
7	40	2	1	2.90e-11	1.46e-11	1.88e-11
8	40	3	1	1.04e-11	5.14e-11	9.12e-11
9	40	3	8	1.15e-11	5.99e-12	1.24e-11
10	40	3	20	0	0	7.20e-12
21	100	0.3	1	8.81e-11	5.74e-11	6.93e-11
22	100	0.5	1	5.77e-11	3.69e-11	4.31e-11
23	100	0.75	1	4.18e-11	4.59e-11	4.39e-11
24	100	0.9	1	4.96e-11	3.42e-11	4.22e-11
25	100	0.9	8	2.91e-11	2.28e-11	2.68e-11
26	100	0.9	20	5.03e-11	3.43e-11	3.88e-11
27	100	2	1	1.59e-11	6.23e-11	2.04e-11
28	100	3	1	7.67e-11	3.15e-11	1.26e-11
29	100	3	8	4.23e-11	3.32e-11	8.29e-11
30	100	3	20	1.28e-11	1.46e-11	0
31	10	0.9	1	1.56e-11	1.12e-11	4.88e-11
32	20	0.9	1	2.66e-11	3.74e-11	1.48e-11

Table : A (contd.)

Expt. #	Input Power (W)	Pressure (mT)	Flow rate (sccm)	Intensities (arbitrary units)		
				3336.13Å	3344.72Å	3358.49Å
33	30	0.9	1	3.23e-11	2.89e-11	1.72e-11
34	50	0.9	1	5.89e-11	3.09e-11	3.49e-11
35	60	0.9	1	5.71e-11	3.68e-11	3.42e-11
36	70	0.9	1	6.15e-11	3.35e-11	4.42e-11
37	80	0.9	1	5.87e-11	4.46e-11	3.44e-11
38	90	0.9	1	6.97e-11	4.41e-11	4.59e-11

Input Power = Incident Power - Reflected Power

Intensities were calculated by measuring the area under the peaks at 3336.13, 3344.72 and 3358.49Å.

APPENDIX B

Table: B Measurements of Ar - H₂ - CH₄ - N₂ Microwave Plasma

P _{inc} (W)	P _{refl} (W)	T _s (°C)	Ar (sccm)	CH ₄ (sccm)	H ₂ (sccm)	2% N ₂ (sccm)	Pressure (Torr)	λ (nm)	Exposure time (s)	Filename
1936	315	1120	100	8	300	0	120	410	4	F1
1936	315	1120	100	8	300	0	120	485	4	F2
1936	315	1115	100	8	300	0	120	650	4	F3
1936	315	1100	200	8	200	0	120	650	4	F4
1936	315	1100	200	8	200	0	120	485	4	F5
1936	315	1100	200	8	200	0	120	410	4	F6
1897	355	1075	400	8	200	0	120	410	4	F7
1897	355	1075	400	8	200	0	120	485	4	F8
1897	355	1075	400	8	200	0	120	650	4	F9
1878	414	1038	600	8	100	0	120	650	4	F10
1878	414	1038	600	8	100	0	120	485	4	F11
1878	414	1038	600	8	100	0	120	410	4	F12

Table: B (contd.)

P_{inc} (W)	P_{refl} (W)	T_s (°C)	Ar (sccm)	CH ₄ (sccm)	H ₂ (sccm)	2% N ₂ (sccm)	Pressure (Torr)	λ (nm)	Exposure time (s)	Filename
1878	473	1020	600	8	50	0	120	410	4	F13
1878	473	1020	600	8	50	0	120	485	4	F14
1878	473	1020	600	8	50	0	120	650	4	F15
1878	493	995	600	8	25	0	120	650	4	F16
1878	493	995	600	8	25	0	120	485	4	F17
1878	493	995	600	8	25	0	120	410	4	F18
1878	532	970	600	8	12	0	120	410	4	F19
1878	532	965	600	8	12	0	120	485	4	F20
1878	532	960	600	8	12	0	120	650	4	F21
1878	591	940	600	8	6	0	120	650	4	F22
1878	591	940	600	8	6	0	120	485	2	F23
1878	591	925	600	8	6	0	120	410	4	F24
1878	591	910	600	8	0	0	120	410	4	F25
1878	591	900	600	8	0	0	120	485	0.656	F26
1878	591	895	600	8	0	0	120	650	4	F27
1878	591	870	600	4	0	0	120	650	4	F28

Table: B (contd.)

P_{inc} (W)	P_{refl} (W)	T_s ($^{\circ}$ C)	Ar (sccm)	CH ₄ (sccm)	H ₂ (sccm)	2% N ₂ (sccm)	Pressure (Torr)	λ (nm)	Exposure time (s)	Filename
1878	591	867	600	4	0	0	120	485	0.656	F29
1878	591	863	600	4	0	0	120	410	4	F30
1878	690	895	600	12	0	0	120	410	4	F31
1878	690	895	600	12	0	0	120	485	0.328	F32
1878	690	895	600	12	0	0	120	650	2	F33
1878	650	1010	600	24	0	0	120	650	0.65	F34
1878	650	1010	600	24	0	0	120	485	0.164	F35
1878	650	1010	600	24	0	0	120	410	0.656	F36
1878	730	895	600	4	12	0	120	410	4	F37
1878	730	895	600	4	12	0	120	485	0.164	F38
1878	730	895	600	4	12	0	120	650	2	F39
1878	493	1100	600	8	200	0	120	650	4	F40
1878	493	1120	600	8	200	0	120	485	0.656	F41
1878	493	1115	600	8	200	0	120	410	4	F42
1878	690	915	600	8	12	0	120	410	4	F43
1878	690	915	600	8	12	0	120	485	0.328	F44

Table: B (contd.)

P_{inc} (W)	P_{ref} (W)	T_s (°C)	Ar (sccm)	CH ₄ (sccm)	H ₂ (sccm)	2% N ₂ (sccm)	Pressure (Torr)	λ (nm)	Exposure time (s)	Filename
1878	690	900	600	8	12	0	120	650	0.656	F45
1878	729	884	600	8	0	0	120	650	0.656	F46
1878	729	885	600	8	12	0	120	650	0.656	F47
1878	710	886	600	8	24	0	120	650	0.656	F48
1878	690	890	600	8	50	0	120	650	0.656	F49
1878	650	915	600	8	100	0	120	650	0.656	F50
1878	591	965	600	8	200	0	120	650	0.656	F51
1878	591	965	600	8	200	0	120	485	0.656	F52
1878	631	910	600	8	100	0	120	485	0.656	F53
1878	670	888	600	8	50	0	120	485	0.328	F54
1878	692	870	600	8	24	0	120	485	0.328	F55
1878	710	870	600	8	12	0	120	485	0.328	F56
1878	730	865	600	8	0	0	120	485	0.328	F57
1878	750	836	600	3	12	0	120	410	4	F58
1878	750	820	600	3	12	1	120	410	4	F59
1878	788	820	600	3	12	2	120	410	4	F60

Table: B (contd.)

P_{inc} (W)	P_{refl} (W)	T_s ($^{\circ}$ C)	Ar (sccm)	CH ₄ (sccm)	H ₂ (sccm)	2% N ₂ (sccm)	Pressure (Torr)	λ (nm)	Exposure time (s)	Filename
1878	788	818	600	3	12	3	120	410	4	F61
1878	788	815	600	3	12	4	120	410	2	F62
1878	788	814	600	3	12	5	120	410	2	F63
1878	788	813	600	3	12	6	120	410	2	F64
1878	788	810	600	3	12	7	120	410	2	F65
1878	808	812	600	3	12	8	120	410	1	F66
1878	808	810	600	3	12	9	120	410	1	F67
1878	808	809	600	3	12	10	120	410	1	F68

 P_{inc} - Incident Microwave Power P_{refl} - Reflected Microwave Power T_s - Substrate Temperature (Observed using an optical pyrometer) λ - Center wavelength of the Spectrometer

APPENDIX C

QBASIC program to read data from the picoammeter connected to the monochromator :

'Author : Jayakumaran Sivagnaname ; Date: July 1998
'Monochromator Spec: 2400 lines/mm grating: offset= 23.5 angstrom
'Mcpherson Monochromator must be scanned with increasing wavelength ONLY

```
DECLARE SUB FILEWRTU ()  
DECLARE SUB FILEWRD (=)  
'$INCLUDE: 'qbdecl4.bas'
```

```
CONST black = 0  
CONST blue = 1  
CONST green = 2  
CONST cyan = 3  
CONST red = 4  
CONST magenta = 5  
CONST brown = 6  
CONST white = 7  
CONST grey = 8  
CONST lightblue = 9  
CONST lightgreen = 10  
CONST lightcyan = 11  
CONST lightred = 12  
CONST lightmagennta = 13  
CONST yellow = 14  
CONST brightwhite = 15
```

```
COMMON resol!, cyc%, count!, pico%, i%, staln!, tottim%, sec%, buff$, temp$, prev
```

```
st1$ = "waveln=["  
st2$ = "value=["  
EN$ = "];"  
path$ = "c:\jay\spec\data"  
10 CLS  
20 SCREEN 0  
30 LOCATE 1, 3  
40 PRINT "Enter the last few digits [mmdtrialno] of the data file";
```

```

50 INPUT filenm$
60 PRINT " Is the filename correct [y/n]";
70 INPUT confirm$
80 IF confirm$ = "n" GOTO 10

CALL IBDEV(0, 3, 0, 10, 1, 1, pico%)
OPEN path$ + "\W" + filenm$ + ".m" FOR OUTPUT AS #1'store wavelength value
  PRINT #1, st1$
  OPEN path$ + "\D" + filenm$ + ".m" FOR OUTPUT AS #2'store current value
  PRINT #2, st2$
LOCATE 2, 3
PRINT "Values of wavelength stored in "; path$ + "\W" + filenm$ + ".m"; " file"
LOCATE 3, 3
PRINT "Values of current stored in "; path$ + "\D" + filenm$ + ".m"; " file"
buff$ = SPACES$(40)
temp$ = SPACES$(40)
cycle! = 4
count! = 1
prev = 1E-11

COLOR green, black
LOCATE 4, 3
PRINT "Program used for the spectrometer with 2400 lines/mm grating"
COLOR white, black
LOCATE 5, 3
PRINT "Enter the initial scan wavelength [A]";
INPUT staln!
COLOR yellow, blue
LOCATE 7, 3
PRINT "Set the counter to"; staln! + (47/2)
COLOR white, black
LOCATE 9, 3
PRINT "Enter the final scan wavelength [A]";
INPUT endln!
LOCATE 10, 3
PRINT "End point as observed from the counter [A]"; endln! + (47/2);
LOCATE 11, 3
PRINT "Enter the speed of scanning drive [A/min]";
INPUT speed!
LOCATE 13, 3
PRINT "Maximum resolution that can be obtained [A]"; speed! / (cycle! * 60);
LOCATE 15, 3
PRINT "Enter the resolution required [A]-(default"; speed! / (cycle! * 60); "A)";

```

```

INPUT resol!
IF resol! = 0 THEN resol! = speed! / (cycle! * 60)
sec! = resol! * (cycle! * 60) / speed!
sec% = sec!
IF (sec% - sec!) > .000001 THEN
    COLOR white, red
    LOCATE 16, 3
    PRINT "Error in calculation is more likely to occur";
END IF
COLOR white, black
LOCATE 17, 3
PRINT "Data acquisition interval [seconds]"; sec%;
temp% = endl! - staln!
IF temp% < 0
    LOCATE 19, 3
    PRINT "Please scan the spectrometer with increasing value of wavelength"
    GOTO 200
ELSE
    LOCATE 19, 3
    tottim% = (endl! - staln!) * 60 / speed!
    PRINT "Total time taken [seconds]"; tottim%;
    endtim% = tottim% / sec%
    LOCATE 21, 3
    PRINT "No. of samples to be taken"; endtim% * cycle!;
    LOCATE 22, 3
    COLOR white, red
    PRINT "Set Scan drive scanning switch to H";
    LOCATE 23, 3
    PRINT "Start the Program and the Scan drive simultaneously";
    COLOR white, black
    LOCATE 24, 3
    PRINT "Hit any key to start";
    WHILE INKEY$ = ""
    WEND
    COLOR green, black
    i% = 1
    TIMER ON
    ON TIMER(sec%) GOSUB disp
    CLS
    LOCATE 1, 1
    PRINT "Program reads data from Picoammeter in"; sec% / cycle!; "second interval";
    LOCATE 2, 1
    PRINT "No. of samples to be taken"; endtim% * cycle!;

```

```

LOCATE 3, 1
PRINT "Total time taken "; tottim%; " seconds";
LOCATE 5, 1
PRINT "Wavelength[A] Current[amps] Sample No. Cycle/Sec. Time remaining[sec.] "
start! = TIMER
DO
LOOP WHILE i% < endtim% + 1
finish! = TIMER
TIMER OFF
PRINT "Total Execution time="; finish! - start!
PRINT #1, EN$
PRINT #2, EN$
OPEN path$ + "\X" + filenm$ + ".m" FOR OUTPUT AS #3'store matlab EXE file
PRINT #3, "clear all;clc;"
PRINT #3, "W" + filenm$
PRINT #3, "D" + filenm$
PRINT #3, "plot(waveln,abs(value),'g');pause(3);sm5;xlabel('Wavelength A');yla-
bel('Current amps');"
PRINT #3, "title('Emission Spectrum');grid;"
PRINT "Execute "; path$ + "\X" + filenm$ + ".m"; " in matlab to view plot"
CLOSE
GOTO 200
END

```

```

disp:
FOR cyc% = 1 TO cycle!
CALL FILEWRT
count! = count! + 1
NEXT cyc%
i% = i% + 1
RETURN

```

```

200 COLOR white, red
PRINT "Switch off the Spectrometer drive";
COLOR white, black
PRINT " Press any key to end.";
WHILE INKEY$ = ""
HTONE = 2000: LTONE = 550: DELAY = 500
FOR count = HTONE TO LTONE STEP -10
SOUND count, DELAY / count
NEXT count
HTONE = 780: RANGE = 650
FOR count = RANGE TO -RANGE STEP -4

```

```

    SOUND HTONE - ABS(count), .3
    count = count - 2 / RANGE
    NEXT count
    WEND
END IF
END

```

```

SUB FILEWRT
    SHARED prev, pico%, cyc%, i%, staln!, resol!, tottim%, sec%, temp$, buff$, count!
    CALL IBRD(pico%, buff$)
    temp$ = MID$(buff$, 5, 40)
    y = VAL(RTRIM$(temp$))
    IF (y > .00001) THEN
        y = prev
    END IF
    prev = y
    staln! = staln! + resol!
    WRITE #1, 2 * staln!
    WRITE #2, y
    LOCATE 7, 1
    PRINT 2 * staln!, y, count!, cyc%, tottim% - (sec% * i%)
END SUB

```

```

SUB ReportError (fd%, errmsg$) STATIC
    PRINT "Error = ", IBERR%; errmsg$
    IF (fd% <> -1) THEN
        PRINT ("Cleanup: taking board off-line")
        CALL IBONL(fd%, 0)
    END IF
    STOP          ' Abort program
END SUB

```

REFERENCES

REFERENCES

- [1] J. Asmussen, J. Mossbrucker, S. Khatami, W. S. Huang, B. Wright and V. Ayres, "The effect of nitrogen on the growth, morphology, and crystalline quality of MPACVD diamond films," Submitted to *Diamond and related materials*.
- [2] D. Zhou, D. M. Gruen, L. C. Qin, T. G. McCauley and A. R. Krauss, "Control of diamond film microstructure by Ar additions to CH₄/H₂ microwave plasmas," *J. Appl. Phys.*, **84**, No. 4, 1998
- [3] A. K. Srivastava, Properties of Electron Cyclotron Resonance Plasma Sources, Ph.D. Dissertation, Michigan State University, 1995.
- [4] A. R. Striganov and N. S. Sventitskii, Tables of Spectral Lines of Neutrals and Ionized Atoms. (IFI/Plenum, New York, 1968).
- [5] H. N. Chu, E. A. Den Hartog, A. R. Lefkow, J. Jacobs, L. W. Anderson, M. G. Lefally and J. E. Lawler, "Measurements of the gas temperature in a CH₄-H₂ discharge during the growth of diamond," *Phys. Rev. A*, **44**, 6, 1991.
- [6] A. N. Goyette, J. R. Peck, Y. Matsuda, L. W. Anderson and J. E. Lawler, "Experimental comparison of rotational and gas kinetic temperatures in N₂ and He-N₂ discharges," *J. Phys. D: Appl. Phys.*, **31**, 1556, (1998).
- [7] A. Thorne, Spectrophysics (Chapman and Hall, New York, 1988)
- [8] A. Gicquel, K. Hassouni, Y. Breton, M. Chenevier and J. C. Cubertaon, "Gas temperature measurements by laser spectroscopic techniques and by optical emission spectroscopy," *Diamond and related materials*, **5**, 366, (1996).
- [9] L. Wolniewicz and K. Dressler, "The *EF* and *GK* $^1\Sigma_g^+$ States of Hydrogen- Adiabatic Calculation of Vibronic States in H₂, HD, and D₂," *J. Mol. Spectrosc.*, **67**, 416, (1977).
- [10] K. Dressler, R. Gallusser, P. Quadrelli and L. Wolniewicz, "The *EF* and *GK* $^1\Sigma_g^+$ States of Hydrogen- Calculation of Nonadiabatic Coupling," *J. Mol. Spectrosc.*, **75**, 205, (1979).
- [11] I. Kovacs, Rotational Structure in the Spectra of Diatomic molecules (American Elsevier Publishing Company, New York, 1969)
- [12] G. H. Dieke, "The Molecular Spectrum of Hydrogen and its Isotopes," *J. Mol. Spectrosc.*, **2**, 494, (1958).

- [13] G. Herzberg, Molecular Spectra and Molecular Structure vol 1, (Van Nostrand, New York, 1950).
- [14] R. Samlenski, C. Haug and R. Brenn, "Incorporation of nitrogen in chemical vapor deposited diamond," *Appl. Phys. Lett.*, **67**, No. 19, 2798, 1995.
- [15] W. Muller-Sebert, E. Wornor, F. Fuchs, C. Wild and P. Kiodl, "Nitrogen induced increase of growth rate in chemical vapor deposition of diamond," *Appl. Phys. Lett.*, **68**, No. 6, 759, 1996.
- [16] T. Hong, S. Chen, Y. Chiou and C. Chen, "Optical emission spectroscopy studies of the effects of nitrogen addition on diamond synthesis in a CH₄-CO₂ gas mixture," *Appl. Phys. Lett.*, **67**, No. 15, 2149, 1995.
- [17] W. Zhu, A. Inspektor, A. R. Badzian, T. Mckenna and R. Messier, "Effects of noble-gases on diamond deposition from methane-hydrogen microwave plasmas," *J. Appl. Phys.*, **68**, 1489, 1990.
- [18] K. J. Clay, S. P. Speakman, G. A. J. Amaratunga and S. R. P. Silva, "Characterization of *a*-C:H:N deposition from CH₄/N₂ rf plasmas using optical emission spectroscopy," *J. Appl. Phys.*, **79**, No. 9, 7227, 1996.



MICHIGAN STATE UNIV. LIBRARIES



31293017718358